ΕΘΝΙΚΟ ΜΕΤΣΟΒΙΟ ΠΟΛΥΤΕΧΝΕΙΟ
Σχολή Πολιτικών Μηχανικών
Εργαστήριο Μεταλλικών Κατασκευών

ΣΧΕΔΙΑΣΜΟΣ ΜΕΤΑΛΛΙΚΩΝ ΒΙΟΜΗΧΑΝΙΚΩΝ ΚΑΠΝΟΔΟΧΩΝ ΕΝΑΝΤΙ ΛΥΓΙΣΜΟΥ

Διπλωματική Εργασία

Ειρήνη Νικολούδη

ΕΜΚ ΔΕ 2015 36

Επιβλέπων: Χάρης Γαντές, Δρ. Πολιτικός Μηχανικός, Καθηγητής ΕΜΠ
Συνεπιβλέπων: Κωνσταντίνος Καλοχαιρέτης, Δρ. Πολιτικός Μηχανικός

Αθήνα, Οκτώβριος 2015

NATIONAL TECHNICAL UNIVERSITY OF ATHENS
School of Civil Engineering
Institute of Steel Structures

DESIGN OF STEEL INDUSTRIAL CHIMNEYS AGAINST BUCKLING

Diploma Thesis of
Irini Nikoloudi

ΕΜΚ ΔΕ 2015 36

Supervisor: Charis Gantes, Dr. Civil Engineer, Professor of N.T.U.A.
Co-supervisor: Konstantinos Kalochairetis, Dr. Civil Engineer

Athens, October 2015

Ειρήνη Νικολούδη (2015)

Σχεδιασμός Μεταλλικών Βιομηχανικών Καπνοδόχων Έναντι Λυγισμού
Διπλωματική Εργασία ΕΜΚ ΔΕ 2015 36
Εργαστήριο Μεταλλικών Κατασκευών, Εθνικό Μετσόβιο Πολυτεχνείο, Αθήνα.

Irini Nikoloudi (2015)

Diploma Thesis EMK ΔΕ 2015 36
Design of Steel Industrial Chimneys Against Buckling
Institute of Steel Structures, National Technical University of Athens, Greece

Ευχαριστίες

Με την παρούσα εργασία κλείνει ο πενταετής, γεμάτος εμπειρίες και γνώσεις, κύκλος σπουδών μου στο Ε.Μ.Π.. Νιώθω την ανάγκη λοιπόν να ευχαριστήσω τους ανθρώπους που ήταν δίπλα μου σε όλη αυτήν την πορεία, μέχρι και το τέλος: την οικογένειά μου, τους φίλους μου, τους καθηγητές μου. Ο επιβλέπων της διπλωματικής μου εργασίας, ο κ. Χάρης Γαντές, ήταν ο καθηγητής και κυρίως ο άνθρωπος που με ενέπνευσε ώστε να επιλέξω την κατεύθυνση των μεταλλικών κατασκευών. Η γνώση, η εμπειρία και η άριστη επικοινωνία του στάθηκαν αρωγός για τη διεκπεραίωση αυτής της εργασίας και τον ευχαριστώ θερμά για αυτό.

Επίσης, θα ήθελα να ευχαριστήσω από καρδιάς τον Κωνσταντίνο Καλοχαιρέτη, διδάκτορα του Ε.Μ.Π., ο οποίος με την αμεσότητα του χαρακτήρα του και τις πολύτιμες συμβουλές του βοήθησε στην επιτυχή ολοκλήρωση της εργασίας μου. Οι ουσιαστικές παρεμβάσεις του και η ευθύτητα της σκέψης του καθόρισαν την τελική της μορφή και επέκτειναν τους πνευματικούς μου ορίζοντες.

Ευχαριστώ ακόμα τον κ . Παύλο Θανόπουλο και τον κ. Τάσο Αβραάμ για τη συμμετοχή τους στην εξεταστική επιτροπή.

Τέλος, είμαι ευγνώμων για την αμέριστη συμπαράσταση της οικογένειάς μου, καθώς και των φίλων μου. Η στήριξη, οι συμβουλές και η παρότρυνσή τους βοήθησαν στις επιλογές μου και μου έδωσαν δύναμη να συνεχίσω.

Ειρήνη Νικολούδη

Οκτώβριος 2015

ΕΘΝΙΚΟ ΜΕΤΣΟΒΙΟ ΠΟΛΥΤΕΧΝΕΙΟ
ΣΧΟΛΗ ΠΟΛΙΤΙΚΩΝ ΜΗΧΑΝΙΚΩΝ
ΕΡΓΑΣΤΗΡΙΟ ΜΕΤΑΛΛΙΚΩΝ ΚΑΤΑΣΚΕΥΩΝ

ΔΙΠΛΩΜΑΤΙΚΗ ΕΡΓΑΣΙΑ
ΕΜΚ ΔΕ 2015 36

Σχεδιασμός Μεταλλικών Βιομηχανικών Καπνοδόχων Έναντι Λυγισμού

Ειρήνη Νικολούδη

Επιβλέπων: Χάρης Γαντές, Δρ. Πολιτικός Μηχανικός, Καθηγητής ΕΜΠ
Συνεπιβλέπων: Κωνσταντίνος Καλοχαιρέτης, Δρ. Πολιτικός Μηχανικός

ΠΕΡΙΛΗΨΗ

Η ανάλυση και ο σχεδιασμός των λεπτότοιχων κατασκευών ξεκίνησε ήδη από τις αρχές του εικοστού αιώνα, όταν προέκυψε η ανάγκη για σχεδιασμό αεροσκαφών, διαστημοπλοίων, ρουκετών, υποβρυχίων και άλλων συναφών κατασκευών. Η σημαντική διαφοροποίηση αυτών των κατασκευών σε σχέση με άλλες γρήγορα έγινε αισθητή, καθώς παρατηρήθηκε ότι ήταν ιδιαίτερα ευαίσθητες σε γεωμετρικές ατέλειες, τοπικό λυγισμό και πλαστικοποιήσεις.

Αρχικά, το ζήτημα του λυγισμού λεπτότοιχων κελυφών αντιμετωπίστηκε κάνοντας χρήση αναλυτικών μεθόδων σε σχετικά απλές εφαρμογές, όπως αυτήν της απλής αξονικής συμπίεσης. Ανάμεσα στους πρώτους ερευνητές που ασχολήθηκαν με το θέμα αυτό ήταν ο Timoshenko, ο Southwell και ο Lorenz, οι οποίοι καθιέρωσαν αναλυτικές μεθόδους που χρησιμοποιούνται ευρέως ακόμα και σήμερα στους σύγχρονους κανονισμούς. Στις επόμενες δεκαετίες, πραγματοποιήθηκαν πολυάριθμα πειράματα, τα αποτελέσματα των οποίων σήμαναν τα μειονεκτήματα που προέκυπταν από τις υποθέσεις των αναλυτικών μεθόδων. Πρόσφατα, η σημαντική εξέλιξη των υπολογιστών και η ανάπτυξη της επιστήμης του πολιτικού μηχανικού κατέστησαν δυνατή τη χρήση πιο ανεπτυγμένων αριθμητικών διαδικασιών.

Στην παρούσα εργασία, μελετάται μία βιομηχανική μεταλλική καπνοδόχος μονάδας παραγωγής ηλεκτρικής ενέργειας. Η καπνοδόχος έχει τα εξής γεωμετρικά χαρακτηριστικά: ύψος 60m, διάμετρος 7m και σταθερό πάχος τοιχωμάτων ίσο με 0.013m. Επίσης, είναι ενισχυμένη με περιφερειακές νευρώσεις, ή δαχτυλίδια, σε σταθερά διαστήματα των 5m. Οι νευρώσεις αυτές έχουν διατομή σχήματος L και διαστάσεις L120/120/10. Το υλικό που χρησιμοποιείται είναι χάλυβας S235 JR, σύμφωνα με τις διατάξεις του EN 13084-7. Ωστόσο, λόγω της θερμοκρασίας που λειτουργεί η καπνοδόχος, τα μηχανικά χαρακτηριστικά του χάλυβα S235 JR μειώνονται (σύμφωνα με τις αντίστοιχες οδηγίες του EN 13084-7). Τελικά, προκύπτει όριο διαρροής ίσο με 160MPa και μέτρο ελαστικότητας ίσο με 2.025×10^{8}kN/m^2. Ακόμα, ο λόγος του Poisson είναι 0.3. Τα φορτία που ασκούνται στην κατασκευή χωρίζονται σε κατακόρυφα και οριζόντια. Τα πρώτα αποτελούνται από τα ίδια βάρη του κελύφους, των νευρώσεων και του εξοπλισμού που αναμένεται να υπάρχει σε τέτοιου είδους κατασκευές. Τα δεύτερα αφορούν φορτία ανέμου σύμφωνα με τις διατάξεις του EN 1991-1-4.

Η αναλυτική διαδικασία που ακολουθείται στην παρούσα εργασία είναι απλοποιημένη υιοθετώντας κάποιες παραδοχές. Πρώτα από όλα, στους αναλυτικούς υπολογισμούς πραγματοποιείται η παραδοχή

της θεωρίας δοκού. Σύμφωνα με αυτήν, η καπνοδόχος συμπεριφέρεται ως πρόβολος και, ως εκ τούτου, η μέγιστη τάση εμφανίζεται στη βάση της κατασκευής, στην πλευρά όπου ο άνεμος την συμπιέζει. Σε ό,τι αφορά τις αναλύσεις, πρώτον, θεωρούνται γραμμικές και ελαστικές συνθήκες, όπου υπολογίζεται η αντοχή λυγισμού, σύμφωνα με την κλασσική ελαστική θεωρία λυγισμού. Δεύτερον, θεωρούνται μη γραμμικές και ανελαστικές συνθήκες, όπου υπολογίζεται η αντοχή κατάρρευσης της κατασκευής, σύμφωνα με τις οδηγίες του κανονισμού CICIND.

Στα πλαίσια αυτής της εργασίας, πραγματοποιούνται αριθμητικές αναλύσεις μέσω του λογισμικού πεπερασμένων στοιχείων ADINA, με σκοπό τον υπολογισμό της απόκρισης και της αντοχής της καπνοδόχου. Ως εκ τούτου, δύο τύποι αριθμητικών προσομοιωμάτων μελετώνται, η μη ενισχυμένη και η ενισχυμένη κατασκευή. Η τελευταία ενισχύεται με εύκαμπτα (μέτρο ελαστικότητας ίσο με $2.025\times10^8 kN/m^2$) και ελαστο-πλαστικά (όριο διαρροής ίσο με 160MPa) ή ελαστικά δαχτυλίδια, στα πλαίσια των μη γραμμικών και γραμμικών αναλύσεων, αντίστοιχα. Τα αποτελέσματα τόσο των γραμμικών (LBA) όσο και των μη γραμμικών (GNA, MNA, GMNA) αναλύσεων παρουσιάζονται μέσω των δρόμων ισορροπίας και κατάλληλων στιγμιότυπων τη στιγμή της κατάρρευσης. Ως δείκτης αντοχής χρησιμοποιείται ένας φορτικός συντελεστής, ο οποίος πολλαπλασιάζει όλα τα φορτία μέχρι την κατάρρευση. Η σύγκριση των αριθμητικών αποτελεσμάτων μεταξύ της μη ενισχυμένης και της ενισχυμένης κατασκευής δείχνει την επίδραση των νευρώσεων στην αντοχή και τις παραμορφώσεις. Η σύγκριση μεταξύ αναλυτικών και αριθμητικών αποτελεσμάτων της μη ενισχυμένης κατασκευής επιτρέπει τον έλεγχο της επάρκειας των αναλυτικών μεθόδων για τον σχεδιασμό μη ενισχυμένων καπνοδόχων.

Επιπρόσθετα, πραγματοποιείται μια παραμετρική μελέτη, στα πλαίσια της οποίας διερευνάται η επίδραση στην αντοχή δύο παραμέτρων: του διαστήματος μεταξύ των νευρώσεων και της δυσκαμψίας των νευρώσεων. Το διάστημα μεταξύ των νευρώσεων ξεκινά από 20m και φτάνει μέχρι και τα 2.5m. Όσον αφορά τη δεύτερη παράμετρο, συγκρίνονται δυο κατασκευές, αυτή με τις εύκαμπτες νευρώσεις και αυτή με τις δύσκαμπτες νευρώσεις. Στην τελευταία, χρησιμοποιούνται πολύ δύσκαμπτα και ελαστικά δαχτυλίδια.

Τελικά, παρουσιάζονται μερικά συμπεράσματα που αφορούν τον πρακτικό σχεδιασμό των λεπτότοιχων καπνοδόχων. Τα συμπεράσματα αυτά είναι βασισμένα στα αποτελέσματα των παραπάνω αριθμητικών αναλύσεων. Έτσι, εκτιμάται η χρήση της κλασσικής ελαστικής θεωρίας λυγισμού στους αναλυτικούς υπολογισμούς. Επιπρόσθετα, μελετάται η αξιοπιστία της τάσης αστοχίας, σύμφωνα με τις οδηγίες του σχεδιαστικού κώδικα CICIND. Τέλος, λαμβάνει χώρα μια μελέτη βελτιστοποίησης της αντοχής, στα πλαίσια της οποίας εξετάζεται η παράμετρος του διαστήματος μεταξύ των νευρώσεων.

NATIONAL TECHNICAL UNIVERSITY OF ATHENS
SCHOOL OF CIVIL ENGINEERING
INSTITUTE OF STEEL STRUCTURES

DIPLOMA THESIS
ΕΜΚ ΔΕ 2015 36

Design of Steel Industrial Chimneys Against Buckling

Irini Nikoloudi

Supervisor: Charis Gantes, Dr. Civil Engineer, Professor N.T.U.A.
Co-supervisor: Konstantinos Kalochairetis, Dr. Civil Engineer

ABSTRACT

The analysis and design of thin-shell structures began during the early 20th century due to the emerging requirements for designing aircrafts, spacecrafts, rockets, submarines and other types of structures. The significant differentiation of such structures from others was quickly observed, as it was found that they are particularly sensitive to geometric imperfections, local buckling and subsequent plastification.

Initially, the problem of shell buckling was investigated by making use of analytical methods in relatively simple problems, such as axial compression. Among the first researchers who worked on shell buckling were Timoshenko, Southwell and Lorenz, who established analytical methods that are widely used by modern design specifications. In the next decades, experimental tests took place and led to useful conclusions, highlighting drawbacks in the assumptions behind the analytical procedures. In the last decades, the development of computer and civil engineering sciences facilitated the use of more advanced numerical procedures.

In the present thesis, an industrial chimney of a combined cycle power plant is investigated. The thesis assumed chimney structure has a height equal to 60m, a diameter equal to 7m and a constant thickness of 0.013m. Additionally, it is stiffened by circumferential stiffeners (rings) at constant intervals of 5m. The geometric type of the stiffeners is L120/120/10. The used material is steel of grade S235 JR, according to EN 13084-7. However, due to the operating temperature, the following reduced mechanical properties for S235 are eventually used: yield stress f_y=160MPa and elasticity module E=2.025×10^{8}kN/m^2. Additionally, the Poisson's ratio is equal to 0.3. The applied loads are divided into vertical and horizontal. The first ones consist of the self-weights of the shell, the stiffeners and the equipment supposed to be present in such chimneys. The second ones are the wind loads as described in EN 1991 Part 1-4.

The analytical process that is followed in this thesis is simplified making some assumptions. First of all, in the analytical calculations the consideration of beam theory is assumed. Based on the latter, the chimney behaves like a cantilever beam and, hence, the largest stress is assumed at the base of the structure, at the most compressed side due to wind. As far as the applied numerical analyses are concerned, firstly, linear and elastic conditions are assumed, where the buckling strength is calculated, according to the classical elastic buckling theory. Secondly, nonlinear and inelastic conditions are considered, where collapse strength is found based on the guidance of the design code CICIND.

In the context of this thesis, numerical analyses are carried out by means of the finite element software ADINA, in order to compute the response and the capacity of the assumed chimney structure. For this reason, two types of numerical models are investigated, the unstiffened and the stiffened one. The latter is stiffened with flexible ($E=2.025\times10^8 kN/m^2$) and elastoplastic ($f_y=160MPa$) or elastic rings for nonlinear and linear analyses, respectively. Linear (LBA) and nonlinear (GNA, MNA και GMNA) numerical analyses are performed and are presented through appropriate equilibrium paths as well as snapshots at the time of failure. As strength indicator the load factor that multiplies all applied loads up to collapse is used. The comparison of the numerical results between the unstiffened and the stiffened model highlights the impact of ring stiffeners on the structure capacity and deformation. The comparison between the analytical and numerical results of the unstiffened structure leads to the investigation of the sufficiency of the assumed analytical process for the design of unstiffened chimney structures.

A parametric investigation is also conducted. In the context of that, the impact of stiffener spacing and the stiffener rigidity on structure's capacity is investigated. The stiffener spacing ranges from 20m to 2.5m. Investigating the stiffener rigidity, two stiffened structures are compared: the flexibly stiffened and the rigidly stiffened one. In the rigidly stiffened model, very stiff elastic rings are used.

Finally, some practical conclusions for the design of thin-shell chimneys are presented. Hence, the use of the classical elastic buckling theory in the analytical calculations is evaluated. Additionally, the reliability of the failure stress according to the design code CICIND is investigated. Finally, an optimization investigation of the capacity in terms of stiffener spacing takes place.

CONTENTS

1 INTRODUCTION

1.1 HISTORIC FLASHBACK ON THIN SHELLS

Many applications of practical engineering require the use of thin-shell structures. Some of them include: aircraft, spacecraft, rockets, submarines, industrial chimneys, nuclear reactors, cooling towers, roofs, tubular towers, silos, tanks, pressure vessels, pipelines and offshore platforms. The particularity of thin-shell buckling has employed many mathematicians and engineers during the last century. Some illustrious names are Love and Rayleigh, who laid the foundations that were built on by Southwell, Timoshenko, von Karman, Novozhilov, Tsien, Koiter, Reissner, Mindlin and Hutchinson [1].

The beginning of the 20th century is regarded as the classical period of thin-shell buckling research. In the period from 1900s up to 1970s, comprehensive studies and long research took place, resulting in some classical analytical solutions that are used even today. Despite that, it was then that the high sensitivity of thin shells to local phenomena and to geometric imperfections was observed, due to the overestimation of experimental results from the existing analytical solutions. It was noticed that geometric imperfections appear during the fabrication process and may be different from the ones predicted in laboratory. It was understood then that the need for more advanced experimental or computational tools was inevitable.

In the 1960s, the advent of high-speed digital computers and the associated advances in computational mechanics offered a new approach to the shell buckling problem. The shell buckling researchers were some of the first research groups to fully exploit the power of modern computer programs, since buckling experiments were often particularly difficult to carry out and could be very unreliable if not properly undertaken.

By the mid-1980s, computer packages for the buckling analysis of shells had been developed to the point where they could deliver realistic buckling loads if realistic imperfections could be modeled. Path-following methods were used extensively and in particular the arc-length method. The latter enabled the implementation of highly nonlinear equilibrium paths, so that the prediction of buckling was near to the realistic one. The range of different analyses that could be used for shell buckling was considerable, so design processes were required to identify how each might be used safely.

1.2 APPLICATION OF THIN SHELLS TO LARGE-DIAMETER INDUSTRIAL CHIMNEYS

As mentioned earlier, a group of engineering applications that require thin-shell structure is the one related to industrial chimneys. Until recently, steel chimney diameters did not use to exceed 4 meters and this is obvious in the relevant technical literature [2]. However, the development of combined cycle power plants, where industrial chimneys have the role of boiler exhaust stacks, made the new generation of engineers to use large-diameter (in the order of 7 meters) chimneys. Hence, many particularities in the buckling design appeared, related to the high sensitivity of such structures to local phenomena. Therefore, the design codes had to adapt properly if safe thin-shell structures were to be erected.

1.2.1 A REALISTIC CASE OF INDUSTRIAL CHIMNEY AS THE BASE OF THIS THESIS

A realistic large-diameter chimney is the base of this thesis. Such a chimney, whose representative model is presented in section 3.2, is used in a completed research project [3]. The latter is sponsored by CICIND [4] (CICIND is a major international design code for the design of steel chimneys) and has been conducted by the following engineers:

- Michael Angelides, Structural Engineer
- Charis Gantes, Structural Engineer, Professor at the National Technical University of Athens
- Konstantinos Kalochairetis, Structural Engineer

The realistic industrial chimney of the above project is a part of a combined cycle power plant. Some subjects, like the operation of power plants and the role of such a chimney in them, are developed subsequently in the next sections.

1.2.1.1 THE COMBINED CYCLE POWER PLANT CHIMNEY

The combined cycle power plant involves two power generation cycles: The gas or open cycle, which consists of a gas turbine and the steam cycle, where the gas turbine exhaust gas is fed into a boiler and produces steam, which drives a steam turbine. This is depicted in Figure 1-1. During the open cycle operation only, the boiler is not in function and it is blocked off by the diverter. In this case, the bypass stack serves as the exhaust for the gas turbine. During combined cycle operation, the diverter blocks off the bypass stack and leads the exhaust gas to the boiler and from there to the main stack [2].

1.2.1.2 GEOMETRICAL PARTICULARITIES AND DESIGN ISSUES

It is usual for both the main and the bypass chimneys in a combined cycle power plant to have diameters in the order of 7 meters. The necessary interruption of the bypass stack by the diverter requires the bypass stack to be placed on a support frame and separated by the diverter through an expansion joint. The stiffness of the support frame must be carefully accounted for in the design of the chimney, because the size of the diverter will not usually allow any bracing in the direction normal to the gas flow [2].

The connection of the main stack to the boiler usually requires an opening with significant dimensions. Usually, the breeching spans about 150° in width and 21 meters in height. These dimensions make the breeching area design and stabilization as one of the important issues in the overall design. Since such an opening size usually exceeds two thirds of the chimney diameter, it is often worth-considering replacing the single opening by a series of equivalent circular openings (Figure 1-2), as also suggested by the CICIND Model Code Commentaries. The expansion joint between the boiler and the stack is

usually larger than the breeching. Thus, a protruding inlet duct of significant dimensions is required to be attached to the stack, as shown in Figure 1-3.

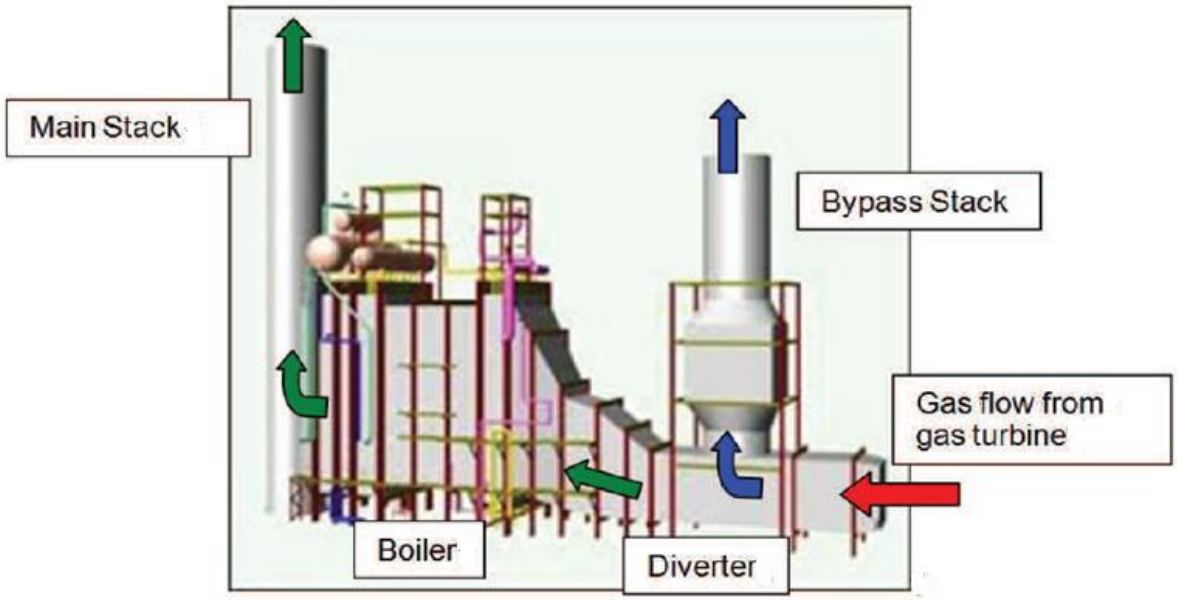

Figure 1-1: Boiler and chimneys in a combined cycle power plant [2]

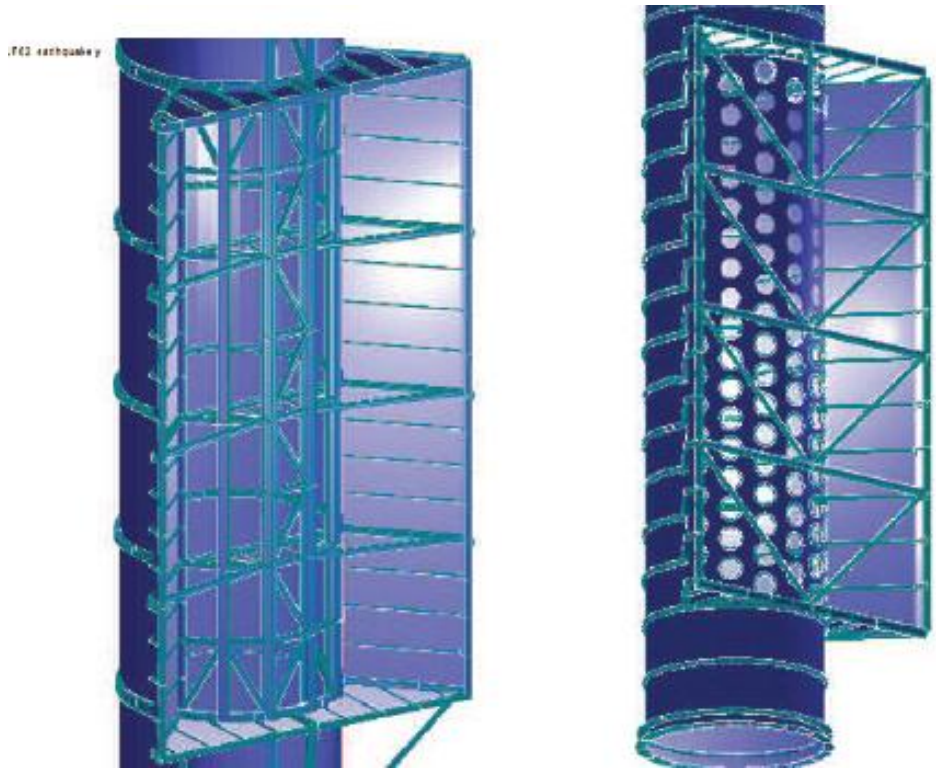

Figure 1-2: Replacement of the single breeching opening (left) by a series of equivalent circular openings (right) [2]

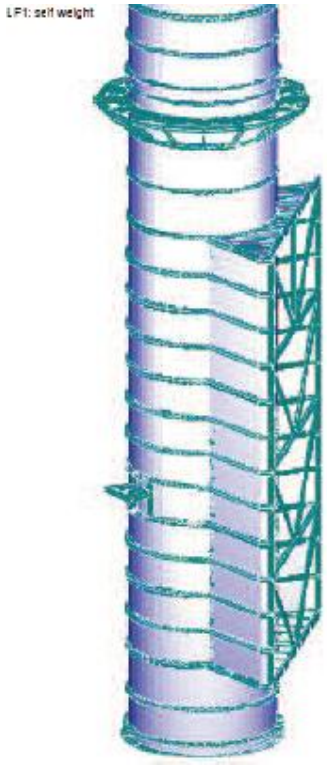

Figure 1-3: Lower part of a main stack with inlet duct [2]

Additionally, it is often required dampers to be installed inside the main stack, in order to control the temperature loss from the boiler during a temporary shut-down. Due to the size of the chimney diameter, these dampers have weights that range from 5 to 15 tons. Similarly, if a silencer needs to be considered inside the chimney, the expected associated weight ranges from 10 to 25 tons. These weights affect the dynamic response of the chimney and require particular measures to introduce them into the shell. The chimney damper is usually installed immediately above the breeching. When the damper is closed, a pressure build-up from the boiler may lead to internal pressure values that can reach up to 6kPa. This pressure distribution constitutes a significant load case, which also contributes to the base moment.

1.2.1.3 FABRICATION, TRANSPORTATION AND ERECTION

Transportation is a significant issue in the case of large-diameter chimneys. Approximately 3 to 4 meters segments can be transferred. Hence, fabrication and shipment in quadrants or 120 deg sections are required. These segments must then be assembled on site into cylindrical cans for the erection of the chimney. Therefore, even if the assembly of cans had been expected to be carried out using bolted flange connections, the transportation restrictions will necessarily require extensive welding on site. This means that a large-diameter chimney will require significantly more site welding than a conventional one. Additionally, the site must be organized to ensure that the necessary tolerances are respected when forming the cylindrical cans, through the use of temporary structures.

The above restrictions have to be documented in the design codes, so that the fabricator and erector to understand clearly the shop and field assemblies and procedures. The use of a 3-Dimensional computer model is required in accomplishing these tasks [2]. The following sample snapshots, shown in Figure 1-4, indicate such fabrication models.

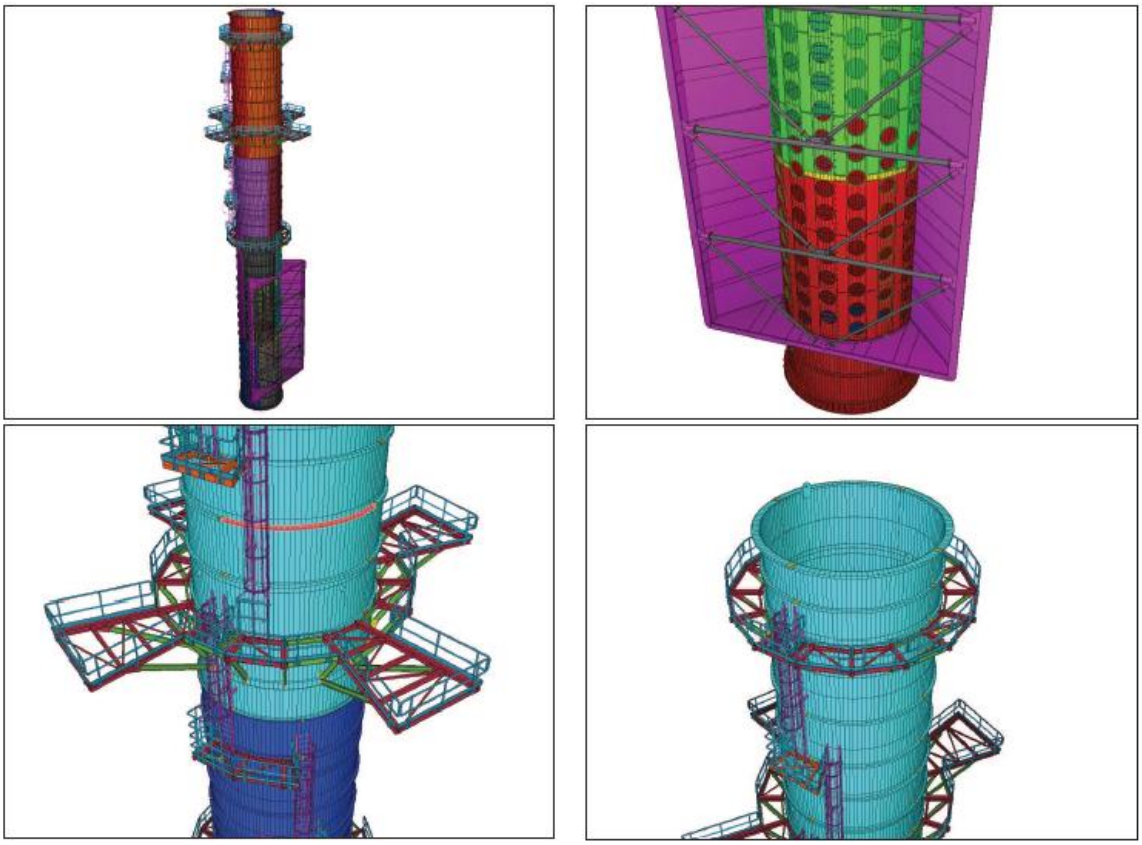

Figure 1-4: Computer model for the fabrication of a 7.20m diameter chimney [2]

1.2.2 THESIS MODEL ASSUMPTIONS BASED ON THE REALISTIC CHIMNEY

The applied simplifications adopted in the present thesis concern the analytical approach to the capacity evaluation and the chimney model description. As far as the simplifications on the analytical calculations are concerned, it is noted that the internal forces are considered at the chimney bottom (see also section 3.3). Such considerations are based on the, so-called, beam theory. In that manner, though, a series of errors may be introduced, taking into account that the most unfavorable internal stresses may be found anywhere along the thin-shell chimney, when wind pressure is applied.

The assumptions of the chimney model refer to chimney's geometric and design characteristics, the used materials and the applied loading. First of all, the thesis model does not use a breeching opening or the equivalent smaller circular openings at the structure base, as they were described earlier. In that way, the chimney is modeled as a long, solid, cylindrical, thin-shell structure. Although the model structure does not include breeching, it can be still regarded a realistic chimney. Therefore, the afore-described chimney equipment is inserted in the thesis model by applying its weights, as vertical forces. In the stiffened model of this thesis, ring stiffeners are used. Stiffeners are longitudinal or circumferential (rings) thin-shell steel equipment, placed along the chimney at constant intervals, usually. Ring stiffeners are considered as necessary for the restriction of the cross-sectional changes. As far as the used materials are concerned, European material grades and European code material properties have been used throughout this work, for consistency purposes. Finally, the thesis assumed loading includes vertical and horizontal forces. The first ones refer to the equipment weights, as mentioned before, while the horizontal ones to the wind pressure, as described in EN 1991 Part 1-4 [5]. The thesis model description is developed thoroughly in section 3.2.

1.3 THE AIM AND THE SUBJECTS OF THE PRESENT THESIS

The basic aim of the present thesis is the thorough investigation of the structural response of unstiffened and stiffened shell structures by making use of advanced numerical tools. Hence, the main topics covered in the present thesis are:

- Investigation of the behavior of the unstiffened model, using advanced numerical tools and comparison of the numerical behavior with the analytical results, according to the existing codes.
- Impact of stiffeners on structure's capacity.
- Impact of the spacing between stiffeners on structure's capacity.
- Impact of the stiffness of stiffeners on structure's capacity.
- Combination of the above results for the estimation of the thesis analytical approach and for an optimization investigation of the structure's capacity.

1.4 STRUCTURE OF THE THESIS

The first (1st) chapter, after a short flashback on thin shells, refers to the use of thin-shell large-diameter industrial chimneys in practical engineering and to the brief presentation of the research project on which this thesis is based. The second (2nd) chapter deals with the past technical insight, where the buckling problem treatment is separated into three aspects: that of analytical calculations, of numerical analyses and of experimental tests. In the third (3rd) chapter, the model description takes place and analytical calculations based on a simplified method are presented. The fourth (4th) chapter initially refers to the description of the numerical model and later to the numerical results of the unstiffened and stiffened structure. The fourth chapter also presents a comparison between analytical and numerical results. The fifth (5th) chapter deals with the impact of stiffener spacing and stiffener stiffness on structure's capacity. The sixth (6th) chapter refers to the estimation of the thesis analytical approach, while an effectiveness investigation of some structural components takes place as well.

In the seventh (7th) chapter, summary and conclusions are presented, while further research for the future is suggested as well. This thesis ends up with the chapter of references, eighth (8th) chapter, where one will find the titles of the references used throughout this work.

2 TECHNICAL INSIGHT FROM THE PAST

2.1 INTRODUCTION

In this chapter, the existing knowledge related to the design of thin shells against buckling is presented. Thin shells are particularly special in the way they collapse under any loading case. Hence, as it will be discussed subsequently in the following sections, many experiments and, more recently, numerical analyses have been conducted with the aim of the strength evaluation of such structures. The results of this extensive research are reflected in many analytical calculations and recently in the related codes. Among the many experiments, the unstiffened and stiffened thin shells under axial compression and external pressure are presented in this chapter. Since numerical analyses could be performed, a variety of models could be investigated under several load-cases. Hence, in the corresponding section, numerical results for unstiffened and stiffened shell structures under wind pressure and other load-cases are indicated. In that way, an introduction to industrial chimneys takes place, since chimneys are thin-shell structures (unstiffened or stiffened), for which the crucial loading is usually the wind pressure.

2.2 ANALYTICAL APPROACHES

Most of the analytical relationships that deal with the strength evaluation of thin shells have resulted from experiments with cylindrical shells under uniform loads. Among the uniform loads, the axial compression is considered as the most prevalent, as long as it guaranties economy in testing, high sensitivity to geometric imperfections and simplicity of testing. Hence, the axially compressed cylinder has been studied more extensively than any other shell buckling problem. The possible induced errors of this approach are usually addressed by means of reduction factors, which are based on experimental observations [6]. In this section, the afore-mentioned analytical approach is presented.

2.2.1 CLASSICAL ELASTIC BUCKLING THEORY

The first theoretical shell buckling stress to be calculated was the, so-called, "classical elastic buckling stress", by Lorenz (1908) [7], Timoshenko (1910) [8] and Southwell (1914) [9]. This buckling stress resulted from experiments on a medium-length cylindrical thin shell under axial compression, with simply supported ends. As a consequence of the uniform axial compression, a membrane (in-plane) prebuckling stress distribution takes place. This prebuckling stress is unaffected by the boundary

conditions and, thus, it is regarded uniform along the cylinder shell. The classical elastic buckling stress is defined in Eq. (4-1).

$$\sigma_d = \frac{E}{\sqrt{3\cdot\left(1-v^2\right)}}\cdot\frac{t}{r} \cong 0.605\cdot E\cdot\frac{t}{r} \tag{2-1}$$

where:

E is the Young's modulus

v is the Poisson's ratio. For the case of circular cylinders v=0.3

t is the shell wall thickness

r is the cylinder radius

In Figure 2-1, the typical load-end shortening relationship is shown, for a geometrically perfect thin elastic cylinder under uniform axial compression. A linear prebuckling path is observed, which suddenly bifurcates into a non-symmetric mode (Figure 2-2(b)), with several full waves of buckling mode around the circumference, and usually several waves up the height. At buckling, the load falls very rapidly, and the cylinder actually increases in length for a while. As the load falls, bifurcation happens again as the mode switches from one circumferential wave number n to another in dynamic jumps, which are particularly difficult to follow with static structural calculations [10]. The bifurcation load is usually slightly lower than the load found by a linear eigenvalue calculation, because nonlinearity in the prebuckling path often leads to additional destabilizing stresses [6].

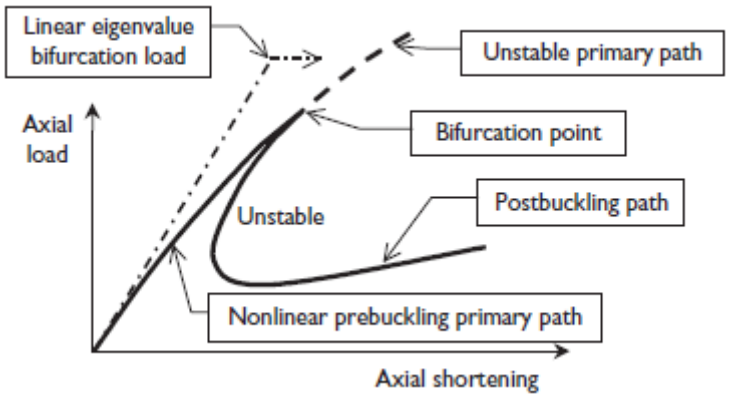

Figure 2-1: Typical load-end shortening relationship for an axially compressed cylinder [6]

At this elastic buckling stress, a very large number of different buckling modes or eigenmodes (sometimes over 100 modes) are all at the same time critical. Many modes appear different "chequer-board" patterns (Figure 2-2(b)), whose wavelengths in the circumferential and axial directions are related by the "Koiter circle" [11], [12]. The steeply falling postbuckling path (Figure 2-1) is related to the proximity of these many modes. It should be noted that Eq. (4-1) also gives the critical stress for axisymmetric buckling, where the cylinder develops a corrugated appearance, with waves only in the axial direction, as shown in Figure 2-2(a). This mode has a stable postbuckling path, and is regarded important when the cylinder is internally pressurized.

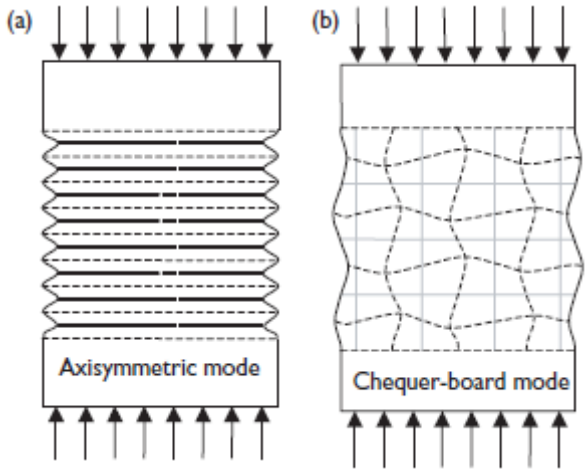

Figure 2-2: Typical buckling modes for axially compressed perfect cylinders: (a) axisymmetric mode (b) non-symmetric mode [6]

For a medium-length cylinder, like the one we investigate in this section, the critical buckling mode that is depicted in Figure 2-2(b) involves square waves, and can be described by the number of full waves n_{cl} around the circumference, given by Eq. (2-2).

$$n_{cl} = \sqrt[4]{\left(\frac{3}{4}\right)\cdot\left(1-\nu^2\right)}\cdot\sqrt{\frac{r}{t}} \cong 0.909\cdot\sqrt{\frac{r}{t}} \tag{2-2}$$

Eq. (2-2) indicates that the number of waves falls progressively as the shell becomes thicker. Additionally, in very thin shells, where the wave number n_{cl} is high, the buckling mode is often much localized, since buckling can occur when a zone of about the size of a single wavelength is critically loaded. However, since a large number of different modes are almost simultaneously critical for our case, Eq. (2-2) does not have great significance. It should also be noted that the wide range of possible modes includes an axisymmetric mode (Figure 2-2(a)) with axial half-wavelength, which is half the half-wavelength of the square chequer-board pattern given by Eq. (2-2). This half-wavelength is given by Eq. (2-3).

$$\lambda_{cl} = \frac{\pi}{\left[12\cdot\left(1-\nu^2\right)\right]^{1/4}}\cdot\sqrt{r\cdot t} \cong 1.728\cdot\sqrt{r\cdot t} \tag{2-3}$$

It is concluded then that a perfect cylinder has a complex buckling behavior, which makes it a popular choice for the extraction of many analytical calculations. Despite that, Eq. (4-1) provides a very poor estimate of the experimental strengths of practical cylinders. However, the critical elastic buckling stress is almost universally used as the reference buckling stress on which other results are based.

2.2.1.1 EFFECT OF THE LENGTH OF THE CYLINDER

Cylindrical shells are usually divided into three basic length categories, according to their buckling response: short cylinders, in which one or two buckle waves take place along the cylinder shell, medium cylinders, in which chequer-board (Figure 2-2(b)), diamond pattern or outward axisymmetric buckles (Figure 2-2(a)) may occur and long cylinders. In short cylinders, the boundary conditions determine the buckling behavior [6]. First, they induce local stresses due to the restraint of radial expansion at the ends, during the prebuckling phase, and also they restrain the buckling displacements. In the prebuckling phase, these local stresses occur in a zone roughly limited by the linear half-wavelength λ of meridional bending from each end, as defined in Eq. (2-4).

$$\lambda = \frac{\pi}{\left[3 \cdot \left(1 - \nu^2\right)\right]^{1/4}} \cdot \sqrt{r \cdot t} \cong 2.44 \cdot \sqrt{r \cdot t} \tag{2-4}$$

Hence, a bound defined as L/λ=2 determines the effect of boundary conditions. The shells with lengths below that bound are expected to have prebuckling stresses affected by end conditions. On the other hand, shells longer than this behave independently of boundary conditions. The latter are defined as medium length cylinders. Short cylinders have a much more stable postbuckling response, which ultimately leads to a lower sensitivity to geometric imperfections. However, a few practical civil engineering problems use short shells. It is pointed out that the EN 1993-1-6:1999 [13] classes cylinders as of medium length if they lie in the range 0.70≤ (L/λ)≤ 0.20(r/t).

2.2.1.2 DISCREPANCIES BETWEEN ANALYTICAL AND EXPERIMENTAL RESULTS

As shown in Figure 2-3, the strengths of cylinders measured in laboratory tests are very scattered and fall far below the ideal strength [6]. Some of the reasons this may happen are the effect of geometric imperfections and the co-existent residual stresses.

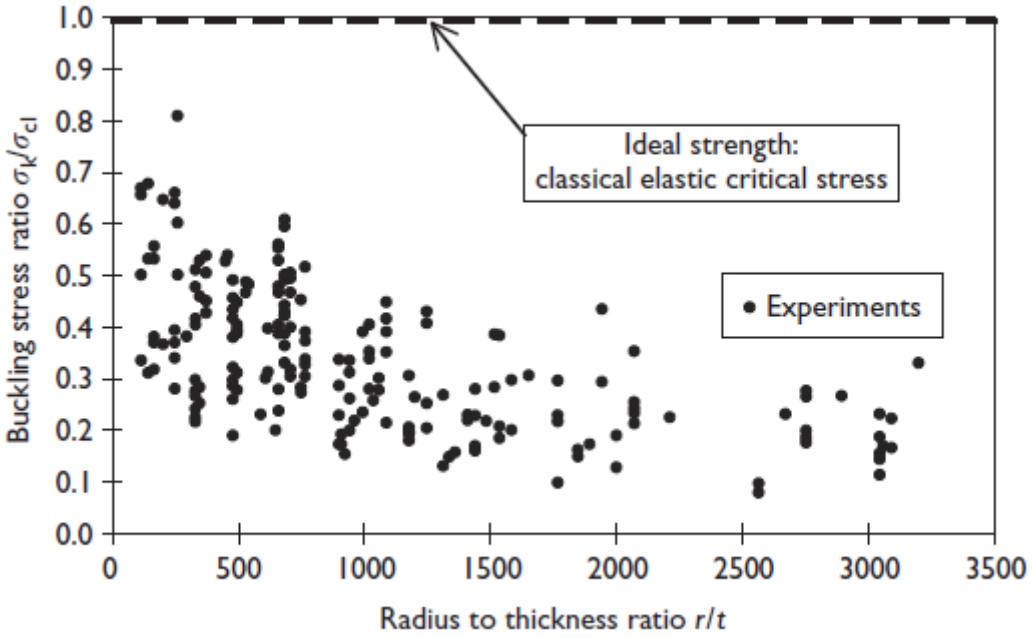

Figure 2-3: Experimental strengths of isotropic axially compressed cylinders [14]

The main of the reasons that a reduced experimental buckling stress takes place is the initial imperfections [15]. In laboratory tests and real structures, during the fabrication process, the introduction of initial geometrical imperfections is inevitable. Therefore, long studies have been carried out to this direction by many researchers, for the prediction of the form and amplitude of initial imperfections. The most notable contributors to this research are von Karman and Tsien (1941), Koiter (1945) [12], Donnell and Wan (1950) [16], Budiansky and Hutchinson (1966) and Yamaki (1984) [17]. Particularly, the matter of the form and amplitude of initial imperfections has been thoroughly investigated by Yamaki (1984). In recent design codes, this significant matter is addressed by the use of reduction factors, as it will be proved later in this section.

As far as the residual stresses are concerned, it is noted that they exist when geometrical imperfections are present and many times they may be quite large. Though, extensive studies have

not been carried out about these stresses. Recently, the researchers (Bornscheuer et al. 1983 [18], Rotter 1988, 1996b [19], Ravn-Jensen and Tvergaard 1990, Guggenberger 1996a [20], Holst et al. 1996a, 2000 [21], [22], Hübner et al. 2003) support that residual stresses do not contribute that much in the elastic buckling stress reduction as they do in columns and beams.

2.2.2 APPROACHES TO THE DESIGN PROBLEM

Many philosophies have developed in the past so as the afore-mentioned disadvantages of the use of the elastic buckling stress to be addressed. In this section, some of them will be presented as proposed by Teng and Rotter (2004) [6], as well as the recent codes, which are based on such philosophies.

2.2.2.1 LOWER BOUNDS ON TEST RESULTS

The adoption of a lower bound, based on the observed test results (Figure 2-3), is considered the oldest of the methods for the treatment of the imperfections matter. This approximation is traced back to Robertson (1928) [23] and Wilson and Newmark (1933) [24]. The most recent studies referred to such an approach are the researchers: Donnell (1934) [25], Timoshenko (1936) [26], Harris et al. (1957) [14], Weingarten et al. (1965a) [27], Hoff and Soong (1967) [28], Almroth et al. (1970) [29], Steinhardt and Schulz (1971) [30] and Bornscheuer (1982) [31].

Despite the simplicity of the method, there are some disadvantages that make the pure use of it inadequate. First of all, some of the tests indicate very low values of strength and thus the design will have to be quite conservative, unreasonably most of the times. The main reason of the insufficiency of this method is the fact that the imperfections introduced by the fabrication process of the laboratory tests are different in form and amplitude than the ones of the real structures, making the test results unrepresentative and the lower bound controversial. However, standards that have adopted this approach had been developed, including API 620 (1978) [32], AWWA D100 (1979) [33], ECCS (1988) [34] and DIN 18800 (1990) [35]. A progress to this empirical approach was carried out mainly by Rotter, 1985 [36] and was related to the use of tolerance measures so as the imperfections to be controlled. For this reason, empirical curves that relate imperfection sensitivity and tolerance measurements were created. Such curves, with changes as proposed by Rotter in 1997 and 1998 [37], [38], are used in EN 1993-1-6:1999 [13].

2.2.2.2 FAILURE STRESS BY EN 1993-1-6:1999

This approach is based on the experimental results (as stated in the previous section). However, since the form and the amplitude of imperfections are unpredictable in both the laboratory models and the real structures and their effect on structure's capacity are undeniable, this method proposes measures for the control of imperfections. As far as the tolerance measurements are concerned, EN 1993-1-6:1999 [13] proposes a group of different measurements (Figure 2-4). Some of them concern other states of loading, but mainly they intend to control the imperfections as introduced by the axially compressed cylinder.

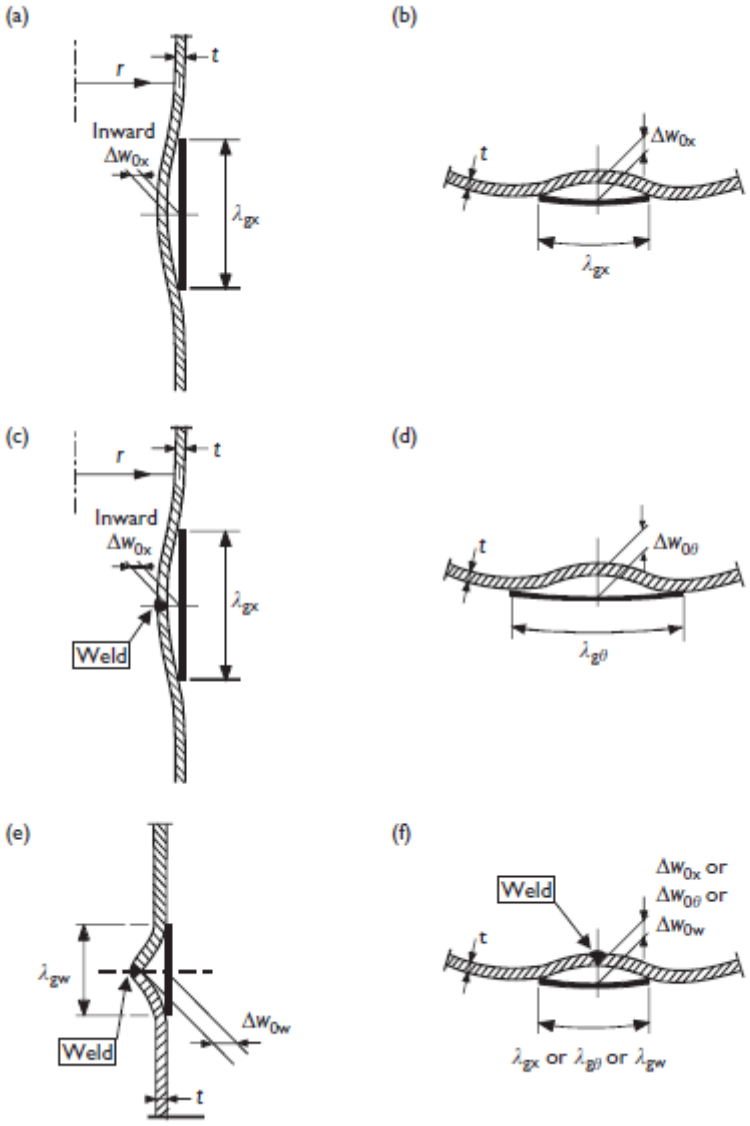

Figure 2-4: Dimple imperfection measurements required by EN 1993-1-6 (a) Measurement on a meridian (b) First measurement on a circumferential circle (c) First measurement across a weld (d) Second measurement on circumferential circle (e) Second measurement across a weld using a special gauge (f) Measurements on circumferential circle across weld

The tolerance measurements are related to the wavelength of the square eigenmode for the perfect shell (Figure 2-2(b)), which has a half wavelength in each direction of $2\lambda_{cl}$ (λ_{cl} was defined in Eq. (2-3). Since λ_{cl} is theoretical and not precise, the normal measuring stick has a length λ_{gx}, as indicated in Eq. (2-5). This reflects the classical eigenmode and is used as the reference worst imperfection.

$$\lambda_{gx} = 4 \cdot \sqrt{r \cdot t} \tag{2-5}$$

A much shorter length λ_{gw}, is used across welds, as described in Eq. (2-6), for the possibility of local plastic failure if deep local deviations occur.

$$\lambda_{gw} = 25 \cdot t \tag{2-6}$$

The measured imperfection is made dimensionless by Eq. (2-7). A tolerance U has to be lower than the maximum value of U_{max}.

$$U_{0x} = \frac{\Delta_{w0x}}{\lambda_{gx}} \tag{2-7}$$

Three different fabrication quality classes are defined, as indicated in Table 2-1, allowing highly controlled fabrication to exploit the higher resulting strength, but requiring less controlled construction to assume a lower buckling load. The characteristic imperfection amplitude Δ_{wx} is found by Eq. (2-8).

$$\Delta_{wx} = \frac{1}{Q} \cdot \sqrt{\frac{r}{t}} \cdot t \tag{2-8}$$

where:

Q is the meridional compression fabrication quality parameter (Table 2-1)

The characteristic imperfection is then used in an empirical relationship for the elastic buckling strength dependency on imperfection amplitude, as defined in Eq. (2-9).

$$\alpha_{x0} = \frac{0.62}{1 + 1.91 \cdot \left(\frac{\Delta_{wx}}{t}\right)^{1.44}} \tag{2-9}$$

Table 2-1: Values for dimple tolerance $U_{0,max}$ and quality parameter Q

Fabrication tolerance quality class	*Description*	*Value of $U_{0,max}$*	*Value of U_n*	*Q*
Class A	Excellent	0.006	0.01	40
Class B	High	0.01	0.016	25
Class C	Normal	0.016	0.025	16

The buckling stress by EN 1993-1-6:1999 for a medium length shell is then found by Eq. (2-10). It is actually a reduced value of the classical elastic buckling stress σ_{cl} by the factor α_{x0}.

$$\sigma_{xcr} = \alpha_{x0} \cdot \sigma_{cl} \tag{2-10}$$

When plasticity is introduced into the buckling problem, the characteristic buckling strength is reduced to σ_{xk}, for lower values of the relative slenderness of the shell λ_x, given by Eq. (2-11). Eq. (2-11) is valid for $\lambda_0 < \lambda_x < \lambda_p$.

$$\sigma_{xk} = \left\{1 - \beta \cdot \left(\frac{\lambda_x - \lambda_0}{\lambda_p - \lambda_0}\right)^{\eta}\right\} \cdot f_y \text{, for } \lambda_0 < \lambda_x < \lambda_p \tag{2-11}$$

where:

β is the plastic range factor. Typically it is equal to 0.6

λ_x is the relative slenderness of the shell. It is defined in Eq. (2-12)

λ_0 is the squash limit relative slenderness. It is regarded equal to 0.2

λ_p is defined in Eq. (2-13)

η is the interaction exponent. The recommended value is 1.00

f_y is the yield stress

$$\lambda_x = \sqrt{\frac{f_y}{\sigma_{cl}}} \tag{2-12}$$

$$\lambda_p = \sqrt{\frac{\alpha}{1-\beta}} \tag{2-13}$$

where:

α $\alpha=\alpha_{x0}$ for an unpressurised axially compressed cylinder

For shells with $\lambda_x<\lambda_0$, the buckling stress σ_{xk} is taken as equal to the yield stress f_y.

2.2.2.3 FAILURE STRESS BY ASME STS-1

According to this design code, the critical buckling stress s_{cl} by ASME STS-1 [39] is given by Eq. (2-14). Similarly to EN 1993-1-6:1999, this code also takes into account the material plasticity and the geometric imperfections.

$$s_{cl} = \frac{E \cdot t \cdot Y}{4 \cdot D} \tag{2-14}$$

where:

Y is equal to 1.00

D is the diameter of the cylindrical shell

2.2.2.4 FAILURE STRESS BY CICIND

CICIND's critical buckling stress σ_k [4] is defined in Eq. (3-17). It is actually a reduced value of the yield stress by a factor, which takes into account material nonlinearity (plasticity), initial imperfections and the wind pressure.

$$\sigma_k = \left[1 - 0.412 \cdot \left(\lambda^*\right)^{1.2}\right] \cdot f_y \tag{2-15}$$

where:

λ^* is calculated in Eq. (3-18)

$$\lambda^* = \sqrt{\frac{f_y}{\alpha \times \sigma_{cl}}} \tag{2-16}$$

where:

α is calculated in Eq. (3-19)

$$\alpha = \frac{\alpha_N \cdot \sigma_N + \alpha_B \cdot \sigma_B}{\sigma_N + \sigma_B} \quad (2\text{-}17)$$

where:

α_N is calculated in Eq. (3-20), where r is the radius and t the thickness of the cylindrical shell

σ_N is the normal stress

α_B is calculated in Eq. (3-21)

σ_B is the bending stress

$$\alpha_N = \frac{0.7}{\sqrt{0.1 + r/100t}} \quad (2\text{-}18)$$

$$\alpha_B = 0.189 + 0.811 \cdot \alpha_N \quad (2\text{-}19)$$

2.3 NUMERICAL PROCEDURES

It is well-known that thin shells require special handling for their strength evaluation [15]. Unlike beams and plates, they are sensitive to initial imperfections induced during the fabrication process. Moreover, shell buckling is a complex phenomenon, since it is described by nonlinear partial differential equations that without advanced computer software are too difficult to solve. Hence, before the use of advanced computational tools and when inadequate number of experimental results was present, the structure's strength was often overestimated. This happened due to the use of simplified analytical approaches that were based on a perfect model under simplified load cases, such as the afore-described classical elastic buckling theory. That is why, the capacity estimation was mainly based on empirical interpretations of experimental data, but this was only available for a limited number of cases, as stated in the previous section.

Nowadays, since the availability of powerful computers is present, the development of sophisticated finite element intends to be an advanced numerical tool of the engineers and researchers, at least as far as the treatment of nonlinear equations is concerned. Despite that, the problem of prediction of the form and amplitude of geometric imperfections still remains unsolved. Therefore, the establishment of numerical results into the design codes, instead of the results of experimental tests is still controversial. Until now, only the EN 1993-1-6:1999 has made substantial steps to this direction, but the need of more research on this matter still remains, as it is stated by Rotter (2004) [15].

2.3.1 NUMERICAL ANALYSES

The analyses can be divided into the following classes, as used in the Eurocode standard (EN 1993-1-6:1999): Linear Elastic (LA), which includes Linear Buckling Analysis (LBA), Geometrically Nonlinear Elastic (GNA), Materially Nonlinear (MNA), Geometrically and Materially Nonlinear (GMNA) and Geometrically and Materially Nonlinear Analysis with geometric Imperfections (GMNIA). Formal definitions of these different types of analysis and the manner in which they can be adopted into the design process according to this standard were set out by Rotter (2002a, b) [40], [41]. Throughout this thesis, the afore-mentioned analyses (except for the last one, which is not applied extensively in this thesis) are more thoroughly described in section 4.2.5.

2.3.1.1 RESTRICTIONS BY THE USE OF NUMERICAL ANALYSES

It is important to note that the numerical analyses do not replace the existent analytical calculations of the Eurocode, which are based on experimental tests. Indeed, the numerical results explain the buckling behavior for specific cases and the corresponding parts of the code are rigorously separated. For example, a Linear Buckling Analysis takes no account of shell nonlinear geometric effects, plasticity, or imperfection sensitivity that is present in all constructions. The result of such analysis therefore needs careful interpretation before it can be adopted into the design process. A Linear Buckling Analysis may be performed to obtain the buckling load of the perfect structure, instead. Reduction factors can be then applied to account for the effects of geometric imperfections and plasticity. This approach is closely linked to the analytical calculations of the modern design codes (see also section 2.2.2), since these also begin with linear buckling (classical) stresses as a starting point.

On the other hand, a fully nonlinear analysis with explicit modeling of geometric imperfections (GMNIA) is expected to give more reliable results. Despite that, the problem of the imperfections definition is still present. Speicher and Saal (1991) [42] were the first to address such difficulty by proposing the first buckling mode as the equivalent form of imperfection and the measurements of the existing tests of axially compressed cylinders as the amplitude. Later, Rotter (1997b) [43] using weld depression imperfections attempted to approximate the problem. However, both of these proposals have only been applied to axially compressed cylinders, and other load cases and shell geometries may indicate different results.

If no information is available on the amplitude or form of realistic imperfections in the structure, and the geometry and load case are complex, the eigenmode method of choosing the imperfections for numerical analysis may be the only satisfactory approach. A better concept, however, would be to develop a statistically based imperfection model for a particular class of shell structures, fabricated using the same process, based on extensive measurements of real geometric imperfections on full-scale structures, as proposed by Arbocz (1991), Rotter et al. (1992) [44] and Ding et al. (1996b) [45].

2.3.1.2 EXPLOITATION OF NUMERICAL ANALYSES BY EN 1993-1-6:1999

As stated earlier, the Eurocode (EN 1993-1-6:1999) was the first code to introduce the finite element and similar computer calculations into the design processes. In an attempt to address the afore-mentioned restrictions, this code separates the different shell buckling problems into distinct parts and carefully defines where to use all the above categories of analysis.

Despite the fact that the GMNIA is considered, according to the code, as the most complete analysis, it is stated that one should not regard the GMNIA's strength as an assured lower bound. This is due to the unpredictable geometric imperfections, which may be different in the realistic structure from the assumed in the numerical analysis. Hence, the Eurocode addresses this matter by means of "appropriate allowances". These are separated into two groups: First, geometric imperfections, such as deviations from the nominal geometry, irregularities at and near the welds (minor eccentricities, shrinkage depressions, rolling curvature errors), deviations from the nominal thickness and lack of evenness of supports. The second group covers material imperfections, such as residual stresses, caused by rolling, pressing, welding, straightening, inhomogeneities and anisotropies. Ground settlements or flexibilities of connections or supports are noted as being additional sources of imperfection.

Hence, the Eurocode defines the amplitude of geometric imperfections as the maximum deviation $\Delta_{w0,eff}$ from the perfect shape, which is based on the fabrication tolerance quality class. This is equal to

the larger value between the $\Delta_{w0,eff,1}$ and $\Delta_{w0,eff,2}$, which are defined in Eq. (2-20) and (2-21), respectively.

$$\Delta w_{0,eff,1} = \lambda_g \cdot U_{n1} \tag{2-20}$$

$$\Delta w_{0,eff,2} = 100 \cdot t \cdot U_{n2} \tag{2-21}$$

where:

λ_g covers all relevant gauge lengths of Figure 2-4

U_{n1}, U_{n2} are defined values of the dimensionless imperfection amplitude (Table 2-1)

Despite this effort at amplitude definition, the strength assessment process must recognize that the worst form of imperfection may not be that assumed by the analyst, and that the amplitude of imperfection that causes the greatest strength loss is not necessarily the largest amplitude of the tolerance restriction. According to this, the Eurocode requires that it should also be verified that an imperfection that is 10% smaller than $\Delta_{w0,eff,2}$ does not yield a smaller value for the limit state load R_{GMNIA}. If this occurs, the procedure should be iterated to find the most damaging amplitude.

Finally, since the above procedure may not be sufficient to cover all situations that may arise, the consideration is required that the same analyses should be applied to comparable shell buckling cases for which characteristic buckling resistance values $R_{k,known,check}$ are known (either from calculation or test). The check calculations define the $R_{k,GMNIA,check}$ and are required to adopt similar imperfection assumptions. They also concern structural configurations that are similar in their buckling controlling parameters (relative shell slenderness, postbuckling behavior, imperfection-sensitivity and material behavior) to the target analysis. From the reliability check calculation, a calibration factor k_{GMNIA} is evaluated in Eq. (2-22).

$$k_{GMNIA} = \frac{R_{k,known,check}}{R_{k,GMNIA,check}} \tag{2-22}$$

The characteristic buckling resistance for the real structure is then obtained by Eq. (2-23).

$$R_k = k_{GMNIA} \cdot R_{GMNIA} \tag{2-23}$$

2.3.2 NUMERICAL ANALYSES FOR TALL CYLNDRICAL SHELLS UNDER WIND PRESSURE

Wind loadings are difficult to be applied in laboratory conditions, since the only place where the measurements would be reliable is the wind-tunnels. Hence, the development of advanced numerical analyses made possible the emulation of wind-pressure and thus more reliable results took place. It is pointed out that all the detailed investigations concern cylinders with constant wall thickness.

A report on numerical studies of this problem is given by Greiner and Derler (1995) [46]. It shows that buckling occurs in the mid-height region of the shell in the stagnation zone, initiated by the axial compression stresses acting there. Realistic results require the use of geometrically non-linear analyses of the imperfect structure (GNIA). These results indicate that this type of buckling is highly affected by the, so-called, ovalization of the cylindrical cross-section in the middle height of the shell. This type of deformation is mainly produced by the effect of the suction forces perpendicular to the wind direction.

Numerical investigations of cylinders with higher slenderness were performed by Schneider and Thiele (1998) [47], who revealed that additional buckling shapes may occur, both at the leeward side of the cylinder. As shown in Figure 2-5, one mode is located at the base area and it fails in the shape of the,

so-called, elephant-foot pattern. The other one occurs in the lower half of the shell, mainly initiated by the ovalization of the shell combined with axial compression due to overall bending ((c) case). Hence, the windward buckling failure may be accounted for in design by combination of the non-uniform wind pressure with the axial membrane stress including ovalization. Also the buckling failure in the base area may be checked due to given design rules. The leeward buckling in the lower half of the shell, however, requires further studies for deriving design specifications.

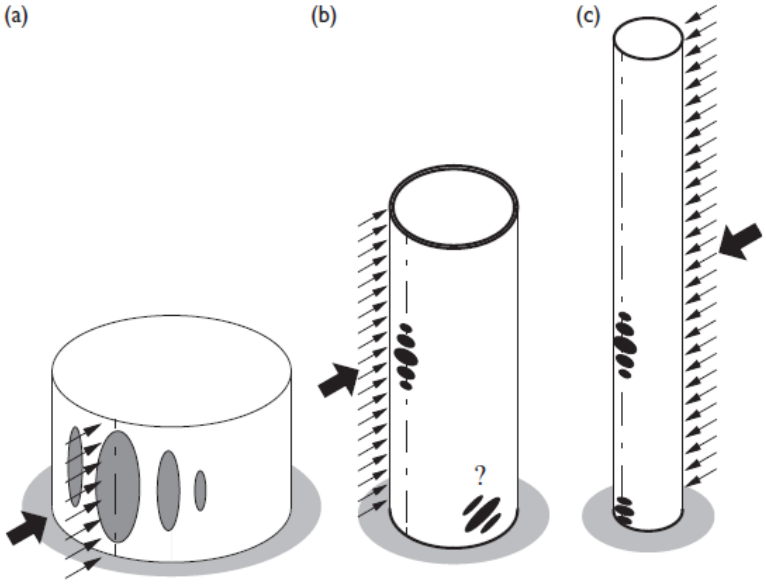

Figure 2-5: (a) Short, (b) long and (c) very long (=slender) wind-loaded cylindrical shell structures [48]

2.3.3 ADVANCED NUMERICAL ANALYSES FOR LARGE-DIAMETER CHIMNEYS UNDER VARIOUS LOAD CASES

In this section, results from numerical analyses, for both unstiffened and stiffened cylindrical shells, under various load cases are presented. These analyses were performed in the context of the afore-presented CICIND funded project by the researchers Michael Angelides, Charis Gantes and Konstantinos Kalochairetis in 2015 [3]. From the performed linear and nonlinear analyses of the project, the LBA results that regard the unstiffened and the stiffened structure are presented hereunder. Additionally, the comparison between the numerical buckling load factors and the classical elastic buckling load factors for the different load cases is shown.

It is noted that the project software is the finite element software ADINA. Additionally, 4-noded shell elements are used and a constant shell thickness is assumed. The boundary conditions are a fully supported bottom. The considered load cases are the following:

- LC1: Pure compression due to a concentrated vertical load applied at the top of the shell.
- LC2: Uniform global bending due to end bending moments of opposite direction.
- LC3: Non-uniform bending along the shell structure due to a concentrated horizontal load applied at the top.
- LC4: Pure compression due to vertical loads-weights applied at different levels. The values of the vertical loads-weights used are the ones given in the afore-mentioned project [3].
- LC5: Pure compression due to vertical loads applied at different levels and self-weight. The values of the weights are the ones presented in the afore-mentioned project [3].

- LC6: Combined loading including vertical load-weights at different levels, the self-weight of the shell structure and wind loading applied normally to the shell according to the design guidance of EN 1991-1-4 [5]. The wind load direction is +X-Direction. This type of loading is considered to be the most realistic one and would be normally used for the analysis and design of such structures.

As far as the unstiffened model is concerned, in Figure 2-6, a comparison between the analytical calculations and the numerically obtained buckling load factors using LBA for several mesh-densities and the different afore-described load cases is presented. It is noted that the analytical calculations are based on the classical elastic buckling theory (section 2.2.1) and the beam theory. It is obvious that for all the load cases except of the last one (LC6), the analytical solution is considered sufficient for the denser meshing. On the contrary, for the most realistic load case (LC6) in which the wind pressure is applied, a denser meshing indicates that the assumptions of the analytical approach (classical buckling theory and beam theory) are not valid.

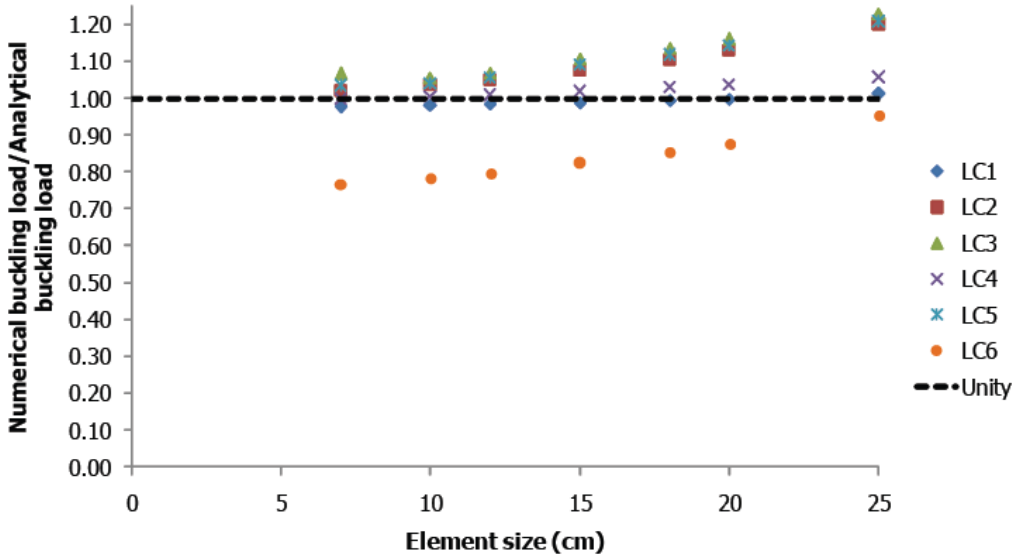

Figure 2-6: Mesh sensitivity using LBA for all load cases considered for the unstiffened model [3]

As far as the stiffened model is concerned, it is pointed out that ring stiffeners are used in this project with cross-section L120/120/10 at 5m intervals. It is interesting to notice the manner in which the stiffener presence affects on the buckling loads and the mode shapes. In Figure 2-7, the comparison between the buckling load factors of the unstiffened and stiffened structure is indicated for the various load cases. It is observed that in any load-case except of the last one (LC6, in which wind pressure is applied) the stiffeners do not contribute to the buckling load. Moreover, in Table 2-2, a comparison between the buckling modes from LBA of the unstiffened and the stiffened structure is shown for the different load cases. The same conclusion is drawn about the effect of stiffeners in the buckling mode shape: Only in the most realistic case, that of LC6, the stiffeners affect the shape of the buckling mode.

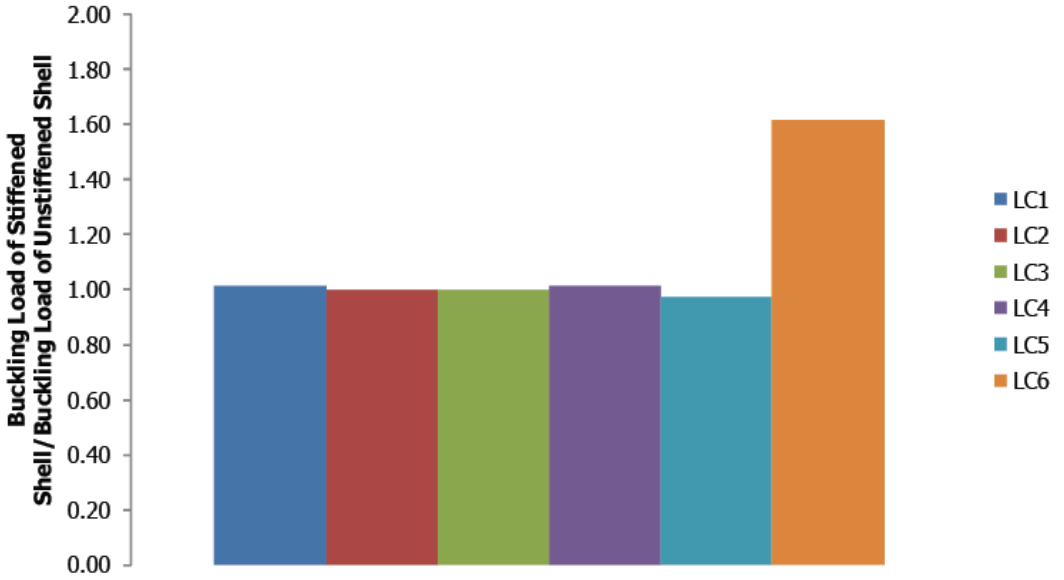

Figure 2-7: Ratio of the buckling loads of the first buckling mode of the stiffened structure to the one of the unstiffened structure for different load cases and based on mesh size equal to 7cm [3]

Table 2-2: Comparison between the first buckling mode shapes found for the unstiffened and the stiffened structures [3]

Load case	Unstiffened shell	Stiffened shell
LC1:Axial compression		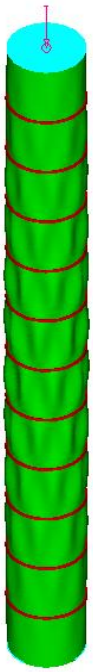

LC2:Uniform bending		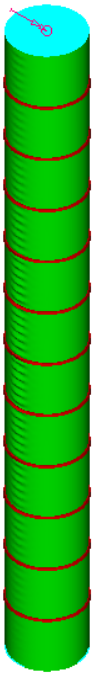
LC3:Non-uniform bending		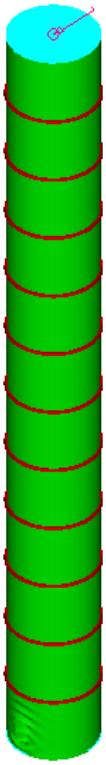

LC4: Attached weights	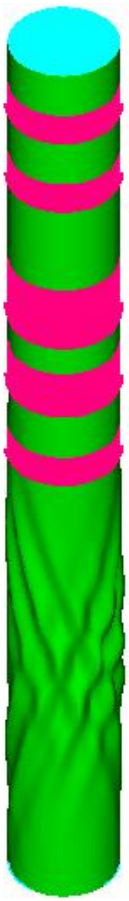	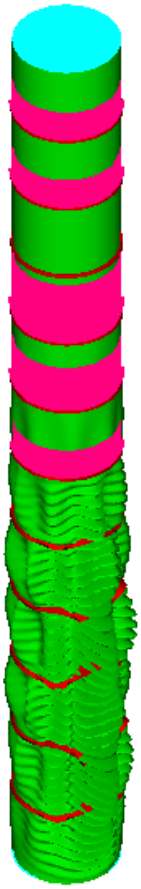
LC5: All weights		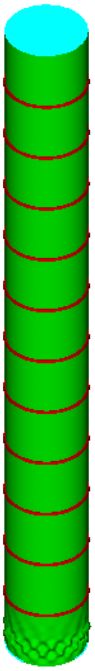

LC6: Combined loading	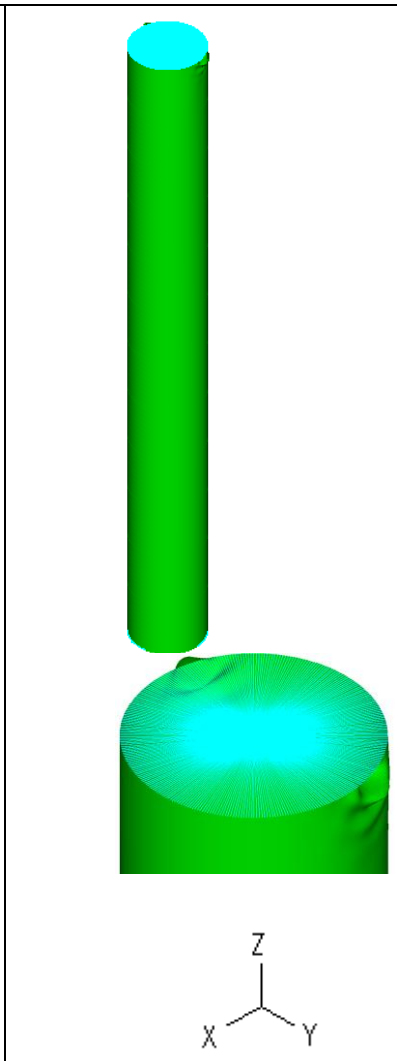	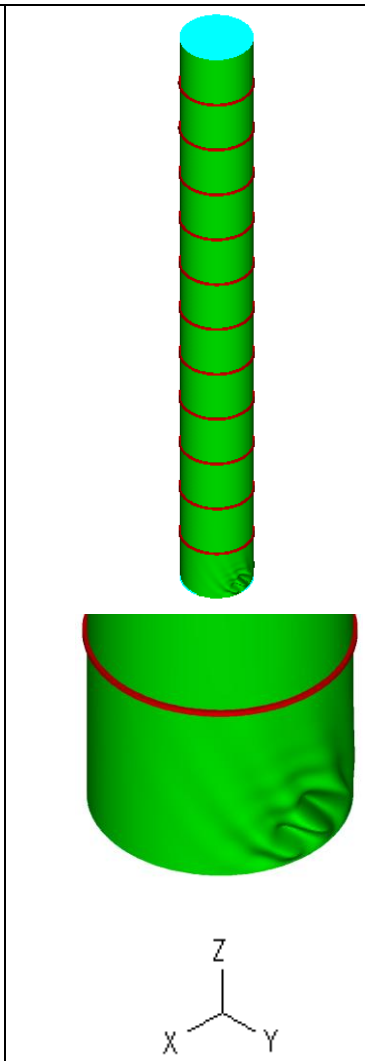

The above observations lead to the conclusion that when wind-pressure is applied on the thin walls of the structure then the use of analytical calculations based on the above assumptions may lead to incorrect strength evaluation. Additionally, the presence of stiffening rings is of importance in thin-shell, large-diameter chimneys under wind-pressure, as far as the strength and the buckling shape are concerned. This may be explained by the restriction offered by the stiffening rings to the cross-sectional changes due to the direct application of wind pressures on the structure shell. However, these conclusions have to be verified against more rigorous and more extensive numerical nonlinear analyses and experimental tests, as proposed by the researchers of the project. The nonlinear results of the wind-pressured chimney are presented, among other numerical results, in this thesis.

2.4 EXPERIMENTAL TESTS

2.4.1 CYLINDRICAL SHELLS UNDER AXIAL COMPRESSION

Axial compression is considered as the most common load case both in realistic structures and in laboratory tests. Hence, as far as the realistic structures are concerned, axial compression may be caused by the weight of the structure. Moreover, in structures like storage tanks with vertical axis the loads up on the roof cause axial compression to the shell walls. In silo structures also the stored solid exerts a normal pressure against the wall, but also applies a frictional drag, which accumulates into a

substantial axial compression. As for the experimental tests, it has been mentioned in this chapter that the tests using the axial compression are regarded simple and economic, despite the insufficiency in structure capacity estimation they may provide. Although the presence of axial compression in every structure is inevitable, in many structures like thin-shell chimneys or towers, it is not the crucial load case, since the wind brings more unfavorable consequences.

Under the axial compression, the surface of shell buckles and suddenly the initial shape changes into a wave-form one. This mode may be symmetric with respect to the axis, forming a single bulge around the circumference, but this only occurs under special conditions. Most commonly, the buckling mode involves alternately inward and outward displacements of the shell wall, termed an asymmetric or non-symmetric buckle (Figure 2-8). The wavelength of the buckles in both the axial and circumferential directions may vary without significantly changing the buckling load. This leads to a variety of possible modes at closely spaced loads. Hence, jumps usually occur from one mode to another as the buckling progresses into the postbuckling region [10]. It is noted that the stiffener presence does not affect the buckling mode shapes for axially compressed cylinders. As a result, buckling is commonly a sudden, dramatic, unpredictable event leading to a substantial loss of load-carrying capacity.

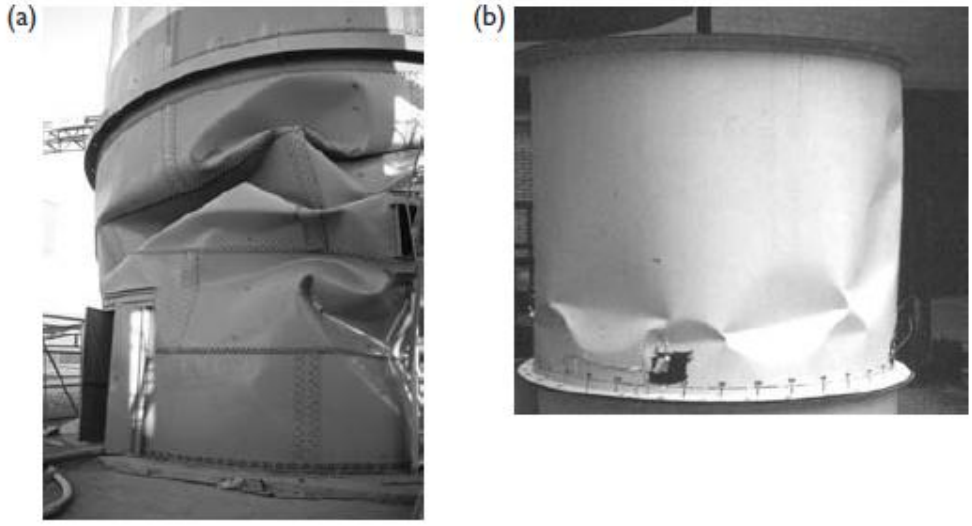

Figure 2-8: Typical appearance of axial compression buckles: (a) failure in service (b) test in laboratory [49]

2.4.2 STIFFENED CYLINDRICAL SHELLS UNDER EXTERNAL PRESSURE OR AXIAL COMPRESSION

In the past, several tests with stiffened cylindrical shells were carried out, since the structure capacity increase has employed the engineers and researchers. Moreover, stiffened shells could not be investigated theoretically or be described by analytically calculated relationships (like the classical elastic buckling theory). Hence, the laboratory tests could turn into reality the investigation of stiffened shells.

It is noted that stiffened cylindrical shells can fail in one of three modes: local shell instability (elastic or inelastic), global (general) instability (elastic or inelastic) or axisymmetric plastic collapse. Some test results conducted in different laboratories by different researchers are shown in Figure 2-9, Figure 2-10 and Figure 2-11. Ring-stiffened cylindrical shells under external pressure were tested and the above types of deformation of stiffened cylindrical shells are depicted. Figure 2-9 indicates the local shell instability. The test was conducted at Technion and regarded a stainless steel ring-stiffened shell, with a radius of 275 mm, R/h=344 and five spot-welded Z-shape rings, spaced at 50 mm distance

(i.e. a/h=63). Because of the wide spacing, the shell buckled in the local shell mode. As the pressure increased, the local buckles spread between the rings, eventually covering most of the shell and transformed into inelastic deformations. In Figure 2-10, the deformation of the general instability is shown, in a test conducted by Krenzke and Reynolds in 1967. The last type of deformation is depicted in Figure 2-11 and regards axisymmetric local plastic collapse in a ring-stiffened cylinder tested by the same researchers.

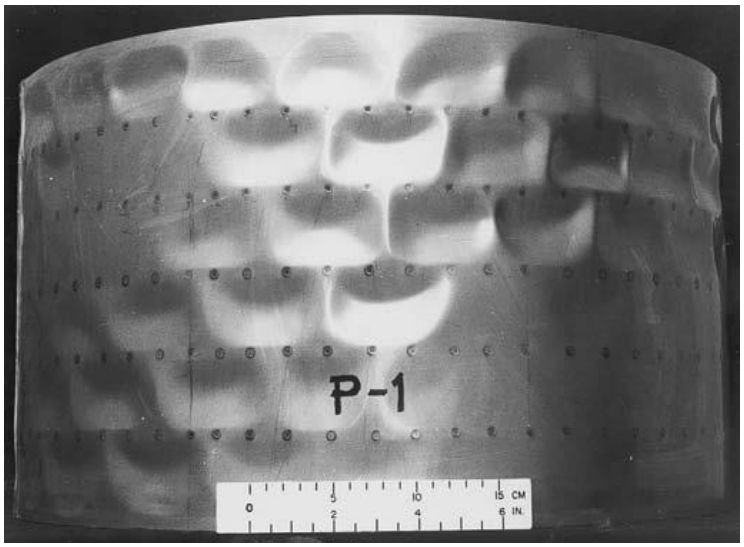

Figure 2-9: Local shell instability of a ring-stiffened cylindrical shell subjected to external pressure

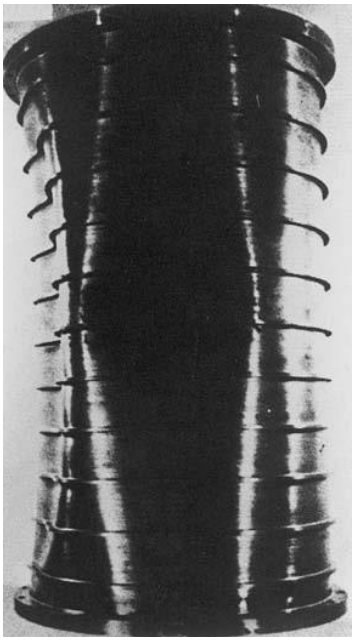

Figure 2-10: General instability (overall collapse) of a ring-stiffened cylindrical shell subjected to external pressure (from Krenzke and Reynolds 1967 [50])

Figure 2-11: Axisymmetric local plastic collapse (yielding) in a ring-stiffened cylindrical shell subjected to external pressure (from Krenzke and Reynolds 1967 [50])

It is noted that subjected to axial compression, the ring-stiffened cylindrical shells behave in a very similar manner. The postbuckling pattern of an axially compressed, widely spaced, ring-stiffened cylinder is shown in Figure 2-12, in the context of a test conducted in DLR Braunschweig by Esslinger and Geier in 1970 and reproduced by Springer and Verlag. The characteristic shape of deformation of local shell buckling between the rings is depicted. Failure by general instability is typical of shells with closely spaced ring-stiffening, as represented in Figure 2-13. This test was carried out at Technion by Rosen and Singer in 1975 and regards closely spaced, ring-stiffened 7075-T6 aluminium alloy cylindrical shell subjected to axial compression. For thicker walled ring-stiffened cylindrical shells under axial compression, the collapse mode may be axisymmetric plastic collapse for both widely and closely spaced stiffening.

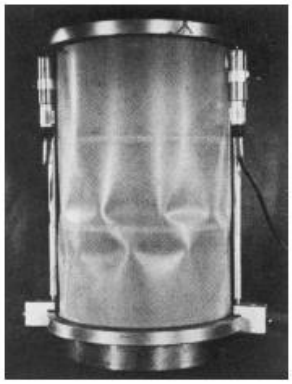

Figure 2-12: Local shell instability of an axially compressed cylindrical shell with widely spaced rings

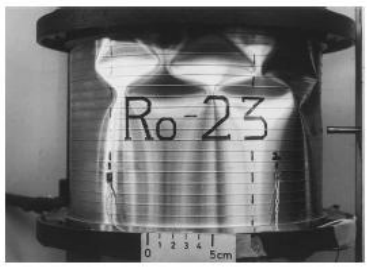

Figure 2-13: General instability of a closely spaced, ring-stiffened 7075-T6 aluminium alloy cylindrical shell subjected to axial compression

2.5 SUMMARY AND CONCLUSIONS

Buckling of thin shells is a matter that has employed many researchers and scientists in the past, as it was obvious in this chapter. The first serious attempt for the estimation of the capacity of such structures carried out at the beginning of the 20th century with the establishment of the, so-called, classical buckling elastic theory. During the next years, many proposals for more precise analytical calculations took place by many researchers, either by means of experimental tests or, more recently, through advanced numerical analyses. Some of these experiments and numerical analyses were presented throughout this chapter. In the context of this thesis, the presented experimental results regarded unstiffened and stiffened shell structures under external pressure or axial compression. In the section of numerical procedures, the matter of initial imperfections was discussed, as well as numerical obtained results for thin shells under wind pressure and other load cases were presented. All the above results contributed to the creation of analytical calculations, which are used in the related design codes.

Nowadays, the prevalent way of thinking is the reduction of the classical elastic buckling stress by appropriate factors. These factors take into account the geometric imperfections induced by the fabrication process, as measured in the laboratory using several cases of structures in several scales. The reduction factors also regard the plasticity of the used material and the realistic loading of wind pressure. Such approach is considered sufficient nowadays and is adopted in the modern codes for the design against the buckling of thin shells.

3 MODEL DESCRIPTION AND ANALYTICAL CALCULATIONS

3.1 INTRODUCTION

In this chapter, the thesis chimney structure is described. In section 1.2.1, it was stated that the thesis chimney is a typical steel chimney serving a HRSG (boiler) at a combined cycle power plant and is based on a CICIND project model [3]. The assumed geometric, material and loading characteristics are described thoroughly in this chapter. Moreover, a simplified analytical approach is described, which intents to present a general view of the capacity evaluation. This process though could not be adopted by engineers as a thorough calculation of strength. In the context of such a process the values of analytical load factors are calculated, through linear and nonlinear results. It is noted that the beam theory assumption is incorporated in the analytical equations (the internal forces are considered at the structure bottom). The analytical results will be later in the next chapter compared with the respective numerical results.

3.2 DESCRIPTION OF THE CHIMNEY STRUCTURE MODEL

3.2.1 GEOMETRY

The thesis chimney model is defined by the following geometric characteristics: the external diameter, which is 7m, the total height of 60m and the thickness of 0.013m. Although an actual chimney would be expected to have a varying shell thickness, in this work a constant thickness is assumed, since initially it is not known the area of collapse [3]. The shell nominal thickness is equal to 16mm, while a shell thickness of 13mm is finally used in calculations, allowing for 3mm for corrosion. In that way, the middle value of cylinder diameter used in the calculations is equal to: 7m-0.013m=6.987m. Additionally, the level of the breeching bottom lies at +4.00m, the breeching height is 22m and the breeching width is at 120 degrees. The chimney's equipment includes: three full perimetric platforms at levels +30.00m, +50.00m and +55.00m, one damper, whose axis lies at level +35.00m, a silencer, whose bottom level is at +35.00m and an inlet duct at the breeching at the chimney bottom. It is noted that in the context of this thesis, breeching is not opened at the structure base and hence the inlet duct is not included in the model's equipment.

The model is stiffened by circumferential stiffeners (rings). The geometric type of the stiffeners is L120/120/10. That means that the stiffeners' geometry is similar to the shape of "L" and the width of the two edges is 120mm. The thickness of both edges is 10mm. Despite the fact that in real structures the stiffeners may not be arranged at constant intervals, in the thesis model a constant spacing of 5m is adopted along the 60m height of the model. The afore-stated geometric characteristics are depicted in Figure 3-1.

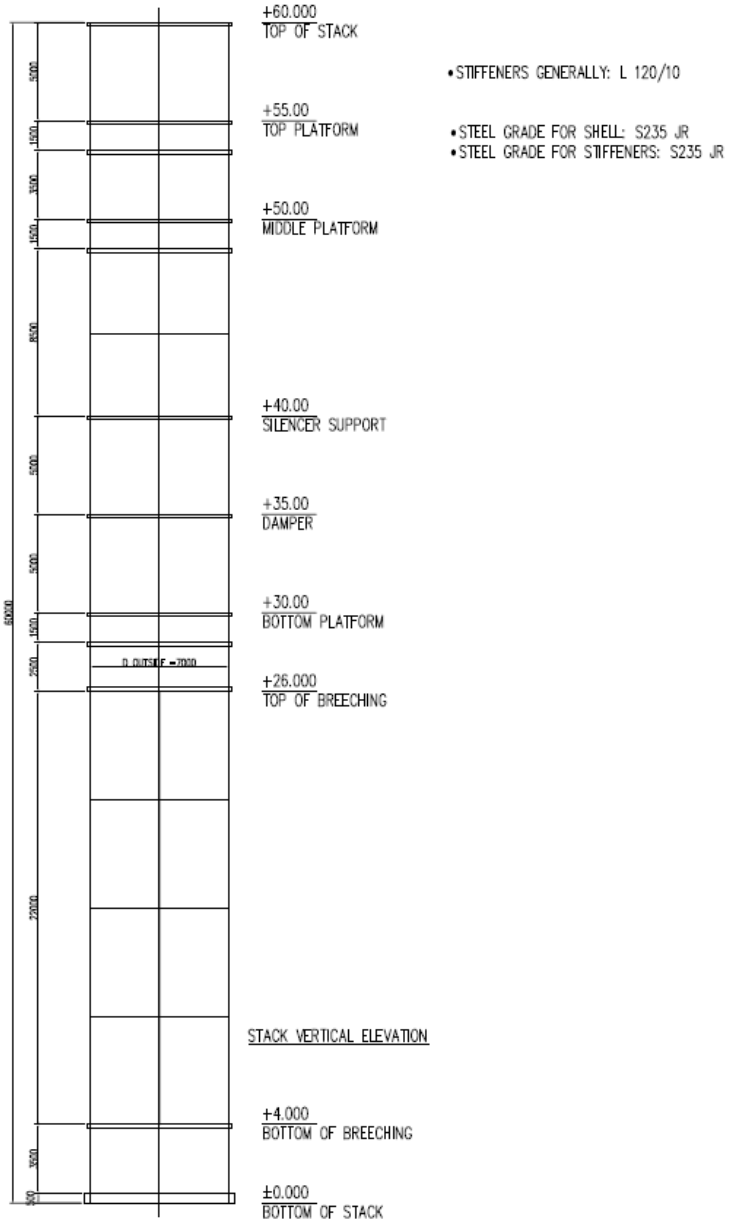

Figure 3-1: General chimney's model

3.2.2 MATERIALS

The applied material of the chimney model is steel and the assumed steel grade is S235 JR, according to the material properties presented in EN 13084-7 [51]. The same material defines both the structure shell and the stiffener shell. However, since an operating temperature of 200 deg C is assumed, the following reduced mechanical properties for S235, as defined in EN 13084-7 [51], are considered: yield stress f_y=160 MPa and elasticity module E=2.025×10^8kN/m^2. Additionally, the Poisson's ratio is equal to 0.3.

3.2.3 APPLIED LOADS

For the purposes of the present work, only vertical loads and wind loads are considered. The vertical loads represent the actual dead loads expected to be present in such a chimney, while the wind loads are calculated according to the European code using assumed wind velocity and terrain category. Hence, the applied loads are separated as following:

3.2.3.1 VERTICAL LOADS

The applied vertical loads of the model refer to the weights of the chimney equipment. As stated earlier, the equipment includes three platforms, one damper and one silencer. Moreover, the structure shell weight and the stiffener weight are calculated.

- Shell weight:

  (7.00-0.013)m×π×0.013m×60m×78.50kN/m^3=1344kN

- Stiffener weight:

  (L120/10: 18.2kg/m, e=33.1mm): [7.00m+2.0×(0.12-0.0331)m]×π×18.2kg/m=410.2kg

- Stiffeners (at 5m intervals): 12×410.2kg=4922.4kg or 49.2kN (assuming 5m intervals along the 60m height of the model, it results approximately 12 stiffeners on the chimney)
- Platforms: 3×7t=210kN
- Damper: 110kN
- Silencer: 150kN

3.2.3.2 WIND LOADS

For the wind loads the methodology described in EN 1991 Part 1-4 [5] is used. Hereunder, the assumptions of the equivalent static method proposed by the EN 1991 Part 1-4 are described. Initially, the basic wind velocity V_b is calculated using Eq. (3-1).

$$v_b = c_{dir} \cdot c_{season} \cdot v_{b,0} \quad (3\text{-}1)$$

where:

v_b is the basic wind velocity, calculated as 30m/s

c_{dir} is the directional factor. The recommended value is 1.0

c_{season} is the season factor. The recommended value is 1.0

$v_{b,0}$ is the fundamental value of the basic wind velocity given in the National Annex. The project assumed value is 30m/s

Subsequently, the mean wind velocity $v_m(z)$ at a height z above the terrain is calculated in Eq. (3-2). The mean wind velocity depends on the terrain roughness and orography and the basic wind velocity v_b. According to Eq. (3-2), $c_r(z)$ is the roughness factor, which is calculated in Eq. (3-3), c_0 is the orography factor, which is taken as 1.0 (EN 1991 Part 1-4), while v_b is the above calculated basic wind velocity. The terrain category is assumed as the second one (Terrain category 2, EN 1991 Part 1-4) (Table 3-1).

Table 3-1: Terrain categories and terrain parameters

Terrain category		z_0 (m)	z_{min} (m)
0	Sea or coastal area exposed to the open sea	0.003	1
I	Lakes or flat and horizontal area with negligible vegetation and without obstacles	0.01	1
II	Area with low vegetation such as grass and isolated obstacles (trees, buildings) with separations of at least 20 obstacle heights	0.05	2
III	Area with regular cover of vegetation or buildings or with isolated obstacles with separations of maximum 20 obstacle heights (such as villages, suburban terrain, permanent forest)	0.3	5
IV	Area in which at least 15 % of the surface is covered with buildings and their average height exceeds 15 m	1.0	10

$$v_m = c_r \cdot c_0 \cdot v_b \tag{3-2}$$

$$c_r = k_r \cdot \ln\left(\frac{z}{z_0}\right) \tag{3-3}$$

where:

k_r is the terrain factor depending on the roughness length z_0. It results 0.19 from Eq. (3-4)

z is the height above ground level (m)

z_0 is the roughness length and equals to 0.05m (Table 3-1)

c_0 The recommended value is 1.0

$$k_r = 0.19 \cdot \left(\frac{z_0}{z_{0,II}}\right)^{0.07} \tag{3-4}$$

where:

$z_{0,II}$ equals to 0.05m (Table 3-1)

The above process targets at the calculation of the external wind induced force F_w, determined by the following general procedure described in EN 1991 Part 1-4 and given by the Eq. (3-5).

$$F_w = c_s c_d \cdot c_f \cdot q_p \cdot A_{ref} \tag{3-5}$$

where:

$c_s c_d$ is the structural factor. The recommended value is 1.1 (EN 1993 Part 1-4, Annex D)

c_f is the force coefficient for the structure given in Eq. (3-6)

q_p is the peak velocity pressure calculated in Eq. (3-10)

A_{ref} is the reference area of the structure. Regarding the steel cylinders, A_{ref} is equal to the total diameter $b=d_{tot}$ of the cylinder (Figure 3-2). The value of d_{tot} (including the eventual external insulation) is equal to 7.20m

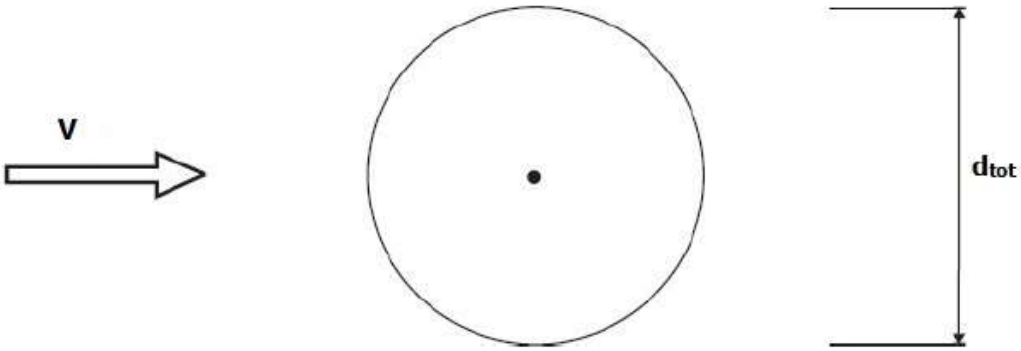

Figure 3-2: Depth of the steel members to be used for A_{ref}

$$c_f = c_{f,0} \cdot \psi_\lambda \tag{3-6}$$

where:

$c_{f,0}$ is the force coefficient without free-end flow calculated in Eq. (3-7)

ψ_λ is the end-effect factor. The project recommended value is 0.675 (EN 1991 Part 1-4)

$$c_{f,0} = 1.2 + 0.18 \cdot \frac{\log(10 \cdot k/b)}{1 + 0.4 \cdot \log(Re/10^6)} \tag{3-7}$$

where:

k is the equivalent surface roughness. It is equal to 0.2mm (Table 3-2)

b is the diameter of the cross section. The value is 7.00m

Re is the Reynolds number as defined by Eq. (3-8)

Table 3-2: Equivalent surface roughness k

Type of surface	Equivalent roughness k (mm)	Type of surface	Equivalent roughness k (mm)
glass	0.0015	smooth concrete	0.2
polished metal	0.002	planed wood	0.5
fine paint	0.006	rough concrete	1.0
spray paint	0.02	rough sawn wood	2.0
bright steel	0.05	rust	2.0
cast iron	0.2	brickwork	3.0
galvanized steel	0.2		

$$Re = \frac{b \cdot v(z_e)}{v} \tag{3-8}$$

where:

b is the diameter of the cross section. The value is 7.00m

$v(z_e)$ is the peak wind velocity at height z_e. It is defined by Eq. (3-9)

v is the kinematic viscosity of the air ($\nu=15\cdot10^{-6}m^2/s$)

$$v(z_e)=\sqrt{\frac{2\cdot q_p}{\rho}} \tag{3-9}$$

where:

q_p is the peak velocity pressure calculated in Eq. (3-10)

ρ is the air density, which depends on the altitude, temperature and barometric pressure. The recommended value is $1.25kg/m^3$

The peak velocity pressure is defined by Eq. (3-10).

$$q_p=\left[1+7\cdot I_v(z)\right]\cdot\frac{1}{2}\cdot\rho\cdot v_m^2(z) \tag{3-10}$$

where:

$I_v(z)$ is the turbulence intensity defined in Eq. (3-11)

ρ is the air density, which depends on the altitude, temperature and barometric pressure. The recommended value is $1.25kg/m^3$

$v_m(z)$ is the mean wind velocity at a height z above the terrain, as described in Eq. (3-2)

Following, the turbulence intensity is defined:

$$I_v(z)=\frac{k_I}{c_0\cdot\ln\left(\frac{z}{z_0}\right)} \tag{3-11}$$

Through the previous process, the wind force distribution for different values of height z is calculated, as shown in Table 3-3. It is noted that the value changes at intervals of 5m (EN 1991 Part 1-4).

Table 3-3: Wind force distribution

z	$\ln(z/z_0)$	$c_r(z)$	$v_m(z)$	I_v	$q_p(z)$	diameter	Re	c_{f0}	c_f	Width	q_w	F_w
0			m/s		kN/m^2	m				m	kN/m^2	kN/m
0.2	3.689	0.701	21.0	0.271	0.80	7.20	1.718E+07	0.772	0.521	7.200	0.459	3.30
5	4.605	0.875	26.2	0.217	1.09	7.20	2.000E+07	0.779	0.526	7.200	0.628	4.52
10	5.298	1.007	30.2	0.189	1.32	7.20	2.209E+07	0.784	0.529	7.200	0.770	5.54
15	5.704	1.084	32.5	0.175	1.47	7.20	2.329E+07	0.786	0.531	7.200	0.859	6.18
20	5.991	1.138	34.2	0.167	1.58	7.20	2.414E+07	0.788	0.532	7.200	0.925	6.66
25	6.215	1.181	35.4	0.161	1.67	7.20	2.479E+07	0.789	0.533	7.200	0.977	7.03
30	6.397	1.215	36.5	0.156	1.74	7.20	2.533E+07	0.790	0.533	7.200	1.021	7.35
35	6.551	1.245	37.3	0.153	1.80	7.20	2.578E+07	0.791	0.534	7.200	1.059	7.62
40	6.685	1.270	38.1	0.150	1.86	7.20	2.617E+07	0.792	0.534	7.200	1.092	7.86
45	6.802	1.292	38.8	0.147	1.91	7.20	2.651E+07	0.792	0.535	7.200	1.121	8.07
50	6.908	1.312	39.4	0.145	1.95	7.20	2.682E+07	0.793	0.535	7.200	1.148	8.27
55	7.003	1.331	39.9	0.143	1.99	7.20	2.709E+07	0.793	0.535	7.200	1.173	8.44
60	7.090	1.347	40.4	0.141	2.03	7.20	2.735E+07	0.794	0.536	7.200	1.195	8.61

3.3 ANALYTICAL APPROACH

In this section, an analytical approach to the buckling problem of the thin-shell unstiffened model takes place. A simplified method is presented, where assumptions concerning the model, the loading and the calculation of the total stress take place. The analytical results will be later in chapter 4

compared with the numerical ones. It is noted, that safety factors do not multiply the analytical stresses, so as the results of both approaches to be directly comparable.

3.3.1 SIMPLIFIED ANALYSIS

Hereunder, the maximum stress appearing in the model is calculated by making use of a simplified approach. According to the simplified method, the chimney model is regarded as a 2-Dimensional beam. Hence, the simplified loading is the wind forces calculated in Table 3-3. Based on the beam theory consideration, the maximum normal stresses appear at the bottom of the support and are calculated for this location. In Figure 3-3, the simplified model and the corresponding loading are illustrated.

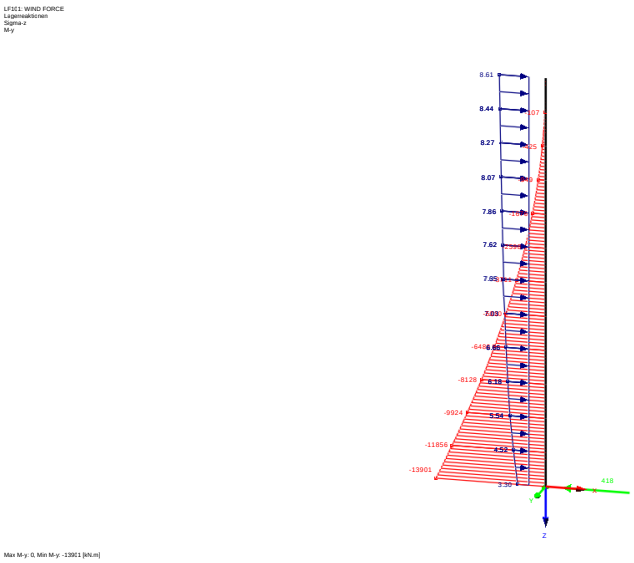

Figure 3-3: Simplified chimney model and the simplified wind force distribution

The mechanical properties of the chimney model are the following:

- Cross section area: A=0.285m^2
- Section elastic modulus: W=0.497m^3

The normal stress σ_N at the chimney bottom is defined by Eq. (3-12).

$$\sigma_N = \frac{N}{A} \tag{3-12}$$

where:

σ_N is equal to 6.5MPa

N is the total axial force. It is equal to 1863kN. It results from the sum of vertical forces according to section 3.2.3.1

The bottom bending moment due to the wind loads, according to section 3.2.3.2, is equal to M=13900kNm. Hence, the bending stress σ_B is defined by Eq. (3-13).

$$\sigma_B = \frac{M}{W} \tag{3-13}$$

where:

σ_B is equal to 27.9MPa

Hence, the total stress at the bottom of the chimney model is calculated in Eq. (3-14) and is equal to σ_{tot}=34.4MPa.

$$\sigma_{tot} = \sigma_N + \sigma_B \quad (3\text{-}14)$$

It is pointed out that the assumption of the 2-Dimensional model is quite simplified and induces errors to the analytical approach. In section 4.6, where the comparison between the analytical and numerical results will be presented, a more realistic analytical approach is assumed. Hence, the internal forces N, M and the total stress at the structure base in chapter 4 differentiate from the calculated in this chapter. However, since the aim of the present work is the investigation of the buckling strength, these differences do not influence to a significant extent the results, but are being noted for completeness.

3.3.2 EVALUATION OF ANALYTICAL CAPACITY

Hereunder, the analytical structure capacity is calculated for the unstiffened model. The analytical calculations are presented by means of linear and nonlinear results. Through the linear results, the buckling load factor is calculated based on the classical elastic buckling theory. On the other hand, according to the nonlinear results the collapse load factor is found, based on CICIND provisions.

3.3.2.1 BUCKLING LOAD FACTOR

Initially, the buckling load factor is found. The classical elastic buckling theory, which has been addressed at the beginning of the 20th century by Lorenz, Southwell and Timoshenko [26], is used. According to this, conditions of elasticity and linearity take place and no initial imperfections are taken into account. Additionally, the classical buckling theory assumes a model subjected to axial compression. Hence, as critical buckling stress is regarded the classical elastic buckling stress and is defined by Eq. (3-15).

$$\sigma_{cl} = k \cdot E \cdot \frac{t}{r} \quad (3\text{-}15)$$

where:

σ_{cl} is the classical elastic buckling stress. The calculated value is 455.89MPa

k for the case of circular cylinders it is defined as 0.605

E is the elasticity module. The thesis value is 2.025×10^8kN/m^2

t is the thickness of the cylinder. Its value is equal to 0.013m (reduced thickness due to corrosion)

r is the radius of the cylinder. Its value is equal to 3.493m (middle radius)

Eventually, the corresponding buckling load factor is defined by Eq. (3-16) and is equal to λ=13.25.

$$\lambda = \frac{\sigma_{cl}}{\sigma_{tot}} \quad (3\text{-}16)$$

where:

σ_{tot} is the final total stress. The adopted value, as described in section 3.3.1, is 34.4MPa

3.3.2.2 COLLAPSE LOAD FACTOR BY CICIND

CICIND's critical buckling stress σ_κ is defined by Eq. (3-17). It is observed that the σ_κ is a reduced value of the yield stress by a factor. In this way the material nonlinearity is taken into account. Additionally, the factor takes into account the geometrical nonlinearity through another factor, the factor alpha (α). The latter provides allowance for the weighted contribution of both axial and bending compressive stresses and reduces the classical elastic buckling stress. Initial imperfections are considered as well. The latter are based on the first buckling mode. Additionally, according to this approach the investigated model is subjected to wind loads.

$$\sigma_\kappa = \left[1 - 0.412 \cdot \left(\lambda^*\right)^{1.2}\right] \cdot f_y \tag{3-17}$$

where:

σ_κ is the CICIND failure stress. It is equal to 107MPa

λ^* is calculated in Eq. (3-18)

f_y is the yield stress. The thesis value is 160MPa

$$\lambda^* = \sqrt{\frac{f_y}{\alpha \times \sigma_{cl}}} \tag{3-18}$$

where:

λ^* results 0.834

σ_{cl} is the classical elastic buckling stress. The calculated value has been found 455.89MPa by Eq. (3-15)

α is calculated in Eq. (3-19)

$$\alpha = \frac{\alpha_N \cdot \sigma_N + \alpha_B \cdot \sigma_B}{\sigma_N + \sigma_B} \tag{3-19}$$

where:

α results 0.504

α_N is calculated in Eq. (3-20), where r=3.49m the radius and t=0.013m the thickness. The calculated value is 0.419

σ_N is the normal stress. It has been found 7.76 in Eq. (3-12)

α_B is calculated in Eq. (3-21). It is equal to 0.529

σ_B is the bending stress. It has been found 27.9MPa in Eq. (3-13)

$$\alpha_N = \frac{0.7}{\sqrt{0.1 + r/100t}} \tag{3-20}$$

$$\alpha_B = 0.189 + 0.811 \cdot \alpha_N \tag{3-21}$$

The corresponding analytical collapse load factor λ by CICIND results then from Eq. (3-22) λ=3.11.

$$\lambda = \frac{\sigma_K}{\sigma_{tot}} \tag{3-22}$$

3.4 SUMMARY AND CONCLUSIONS

In this chapter, the geometrical characteristics, the materials used and the applied loads were described in detail. Especially, the evaluation of the wind loads was presented thoroughly. Moreover, analytical calculations related to the structure's capacity were presented. Initially, the buckling load factor was calculated by making use of the maximum stress obtained with simplified beam theory analysis and of the buckling stress referring to axial compression. Afterwards, the collapse load factor was evaluated by using again the maximum stress found with beam theory and the collapse stress proposed by CICIND.

4 NUMERICAL RESULTS FOR THE UNSTIFFENED AND STIFFENED MODEL

4.1 INTRODUCTION

In the present chapter, the buckling problem is approached through the second option presented in chapter 2, that of numerical procedure. Hence, initially a description of the numerical model is made, together with the assumptions made as far as the applied loading, the geometrical characteristics and the materials are concerned. In this chapter, the applied numerical analyses are also presented, the results of which will subsequently be compared with the relevant analytical calculations of chapter 3. The numerical analyses are applied for two different structures, the unstiffened and the stiffened one, while the comparison of the two structures will provide information about the impact of stiffeners on the structure's capacity. It is important to note that despite the fact that the realistic model, as described in chapter 3, is stiffened, the unstiffened model is examined as well, as it is also regarded a realistic chimney structure and may lead to useful conclusions.

4.2 DESCRIPTION OF THE NUMERICAL CHIMNEY STRUCTURE

4.2.1 APPLIED SOFTWARE

For the numerical model the finite element software ADINA is used. ADINA has been used in the past by many researchers for calculating the response of many types of structures, including shells [3]. For the chimney model, 4-noded shell elements were used, as it is about a surface problem, taking into account that the thickness of the shell is much smaller than its other two dimensions. The applied size of the meshing emerged after performing a mesh sensitivity investigation, as it will afterwards be explained more extensively. The length of each finite element is selected to be equal to 0.07m. The mesh-size is kept constant in the whole structure, considering that in tall shell structures subjected to wind-loading the region of failure is not known in prior.

4.2.2 GEOMETRY

The geometrical characteristics remain the same as the ones described in the analytical model, in section 3.2.1. Hence, the representative chimney has a diameter equal to 6.987m and a radius equal

to 3.49m. It is noted that this leads to a slightly smaller surface on which the wind pressure is applied, compared with the external diameter of 7m of the realistic structure. This differentiation is not expected to have a significant effect on the results. The height of the numerical model is 60m and the nominal thickness is 16mm, but due to corrosion it is reduced to 13mm, which is finally used. Only the shell and stiffeners are modeled. In the context of the present thesis, two structures are investigated, the unstiffened and the stiffened one, for which the same analyses are carried out. Both in the unstiffened and stiffened model, the same geometric characteristics of the shell structure are used. Moreover, in the stiffened one, a constant stiffeners' spacing of 5m is used. The stiffeners that are selected are circumferential and have an L120x120x10 cross-section.

The support is considered at the bottom of the chimney and is modeled by making use of rigid links, as shown in Figure 4-1. At this point all degrees of freedom are restricted and the support behaves as a fixed one. It should also be noted that rigid links are used at the top plane of the chimney model, as shown in Figure 4-2, because it is considered that at this location a relatively rigid ring exists. This ring leads to a rigid diaphragm and the cross-sectional shape of the cross-section at the top remains circular at at all stages of analyses. Translational degrees of freedom are restricted in this plane.

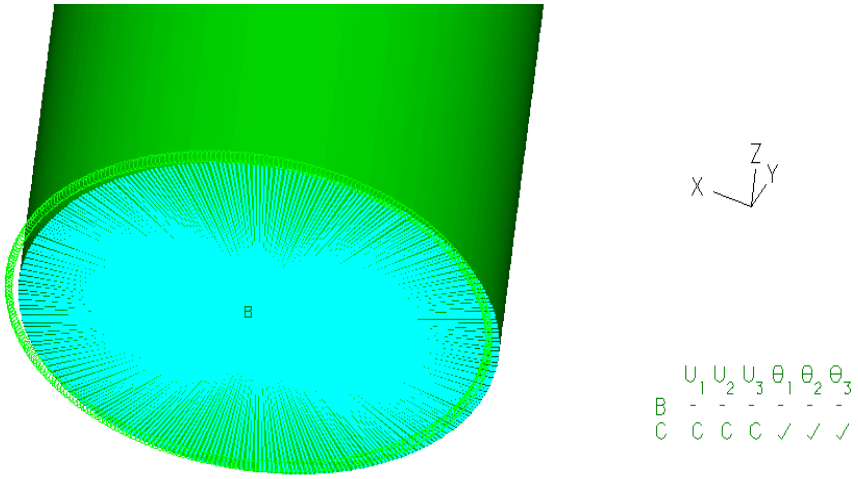

Figure 4-1: Full fixity at the center bottom point

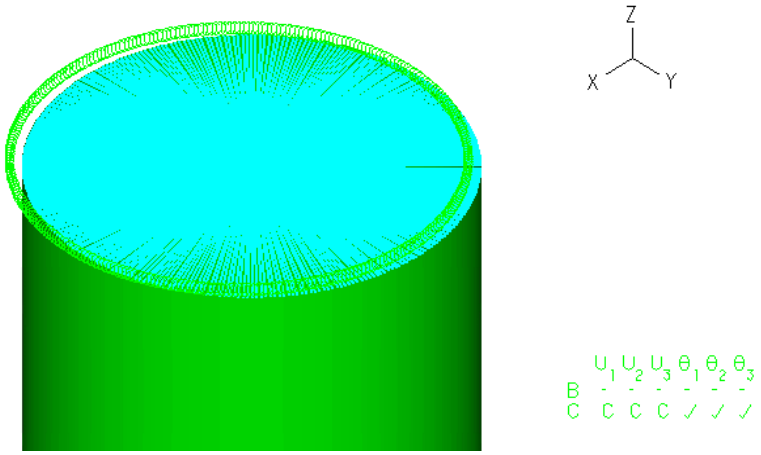

Figure 4-2: Rigid link at the top of the structure

4.2.3 MATERIALS

As presented in section 3.2.2, where the analytical simplified model was described, European material grades and European code material properties have been used throughout this work, for consistency

purposes. Hence, the material used in the numerical model is also steel S235 JR. Similarly to the analytical model, due to the assumed operating temperature of 200 deg C, the same reduced mechanical properties for S235 (EN 13084 Part 7 [51]) emerge:

- f_y=160MPa (Yield stress)
- E=2.025×10^8kN/m^2=202.5GPa (Elasticity module)
- v=0.3 (Poisson's ratio)

It is noted that elastoplastic material with yield stress equal to 160000kN/m^2 is used in the shell structure when materially nonlinear analyses take place, while when elastic analyses are carried out elastic steel is assumed (for the relevant analyses see section 4.2.5). As far as the stiffeners are concerned, the used material is, in any case, the same as the one used for the shell of the structure.

4.2.4 APPLIED LOADS

The applied loads of the chimney model were described in section 3.2.3. The same loads are used in the numerical model, as well. Hence, in every model case (the unstiffened and stiffened structure), the same loads (vertical and horizontal) are applied. Vertical loads refer to the weights of the chimney equipment, while the horizontal ones to the wind pressure, which result from the wind forces, as calculated in section 3.2.3.2. The final values of the applied loads are presented hereunder once again for completeness.

4.2.4.1 VERTICAL LOADS

First of all, the weight of the shell structure and of the stiffening rings is directly taken into account by the finite element software. Therefore, any additional considerations for their self-weight are not required. On the other hand, the additional equipment that exists on the structure is accounted for by appropriately applying uniformly distributed loads. The total weights of the main components are summarized as:

- Platforms: 3 full perimetric platforms at levels +30.00, +50.00, +55.00 with 7.0 tons weight each one.
- Damper: Damper axis at +35.00, Damper weight: 11.00 tons.
- Silencer: Silencer bottom level at +40.00, Silencer weight: 15.00 tons.

4.2.4.2 WIND LOADS

For the wind loads modeling, the methodology described in EN 1991 Part 1-4 [5] is used, as it was presented thoroughly in section 3.2.3.2. Moreover, the wind pressure is distributed around the circumference according to EN 1991, as shown in Figure 4-3, and its values are calculated according to the formula described in Eq. (4-1).

$$w_e = q_p(z_e) \cdot c_{pe} \tag{4-1}$$

where:

q_p is the peak velocity pressure calculated in Eq. (3-10)

c_{pe} is the wind pressure coefficient, calculated at specific angles in Eqs. (4-2), (4-3), (4-4), (4-5), (4-6)

The angles, for which the value of wind pressure is calculated, are indicated in Figure 4-3. The relevant values of c_{pe} are calculated in Eqs. (4-2), (4-3), (4-4), (4-5), (4-6) and shown in Table 4-1 for every level of height z, as well.

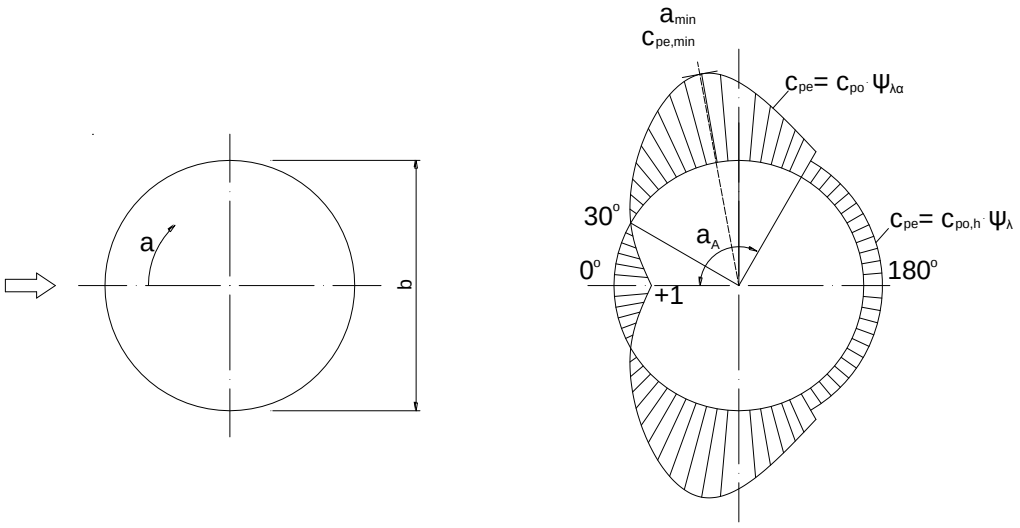

Figure 4-3: Wind pressure distribution in a plan view

$c_{pe} = 1$, for α=0° (4-2)

$c_{pe} = 0$, for α=30° (4-3)

$c_{pe} = c_{p0,min} \cdot \psi_{\lambda,min}$, for $\alpha=\alpha_{min}=75^{o}$ (4-4)

where:

$c_{p0,min}$ is the value of the minimum pressure coefficient (°)

$\psi_{\lambda,min}$ is the value of the minimum end-effect factor. The recommended value is 1

$c_{pe} = c_{p0} \cdot \psi_{\lambda\alpha}$, for $\alpha=\alpha_A=105^{o}$. The calculated value is -0.74 (4-5)

$c_{pe} = c_{p0,h} \cdot \psi_{\lambda}$, for $\alpha_A<\alpha<255^{o}$ (4-6)

where:

c_{p0} is a pressure coefficient (°)

$c_{p0,h}$ is the base pressure coefficient (°)

ψ_{λ}, $\psi_{\lambda\alpha}$ are the end-effect factors. The recommended value is 0.675

The corresponding pressure coefficients and the resulting wind pressure, per m height of the stack, are shown in Table 4-1. Hence, the final values of wind pressure, used in the numerical model, for the different angles of the plan view and the different levels of height (5m intervals), are presented in Table 4-2.

Table 4-1: Wind pressure distribution

												$c_{pe} = c_{p0}\,\psi_\lambda$			$w_e = q_p(z_e)\,c_{pe}$		
z	$\ln(z/z_0)$	$c_r(z)$	$v_m(z)$	I_v	$q_p(z)$	diameter	Re	α_{min}	$c_{p0,min}$	α_A	$c_{p0,h}$	α=0°	α_{min}	α_A	α=0°	α_{min}	α_A
0			m/s		kN/m^2	m											
0.2	3.689	0.701	21.0	0.271	0.80	7.00	1.670E+07	75	-1.5	105	-0.8	1.0	-1.5	-0.74	0.80	-1.20	-0.59
5	4.605	0.875	26.2	0.217	1.09	7.00	1.945E+07	75	-1.5	105	-0.8	1.0	-1.5	-0.74	1.09	-1.63	-0.80
10	5.298	1.007	30.2	0.189	1.32	7.00	2.147E+07	75	-1.5	105	-0.8	1.0	-1.5	-0.74	1.32	-1.98	-0.98
15	5.704	1.084	32.5	0.175	1.47	7.00	2.264E+07	75	-1.5	105	-0.8	1.0	-1.5	-0.74	1.47	-2.21	-1.09
20	5.991	1.138	34.2	0.167	1.58	7.00	2.347E+07	75	-1.5	105	-0.8	1.0	-1.5	-0.74	1.58	-2.37	-1.17
25	6.215	1.181	35.4	0.161	1.67	7.00	2.411E+07	75	-1.5	105	-0.8	1.0	-1.5	-0.74	1.67	-2.50	-1.23
30	6.397	1.215	36.5	0.156	1.74	7.00	2.462E+07	75	-1.5	105	-0.8	1.0	-1.5	-0.74	1.74	-2.61	-1.29
35	6.551	1.245	37.3	0.153	1.80	7.00	2.506E+07	75	-1.5	105	-0.8	1.0	-1.5	-0.74	1.80	-2.70	-1.33
40	6.685	1.270	38.1	0.150	1.86	7.00	2.544E+07	75	-1.5	105	-0.8	1.0	-1.5	-0.74	1.86	-2.79	-1.37
45	6.802	1.292	38.8	0.147	1.91	7.00	2.577E+07	75	-1.5	105	-0.8	1.0	-1.5	-0.74	1.91	-2.86	-1.41
50	6.908	1.312	39.4	0.145	1.95	7.00	2.607E+07	75	-1.5	105	-0.8	1.0	-1.5	-0.74	1.95	-2.93	-1.44
55	7.003	1.331	39.9	0.143	1.99	7.00	2.634E+07	75	-1.5	105	-0.8	1.0	-1.5	-0.74	1.99	-2.99	-1.47
60	7.090	1.347	40.4	0.141	2.03	7.00	2.659E+07	75	-1.5	105	-0.8	1.0	-1.5	-0.74	2.03	-3.04	-1.50

Table 4-2: Wind pressure distribution coefficients used in the numerical model

Levels of height (m)	**Wind pressure at specific angles:**			
	0	**a_{min}**	**a_A**	**180°**
0-0.2	0.8	-1.2	-0.592	-0.432
0.2-5	1.09	-1.635	-0.8066	-0.5886
5-10	1.32	-1.98	-0.9768	-0.7128
10-15	1.47	-2.205	-1.0878	-0.7938
15-20	1.58	-2.37	-1.1692	-0.8532
20-25	1.67	-2.505	-1.2358	-0.9018
25-30	1.74	-2.61	-1.2876	-0.9396
30-35	1.8	-2.7	-1.332	-0.972
35-40	1.86	-2.79	-1.3764	-1.0044
40-45	1.91	-2.865	-1.4134	-1.0314
45-50	1.95	-2.925	-1.443	-1.053
50-55	1.99	-2.985	-1.4726	-1.0746
55-60	2.03	-3.045	-1.5022	-1.0962

For simplification, the variation of the wind distribution in plan is assumed to be linear, as shown in Figure 4-4. The wind pressure distribution (red color), as shown in the finite element software ADINA, is presented in Figure 4-5.

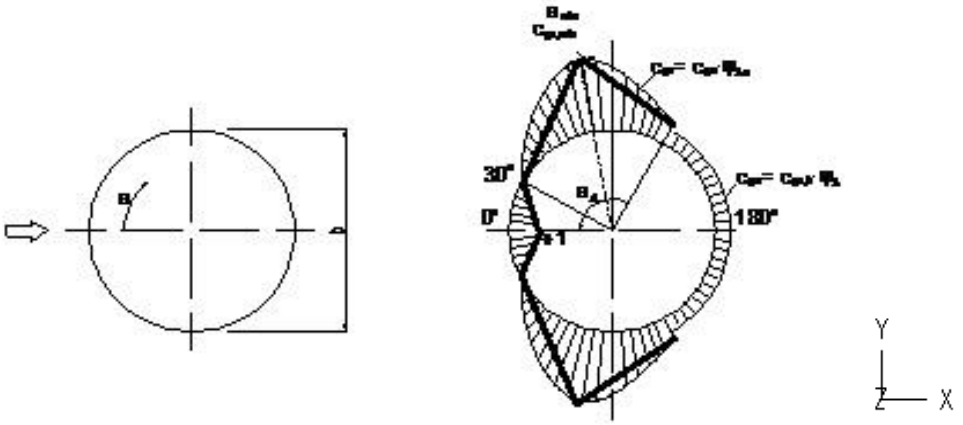

Figure 4-4: Simplification of wind pressure distribution in plan

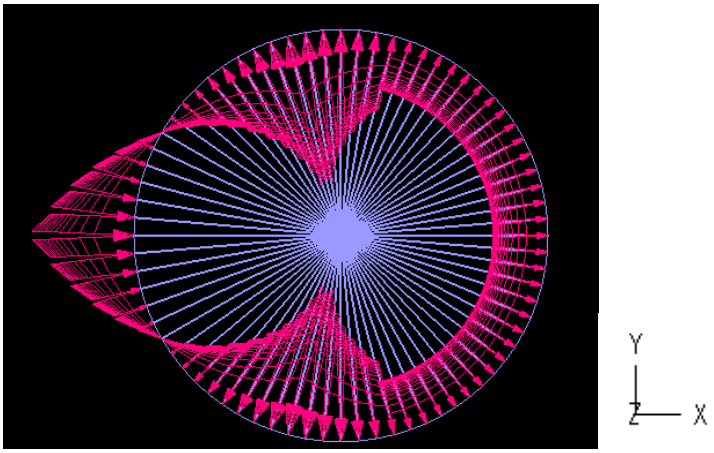

Figure 4-5: Wind pressure distribution as applied in ADINA

4.2.5 APPLIED ANALYSES AND RESULTS PRESENTATION

The types of analyses that are used in the present thesis can be separated into two basic categories: linear and nonlinear analyses. The linear analyses are based on two fundamental assumptions. The first one is related to elastic material and the second one to geometrical linearity, which means that the undeformed shape of the structure is used for the formation of the equilibrium conditions. In general, linear elastic analyses are used by engineers of practice for designing common structures. The linearity of the material's behavior and of the geometrical response is usually valid for stiff structures and/or small levels of loading [52].

A more accurate estimation of the structural response can be achieved by making use of nonlinear analyses, either materially or geometrically or both. These types of analyses are more complicated, require more computational effort and can be performed by a limited number of commercial software. Nonlinear types of analyses are basic for the research performed in this thesis and they represent the main type of analyses used. A thorough presentation of the possible types of analyses is made in the next sections by presenting the purposes they serve in our case.

4.2.5.1 LINEAR ELASTIC ANALYSIS

Linear Elastic Analysis is selected so as to extract information about the most stress-intensive areas of the model. It is a static (one step of loading), linear (geometrical linearity) and elastic (material linearity) analysis, where equilibrium equations are based on the undeformed structure. This type of analyses also serves, in our case, verification purposes.

4.2.5.2 LINEARIZED BUCKLING ANALYSIS (LBA)

In LBA the material is elastic and the equilibrium equations are based on the deformed shape of the structure. LBA results in the calculation of the buckling mode shapes and elastic buckling loads, which are an upper bound of the structure's strength.

4.2.5.3 GEOMETRICALLY NONLINEAR ANALYSIS (GNA)

In GNA the material is elastic and the equilibrium equations are based on the deformed shape of the structure, taking in this way into account the geometrical nonlinearity.

4.2.5.4 MATERIALLY NONLINEAR ANALYSIS (MNA)

In MNA the material is elastoplastic and the equilibrium equations are based on the undeformed shape of the structure. In this way only the material plastification leads to nonlinear response. The material plasticity is based on the flow rule of plasticity, which is a commonly scientifically acceptable way for modeling plastification of steel. In the cases presented herein, an elastic-perfectly plastic material is considered.

4.2.5.5 GEOMETRICALLY AND MATERIALLY NONLINEAR (IMPERFECTION) ANALYSIS (GMN(I)A)

In GMNA the material is elastoplastic and the equilibrium conditions are based on the deformed shape of the structure. In this way, both types of non-linearity are taken into account and this type of analysis is considered to be one of the most advanced and sophisticated tools in the hands of a civil engineer for the evaluation of the stiffness and capacity of the structure. Additionally, when initial imperfections are taken into account, they are based on the first buckling mode of the LBA, in the context of the present thesis.

4.2.5.6 SOFTWARE ASSUMPTIONS

As far as the LBA is concerned, the option "Large displacements" in the ADINA tab of "Control" is activated, so as the equilibrium equations to be formed based on the deformed shape of the structure. Additionally, in the tab of LBA "Parameter Options", the selected number of buckling modes is four (4) and the applied "Method of Generating Starting Vectors" is "Standard", instead of "Lanczos", as the first one describes better the classic concept of Linearized Buckling.

The type of nonlinear analyses applied in this project is collapse analyses, meaning that the arc-length method is used. In this way, it is possible to extract the declining part of the equilibrium path and, hence, the limit point emerges, which shows the strength of the structure. When a collapse analysis is used in this thesis, the following parameters are selected:

- The top central node is selected to indicate the prescribed displacement, along the X-Translation degree of freedom (X-Translation is the predominate direction of wind-loading).
- The initial displacement is 0.0001m, so as the analysis to begin.
- The maximum allowed displacement is 1m.
- The choice of "Continue after the critical point is reached" is also selected.

4.2.5.7 RESULTS PRESENTATION

The results are presented by using equilibrium paths as well as stress distributions and deformed shapes at characteristic locations along the equilibrium paths, as proposed by Gantes and Fragkopoulos (2010) [53]. At graphs of equilibrium paths, X-Coordinate indicates the horizontal displacement along X-Direction of the central point at the top of structure, while Y-Coordinate

indicates the load factor λ, which multiplies all the applied loads up to collapse. In this way, qualitative and quantitative conclusions can be drawn, which focus mainly on the pre-failure response, including the elastic stiffness and the ultimate strength of the structure. A similar procedure for the evaluation of the structural response of steel shells of wind turbines was used by Dimopoulos and Gantes (2012) [54].

It is pointed out that the load factor λ multiplies all the loads, both vertical and wind ones. In general, the dead loads do not vary so much as the wind loads and, therefore, using a common variation factor for both of them is a simplified assumption, but is not far from reality (the safety factor for the dead loads is 1.35 and for the live loads 1.50).

4.3 UNSTIFFENED STRUCTURE

In this section, the numerical results obtained with linear and nonlinear analyses, performed for the unstiffened structure, are presented. The geometric characteristics of the numerical unstiffened model have already been described in section 4.2.2. In Figure 4-6 the unstiffened model, as presented in ADINA, is shown.

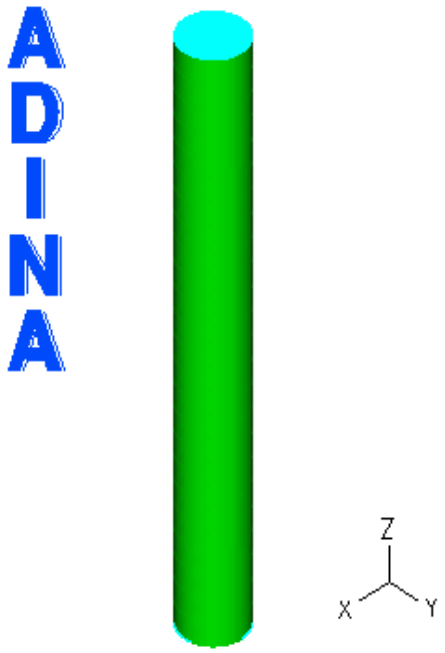

Figure 4-6: The unstiffened structure as modeled in ADINA

4.3.1 LINEARIZED BUCKLING ANALYSIS

The used material is elastic steel, as LBA is a materially linear approach. The used mesh density is 0.07m, as this resulted to be, after an investigation, the most accurate and computationally convenient. The investigation was necessary, as it is known that thin shell calculations are mesh size dependent and, even more, a finite element eigenvalue analysis is more sensitive to mesh size than it is in regular displacement analyses [55]. According to that, the LBA of unstiffened model was carried out for different sizes of mesh density (using length of finite elements): 0.15m, 0.10m, 0.07m, 0.04m. The smallest considered mesh size (0.04m) leads to very computationally demanding analyses and any further decrease is not possible. As it will be shown by the following numerical investigation, the mesh size of 0.07m is considered sufficient for the purposes of the present work. The buckling loads

of LBA for these different mesh densities were then compared, so as to make the decision about the final used mesh size of LBA of the unstiffeend model, according to the afore-mentioned criteria. In Table 4-3, the list of buckling loads (only for the first buckling mode), for the different mesh densities, is shown. As it is indicated, the convergence between the buckling loads of the two last mesh sizes is 1.3%, which is considered sufficient for the purposes of this project, and the mesh size of 0.07m is kept for the case of LBA of unstiffened model.

Table 4-3: Comparison of buckling loads between different mesh sizes of the unstiffened model

Mesh size (m)	Buckling load
0.15	13.17
0.10	12.57
0.07	12.3
0.04	12.14

4.3.1.1 NUMERICAL RESULTS BASED ON LBA

Looking at the first LBA buckling mode of the unstiffened model in Figure 4-7, it is observed that buckling occurs at the top of the structure and at a location that does not correspond to the more compressed side according to beam theory, as shown in Figure 4-8. It is also interesting to notice the expected almost symmetrical deformation, due to the respective symmetrical wind-loading. The initially unexpected fact is that this symmetrical deformation occurs along Y-Direction, while the predominant wind loading direction is along X-Direction. This observation shows that the assumptions of beam theory are insufficient for load cases where loading appears as pressure directly applied to shell structures, since it describes better 2-Dimensional problems. A buckling load factor (factor multiplying the loads) approximately equal to 12.3 is required for the first buckling mode to occur (Figure 4-7).

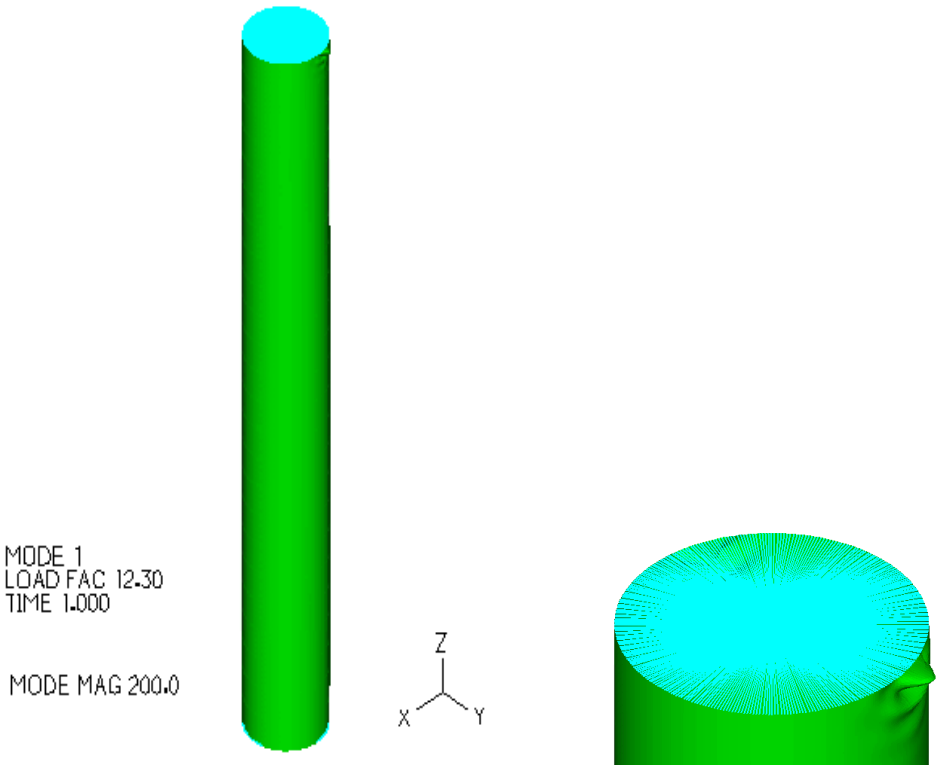

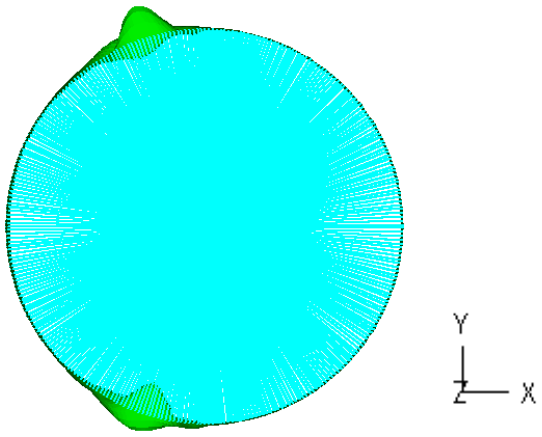

Figure 4-7: First buckling mode views and buckling load of the unstiffened structure

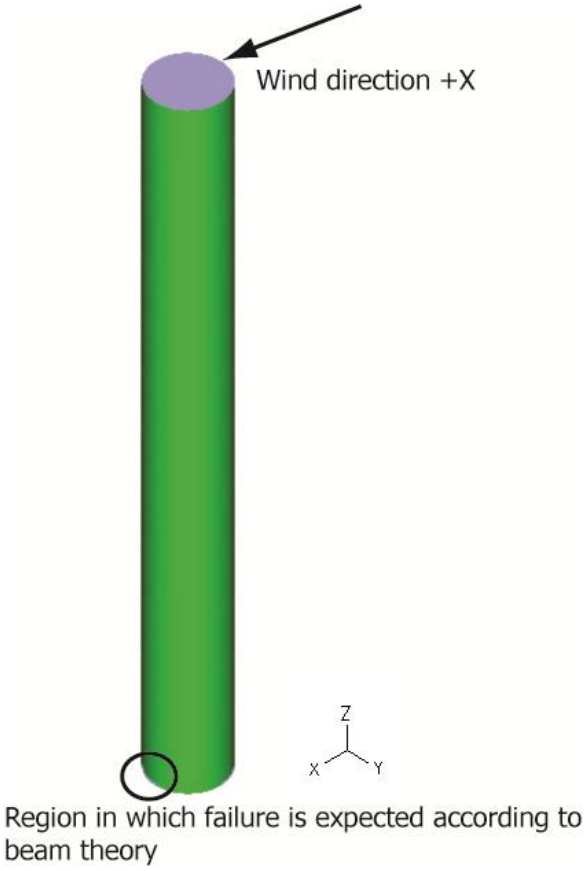

Figure 4-8: Wind direction and region in which failure is predicted based on beam theory

Even if we know, looking at real structures, that using rigid links at the top of the shell is closer to reality than leaving it free, for investigation reasons, the case without rigid links at the top is also analyzed by making use of Linearized Buckling Analysis. When the top of the shell is free, the buckling waves appear at the bottom of shell and the buckling load is equal to 6.3. Again, the buckling waves appear in Y-Direction and not in the, expected for beam theory, +X-Direction. Hence, two main conclusions can be extracted by this result, for our case. First of all, the use of a rigid stiffener at the top of the structure increases the buckling strength of the structure by two times. That is why, it is important to use such a ring. Secondly, it shows that LBA is based clearly on the maximum compressive stresses. Therefore, by the time a rigid ring is placed at the top, a concentration of stresses takes place and buckling occurs there (the rigid ring at the top is a restriction of

deformations). The comparison between the models without and with rigid links at the top is presented in Figure 4-9.

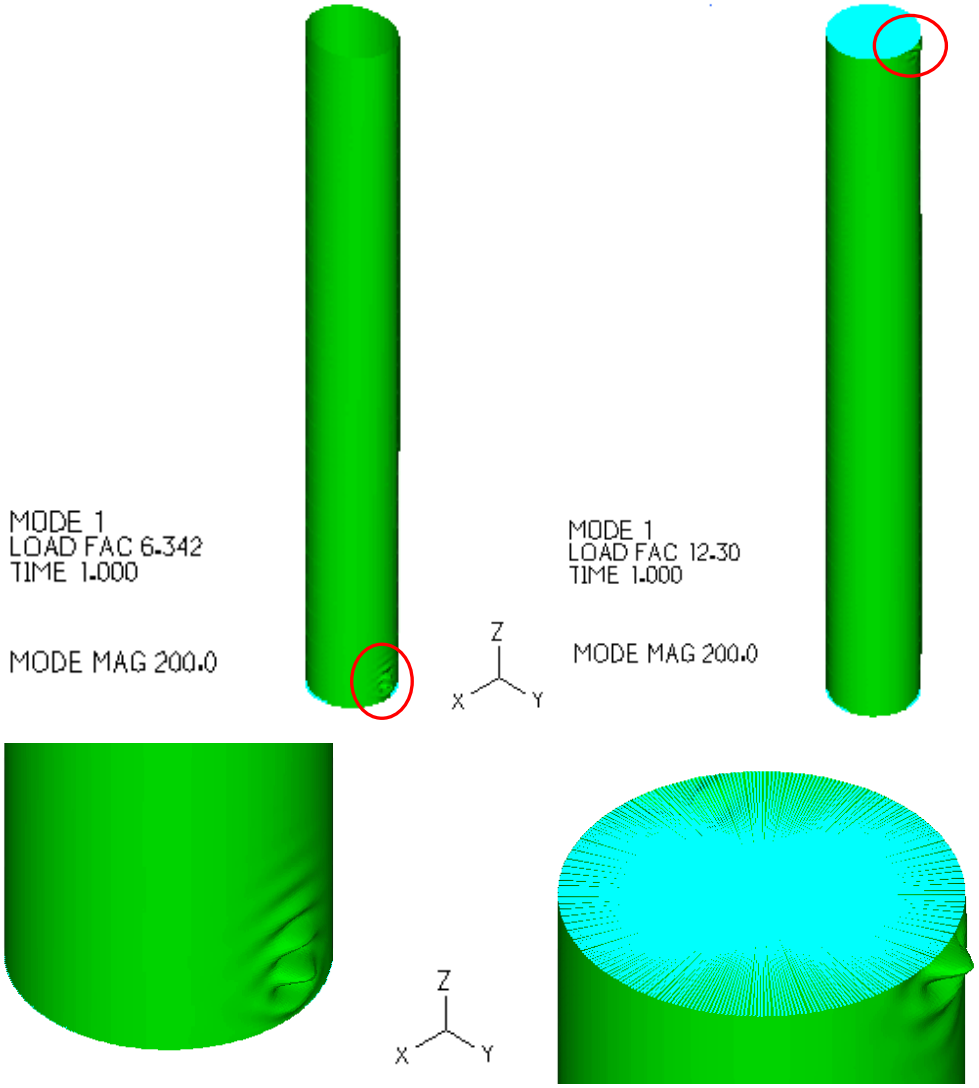

Figure 4-9: Comparison between the first buckling mode shapes of the cases in which rigid links are used (right) and not used (left)

4.3.2 NONLINEAR ANALYSES

The finite element model is exactly the same as the one used for LBA. The analyses performed are nonlinear taking into account a yield stress equal to 160MPa, when material nonlinearity is considered and large deformations, when geometrical nonlinearity is taken into account. It was seen that, based on LBA (that is relatively sensitive to the mesh density), a mesh size equal to 0.07m is sufficient and no further reduction is required. A similar conclusion is drawn according to GMNA, as shown in Figure 4-10. The stiffnesses and ultimate strengths predicted by mesh sizes of 0.07m and of 0.04m are very close to each other, indicating that the first one (which is less computationally demanding) is sufficient for the purposes of our research.

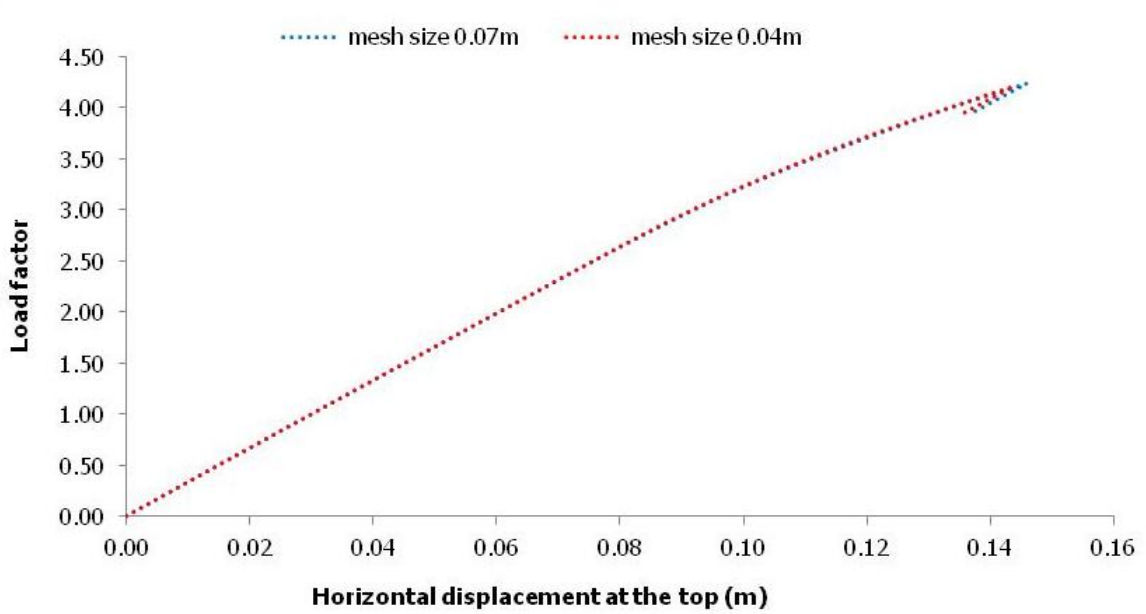

Figure 4-10: Comparison of equilibrium paths obtained with GMNA of the unstiffened model between 0.07m and 0.04m mesh size

4.3.2.1 NUMERICAL RESULTS BASED ON NONLINEAR ANALYSES

In Figure 4-11, the results obtained with GNA are shown. It can be seen that the structure's collapse load factor is equal to 6.7. This load factor is almost half of the corresponding value of LBA, where 12.3 had been found, meaning that prebuckling deformations are of major significance for this case and, hence, nonlinear analyses are required for the structure capacity evaluation. It is interesting to note that the stiffness of the structure is not significantly reduced as the load factor increases. This means that the prebuckling deformations lead to a significant decrease in the collapse load factor, but do not have an important effect on the elastic stiffness of the structure.

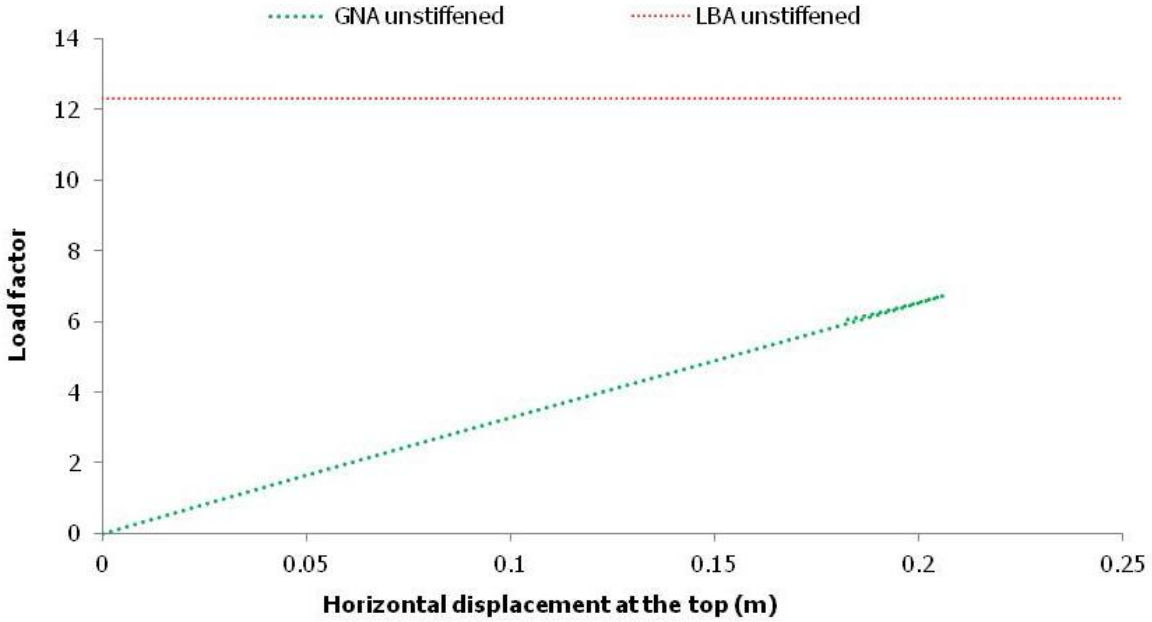

Figure 4-11: GNA results of the unstiffened structure

In Figure 4-12, the results obtained with MNA are presented. With a collapse load factor equal to 7.4, it seems that MNA does not differ that much from GNA, as far as the total capacity is concerned. However, it is noticed a gradual reduction of stiffness as the loading increases. Since geometrical linearity takes place, it is obvious that the elastoplastic material affects not only the structure capacity, but also the stiffness, which is being reduced gradually up to collapse. A combination of the geometrical and material nonlinearity, as taken into account in GMNA, is expected to have a significant effect on the ultimate strength.

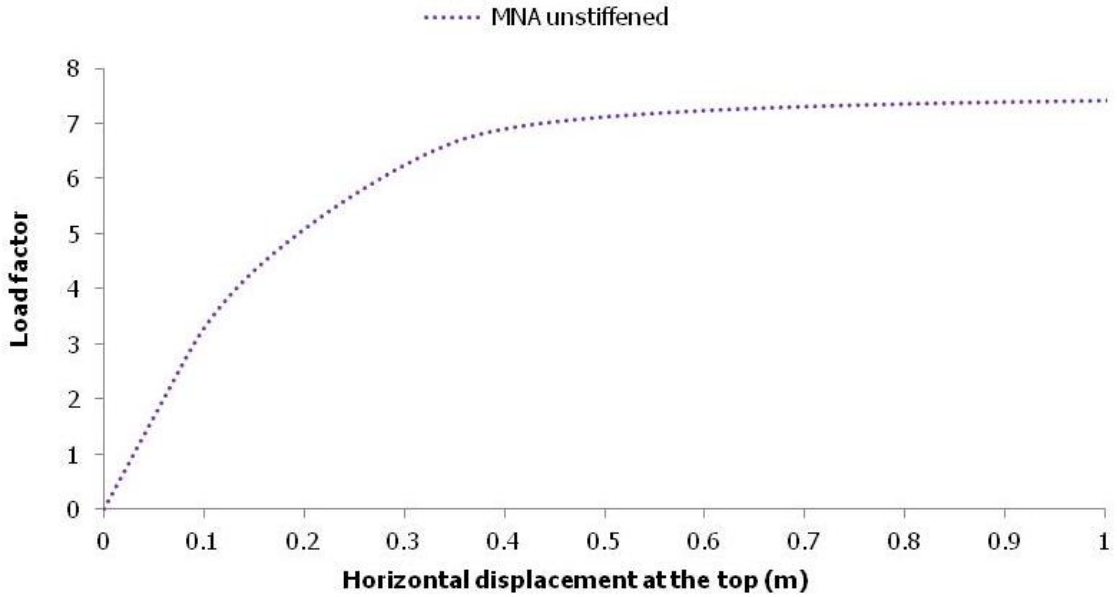

Figure 4-12: MNA results of the unstiffened structure

The results related to GMNA are presented in Figure 4-13. The ultimate collapse load factor is close to 4.3, a value smaller than the one predicted by GNA and MNA, verifying the expected conclusion that a combination of the nonlinearities leads to an even greater reduction of the collapse load factor. The decrease of the stiffness of the structure is clearly attributed to the material nonlinearity, as no reduction of the stiffness is observed in GNA. As GMNA is considered to be the most accurate available tool for the evaluation of the structural response of the chimney, the value of 4.3 is the final capacity of such a structure. Of course, no initial imperfections, based on buckling mode shapes, are inserted in the analyses, but the wind loads that are directly applied to the thin shell surface induce a type of imperfection by modifying the cross-sectional shape, as shown in Figure 4-16.

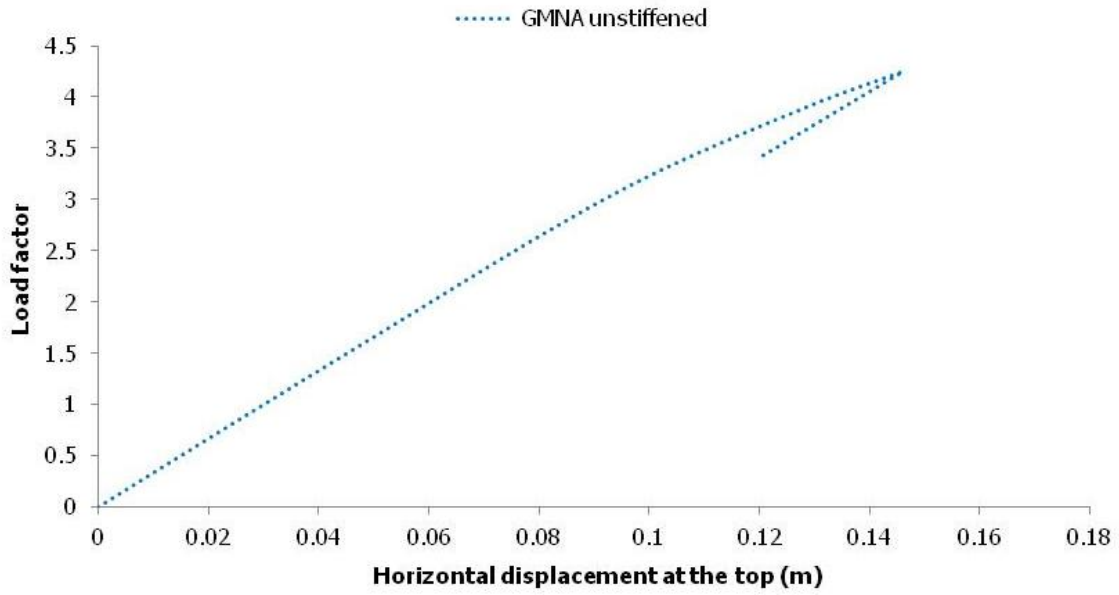

Figure 4-13: GMNA results of the unstiffened structure

The equilibrium paths for all the analyses of the unstiffened structure are shown in Figure 4-14. It can be seen that an upper strength bound is provided by LBA, with a load factor equal to 12.3. The maximum load factors achieved by GNA and MNA are practically of similar magnitude, as already has been stated. A combination of the nonlinearities in GMNA leads to a reduced collapse load factor, which is equal to 4.3. It is also worth noticing that all the nonlinear analyses show the same stiffness up to a point. MNA and GMNA results diverge from the initial stiffness in the same way, as shown in Figure 4-15, while GNA is still linear and maintains a stiffness close to the initial stiffness. This practically means that the decrease of the stiffness is attributed to material nonlinearity, while the decrease of the collapse load factor to both material and geometrical nonlinearity, as also indicated in Figure 4-16 and Figure 4-17.

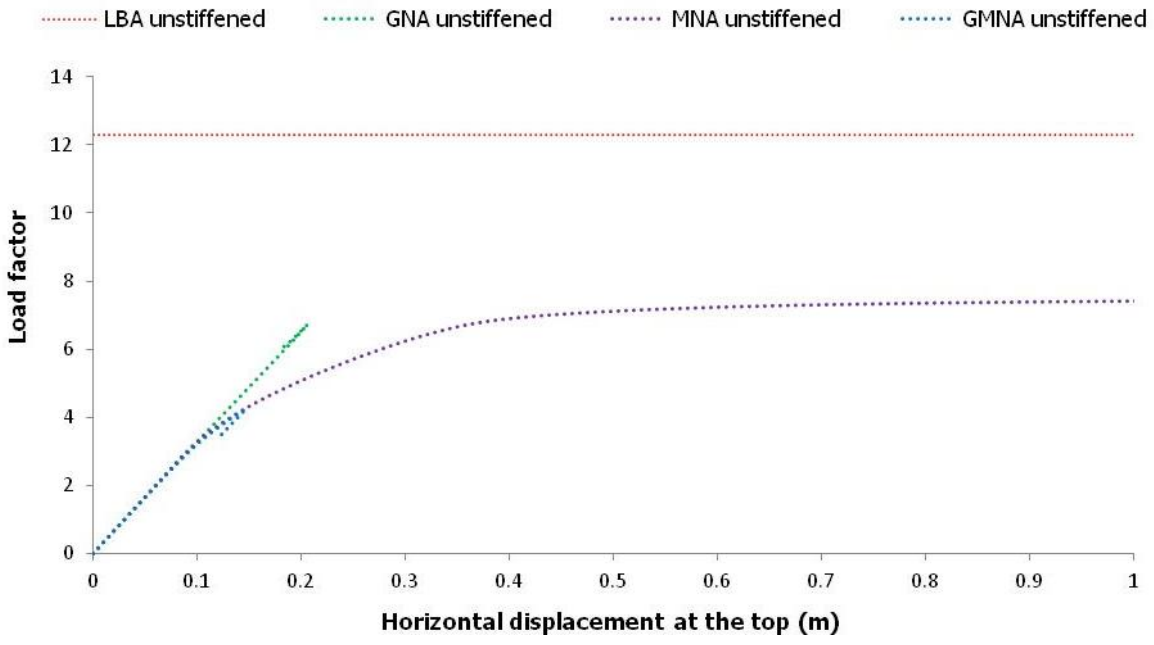

Figure 4-14: Numerical analyses results of the unstiffened structure

Figure 4-15: Detail of equilibrium paths of nonlinear analyses of the unstiffened structure

The magnified deformed shapes of the unstiffened structure at failure from GMNA are shown in Figure 4-16. It is interesting to note that the cross-sectional shape is significantly different from the circular one (undeformed shape) due to the wind pressure application. It is also interesting to mention that the deformed shape is significantly different from the buckling mode shape predicted by LBA. Hence, the previously drawn conclusion that prebuckling deformations are of significant importance in the present case, is now reinforced. It is also concluded that the application of the pressure directly to the perimeter of the shell structure leads to a 3-Dimensional deformation of the thin shell that cannot be captured by beam theory. Therefore, two main components can be distinguished for the deformation of structure:

- The first is related to the overall deformation as a cantilever, where the cross-sectional shape is not modified and the cross-sections remain circular.
- The second deals with the local deformation of the surfaces, where the cross-sectional shape is significantly modified and the cross-sections do not remain circular.

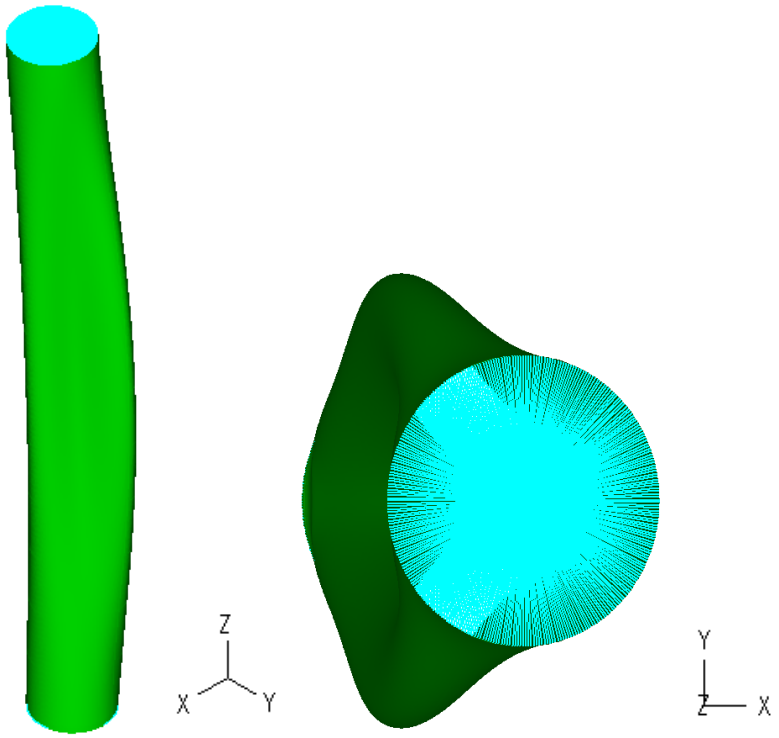

Figure 4-16: 3-Dimensional view and plan view of deformed shapes of the unstiffened structure at failure from GMNA

The distribution of the plastification in the shell structure at failure is presented in Figure 4-17. It can be observed that plastification appears in several regions at the top and bottom of the structure, coming in contrast with what beam theory would predict. According to beam theory, the failure of a

cantilever subjected to these loads occurs at the base support. The following plastification pictures also verify the conclusion that collapse takes place due to both plastification (material nonlinearity) and large deformations (geometrical nonlinearity) of the unstiffened structure.

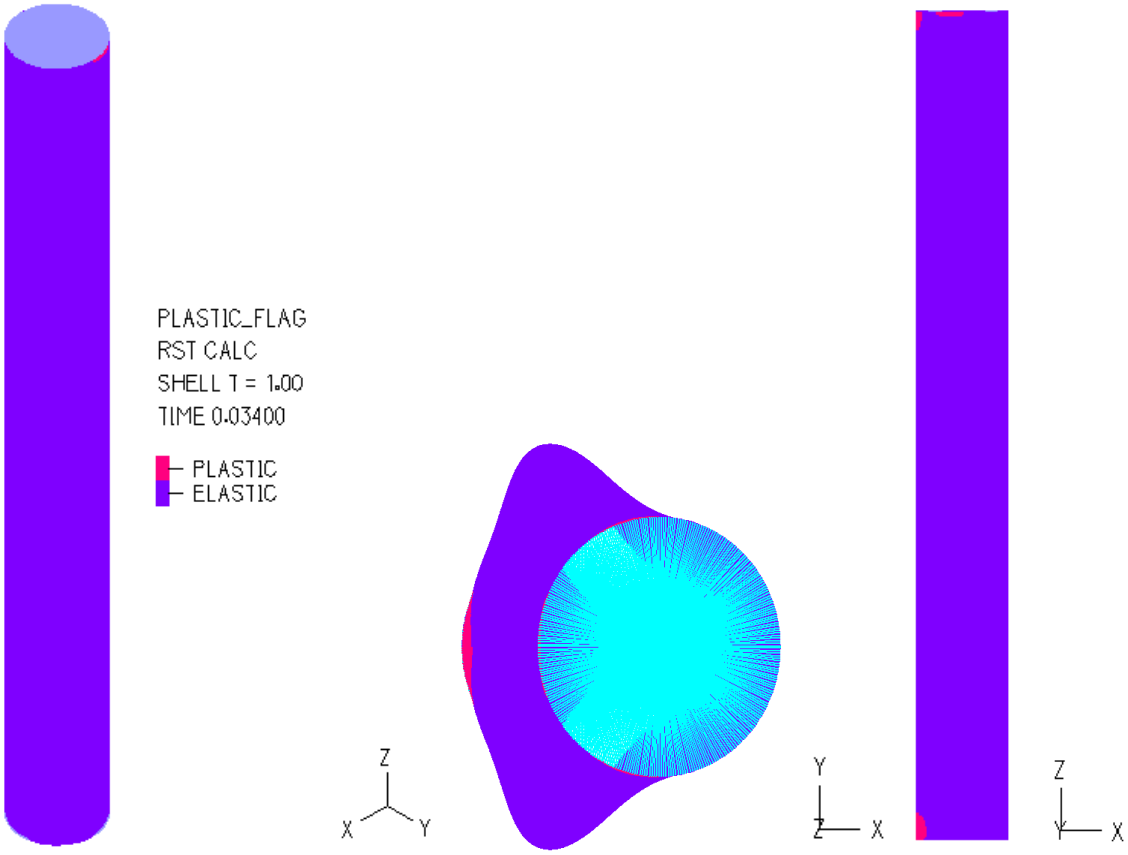

Figure 4-17: Plastic and elastic regions of the unstiffened structure at failure from GMNA

4.4 STIFFENED STRUCTURE

In this section, the numerical results obtained with linear and nonlinear analyses, performed for the stiffened structure, are presented. The geometric characteristics of the numerical stiffened model (both of the shell and stiffeners) have already been described in section 4.2.2. In Figure 4-18, the stiffened model, as presented in ADINA, is shown. The different colors between the shell and stiffeners indicate the different, so-called, element groups. A different thickness of finite elements is used in each element group, as also stated in the numerical description of the model (section 4.2). Hence, the model shell thickness is 0.013 m, while the stiffeners' thickness is 0.01m.

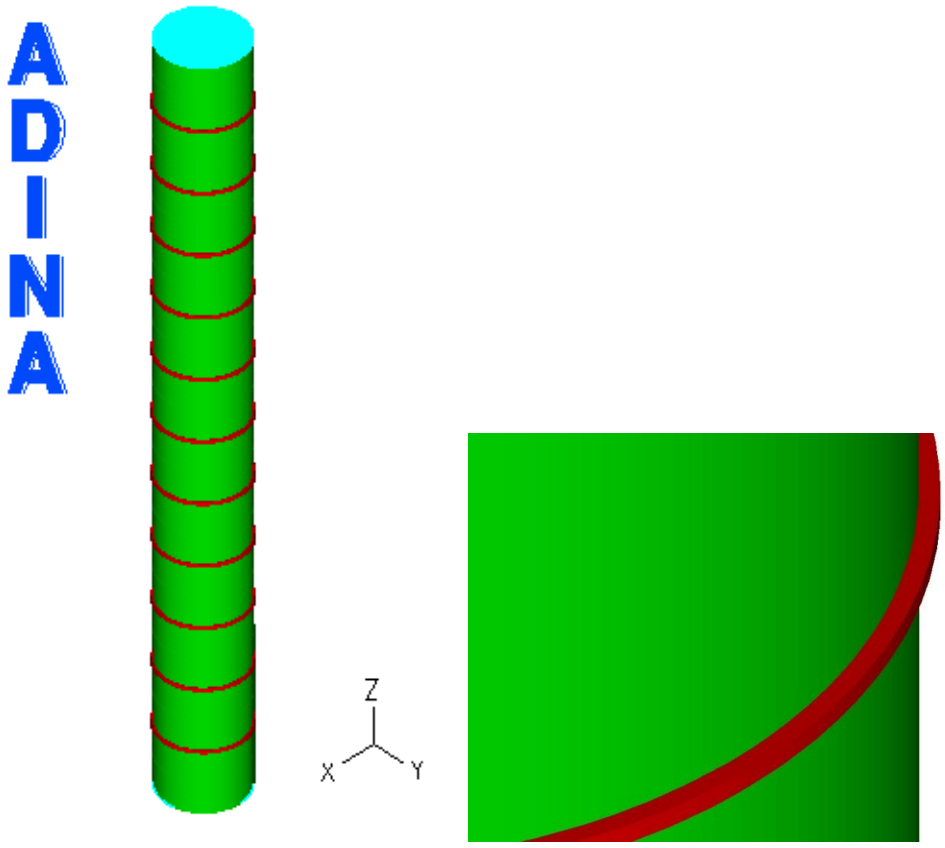

Figure 4-18: The stiffened structure as modeled in ADINA

4.4.1 LINEARIZED BUCKLING ANALYSIS

The material of the stiffeners for LBA is elastic steel, which is the same as the one used in the shell of the structure. In this case, only the load factors of two mesh sizes (0.04m and 0.07m) were compared. In the case of the unstiffened model, a convergence of the order of 1.3% was observed between the buckling loads of these two densities. In the case of the stiffened structure, the observed difference between the buckling loads of the two mesh densities is 1.4% (Table 4-4) and this leads to the final application of a mesh size of 0.07m for LBA of the stiffened model, too.

Table 4-4: Comparison of buckling loads between different mesh sizes of the stiffened model

Mesh size (m)	Buckling load
0.07	19.91
0.04	19.63

4.4.1.1 NUMERICAL RESULTS BASED ON LBA

Looking at the views of the first buckling mode in Figure 4-19, an interesting observation is that buckling is observed at the bottom of the structure. This behavior is close to what beam theory would predict, but not close enough so as beam theory to be valid, due to the Y-Direction of deformation. Additionally, looking at the plan view, despite the fact that symmetrical loading is applied upon the structure, an unsymmetrical deformation of the cross section is observed. This is possibly explained by the imperfections induced by the software itself, during the meshing process.

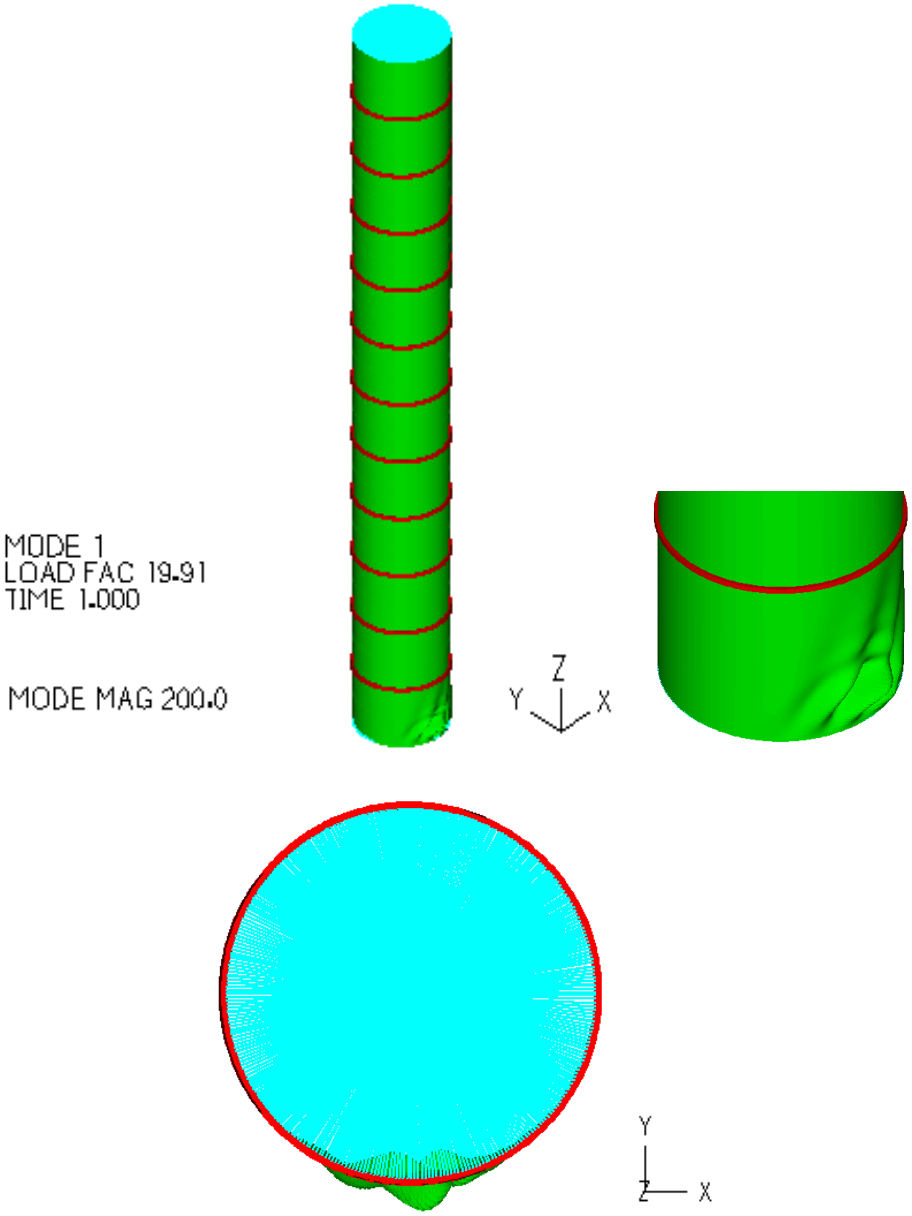

Figure 4-19: First buckling mode views and buckling load of the stiffened structure

4.4.2 NONLINEAR ANALYSES

The stiffened finite element model used in nonlinear analyses is the same as the LBA's model. Elastoplastic material with a yield stress equal to 160MPa is used, when material nonlinearity is considered, while elastic material is applied when geometrical nonlinearity is taken into account. It is noted that, in any case, the material of the shell and stiffeners is the same. As far as the applied mesh size for the nonlinear analyses of the stiffened model is concerned, the ultimate mesh density resulted in 0.07m. This is explained by the insignificant difference between the capacities, obtained with GMNA, using the mesh sizes 0.07m and 0.04m, as shown in Figure 4-20.

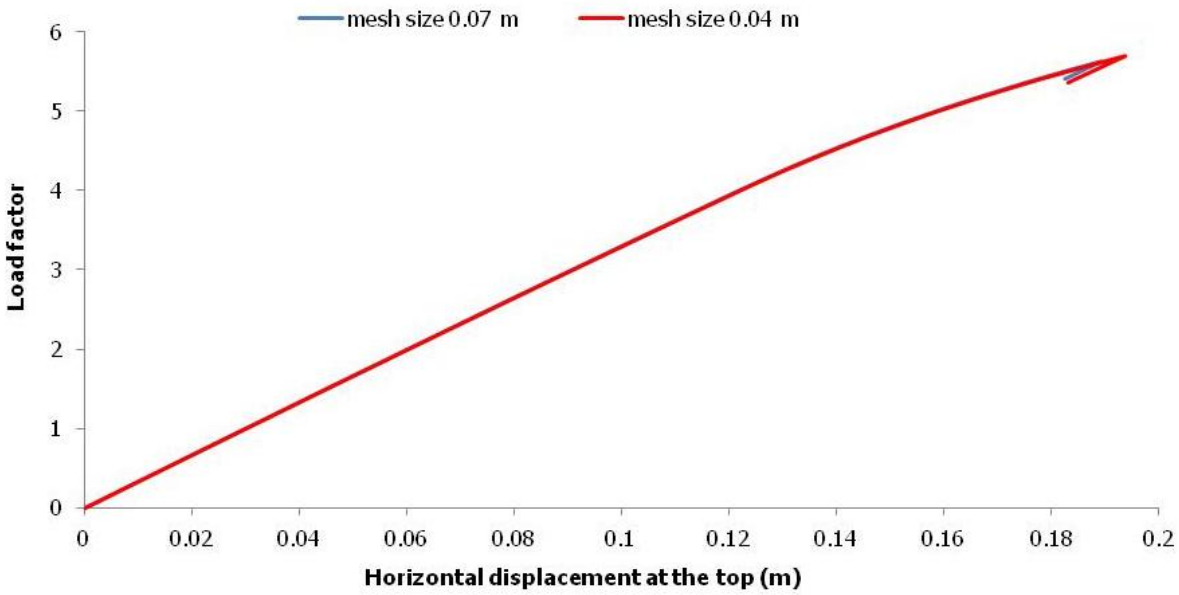

Figure 4-20: Comparison of the equilibrium paths obtained with GMNA of the stiffened model between 0.07m and 0.04m mesh size

Another matter of investigation is the efficiency of the mesh size of 0.07m in indicating the stiffeners yield, because their geometry (0.12m width) allows the existence of only two finite elements along the width of each shell of stiffener. Hence, the finite elements may not be square, as shown in Figure 4-21, but many times they tend to be triangular, making the results controversial. On the other hand, using the mesh size of 0.04m, each one of the two stiffener shells is meshed by three finite elements and, thus, the previously mentioned problem does not exist anymore, as it is clear in Figure 4-22.

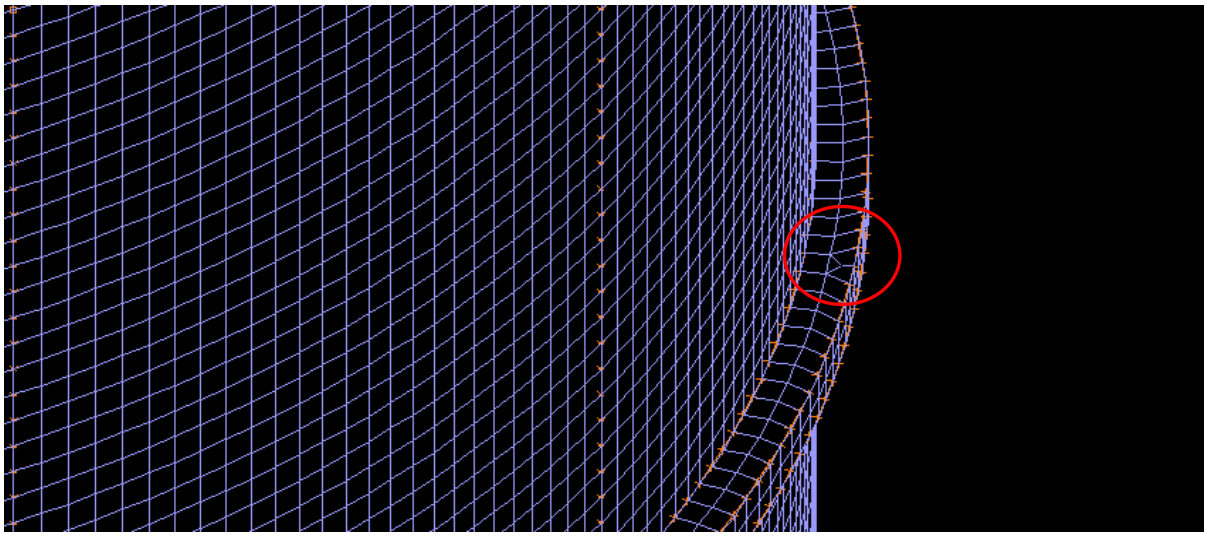

Figure 4-21: Detail of meshing using 0.07m mesh size

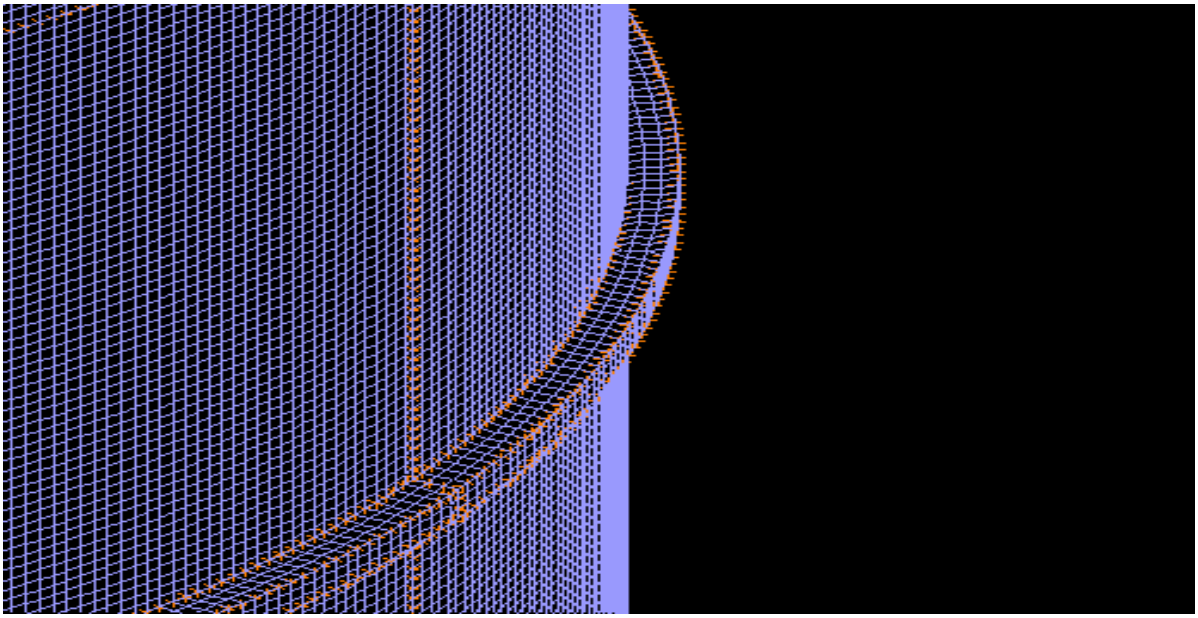

Figure 4-22: Detail of meshing using 0.04m mesh size

To shed light into this matter, plastification views must be observed. What is interesting, looking at Figure 4-23, Figure 4-24, Figure 4-25 and Figure 4-26, is that plastification views of the two mesh sizes do not differ that much. Hence, the computational cost is the only criterion based on which the final decision on the ultimate mesh density for the nonlinear analyses of the stiffened model is taken. Therefore, the final mesh density for the stiffened model is 0.07m.

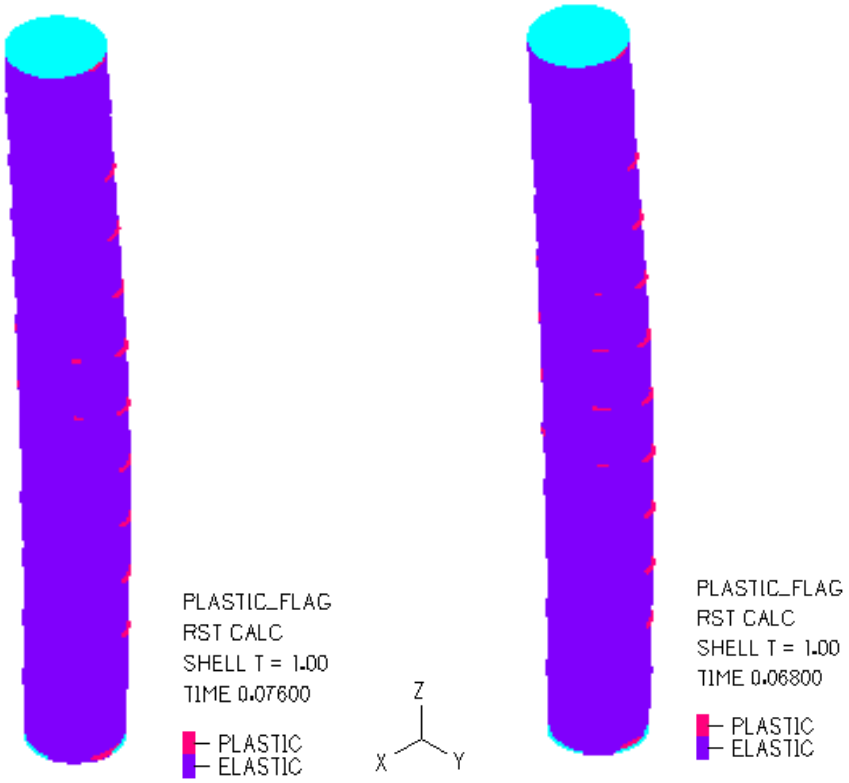

Figure 4-23: Comparison of 3-Dimensional views of the stiffened model between the 0.07m and 0.04m mesh size

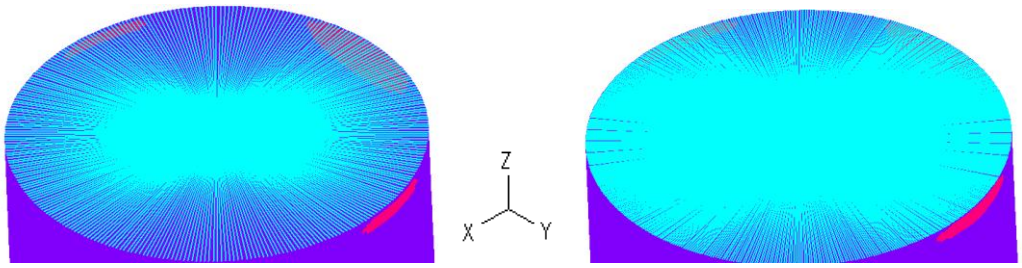

Figure 4-24: Comparison of the top of 3-Dimensional views of the stiffened model between the 0.07m and 0.04m mesh size

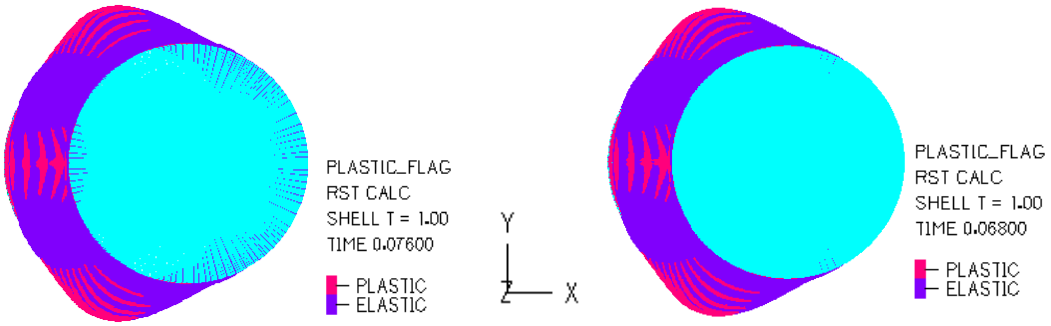

Figure 4-25: Comparison of the plan views of the stiffened model between the 0.07m and 0.04m mesh size

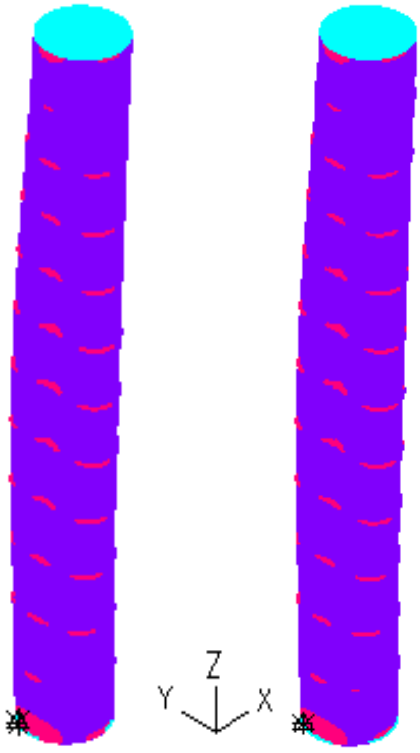

Figure 4-26: Comparison of the second 3-Dimensional views of the stiffened model between the 0.07m and 0.04m mesh size

4.4.2.1 NUMERICAL RESULTS BASED ON NONLINEAR ANALYSES

Looking at Figure 4-27, a first observation is that the final structure capacity given by GNA (with a load factor equal to 18.7) is really close to the buckling load found by LBA. This leads to the conclusion that prebuckling deformations, which LBA cannot capture, are not of significant importance

for the case of the stiffened structure. This may be explained by the impact of stiffeners on the shell deformation. It is also observed that the stiffness of the structure is not significantly reduced as the load factor increases. This means that the prebuckling deformations neither decrease the collapse load factor nor affect the elastic stiffness of the structure. It is, then, concluded that the presence of stiffeners reduces dramatically the prebuckling deformations.

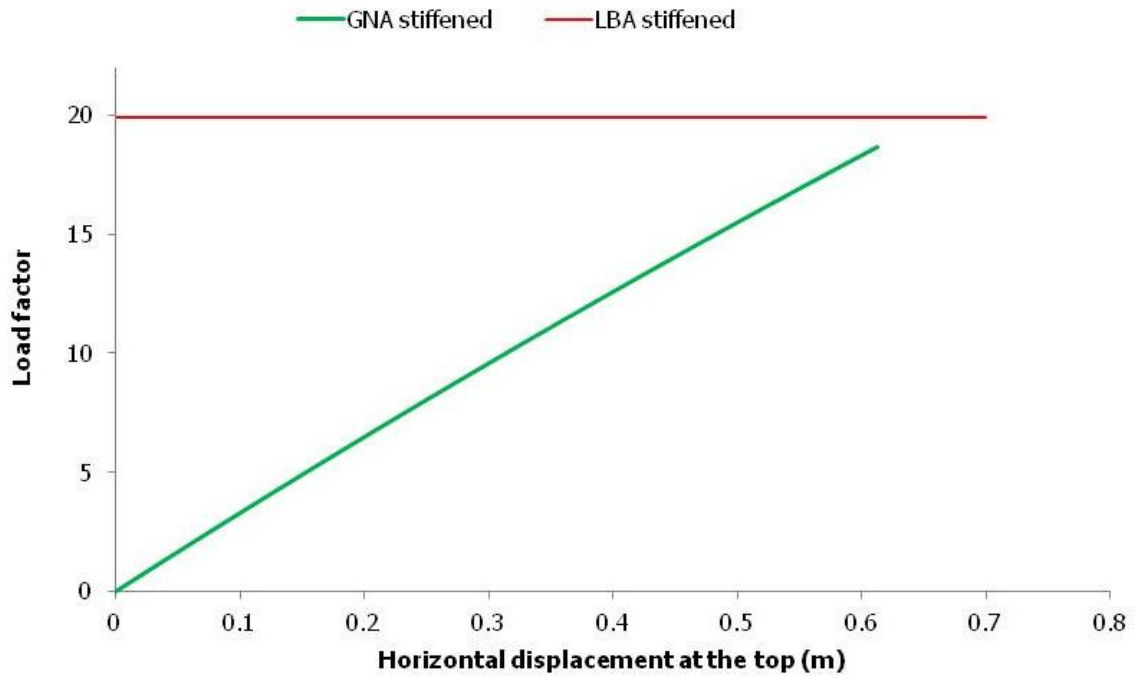

Figure 4-27: GNA results of the stiffened structure

MNA's capacity, though, seems to differ from the result of GNA. As it is shown in Figure 4-28, MNA's collapse load factor is equal to 8, a value much smaller than the one found by GNA (where a load factor equal to 18.7 had been found). It is, then, concluded that material nonlinearity is of significant importance for the stiffened structure. A combination of both nonlinearities is expected to reduce even more the ultimate capacity.

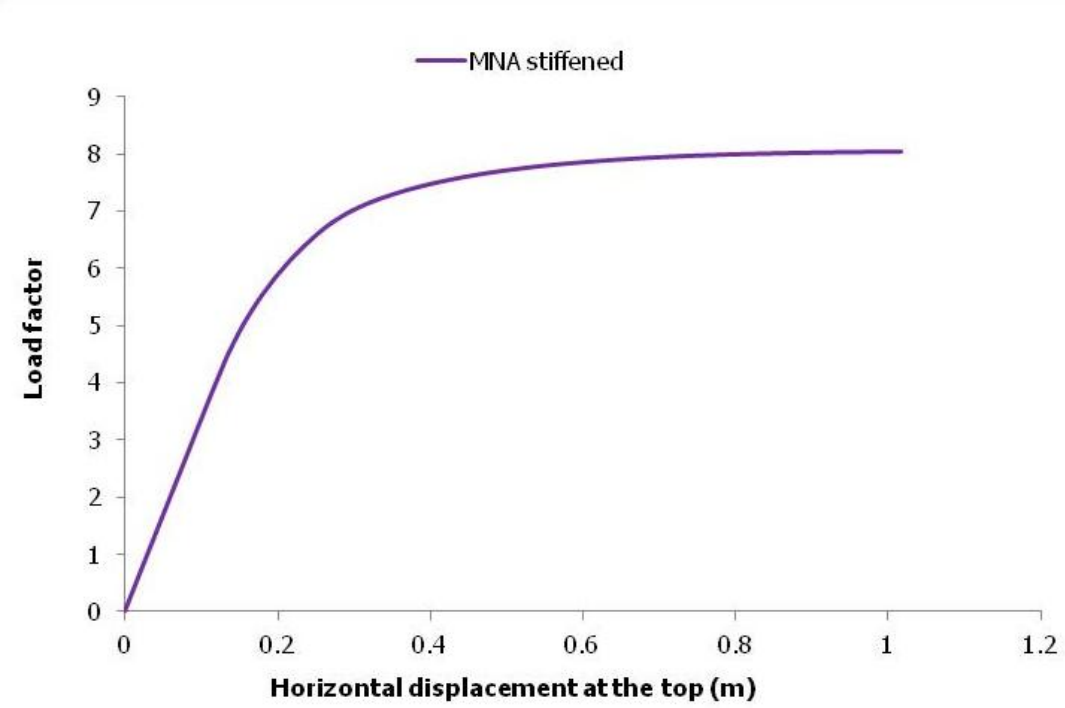

Figure 4-28: MNA results of the stiffened structure

The capacity found by GMNA (with load factor equal to 5.6) is significantly smaller than the one found by both GNA and MNA. Since in GMNA both nonlinearities are inserted, the fact that the final capacity is closer to the one found by MNA leads to the conclusion that the material nonlinearity governs the failure and is the main reason for the reduced collapse load.

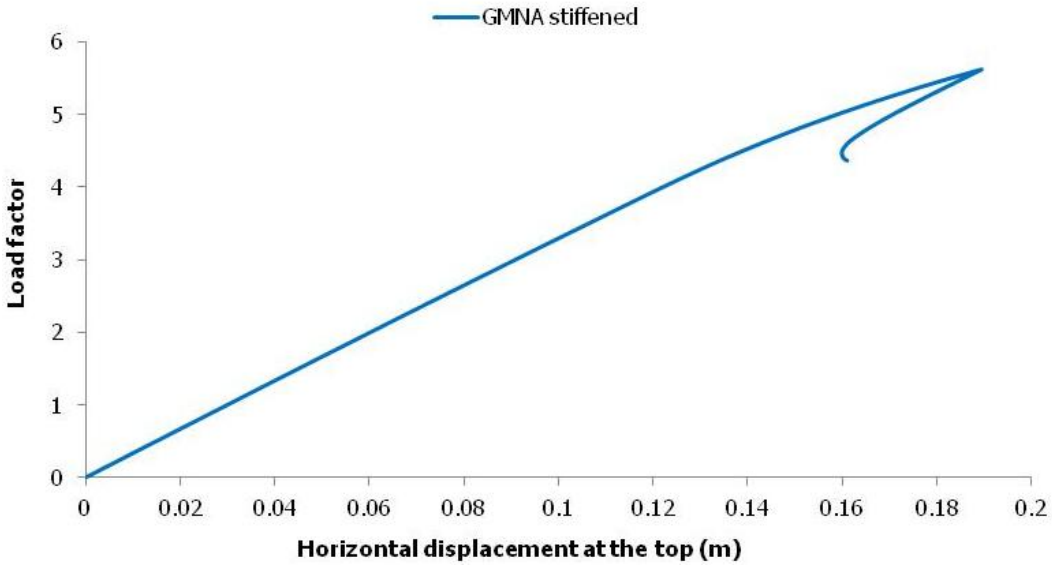

Figure 4-29: GMNA results of the stiffened structure

In Figure 4-30, the comparison between the equilibrium paths, obtained with different analyses, for the stiffened model, is presented. In Figure 4-31, a detail of the equilibrium paths shows that the material nonlinearity is predominant, in the case of GMNA, as its equilibrium path actually follows the one of MNA, but stops earlier, reaching a collapse load factor slightly smaller than the one found by MNA. Deformations and plastification distributions, in the case of GMNA, are presented in Figure 4-32

and Figure 4-33. It can be seen that changes of the cross-sectional shape are significantly restricted due to the appearance of the stiffening rings. Additionally, the regions in which failure is observed are again distributed in the structure and therefore the validity of the beam theory consideration that predicts failure at the base support is not valid.

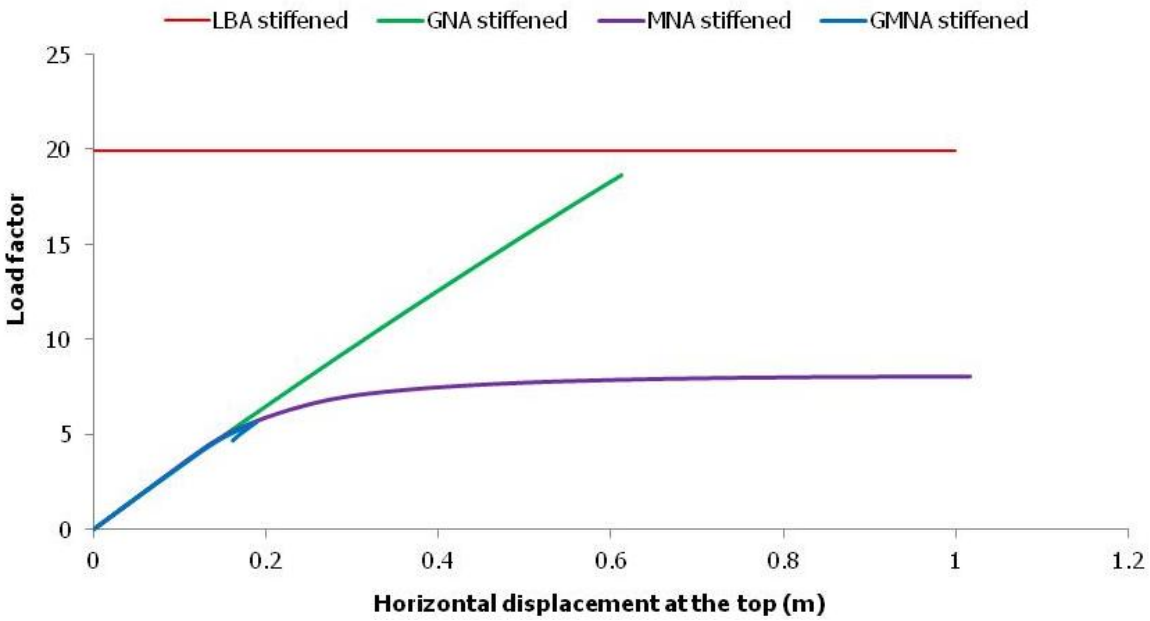

Figure 4-30: Numerical analyses results of the stiffened structure

Figure 4-31: Detail of equilibrium paths of nonlinear analyses of the stiffened structure

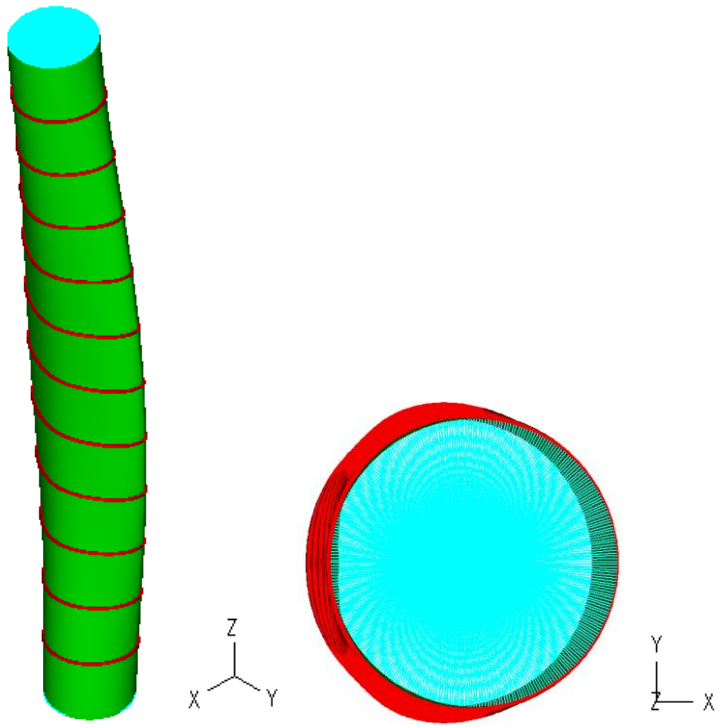

Figure 4-32: 3-Dimensional view and plan view of deformed shapes of the stiffened structure at failure from GMNA

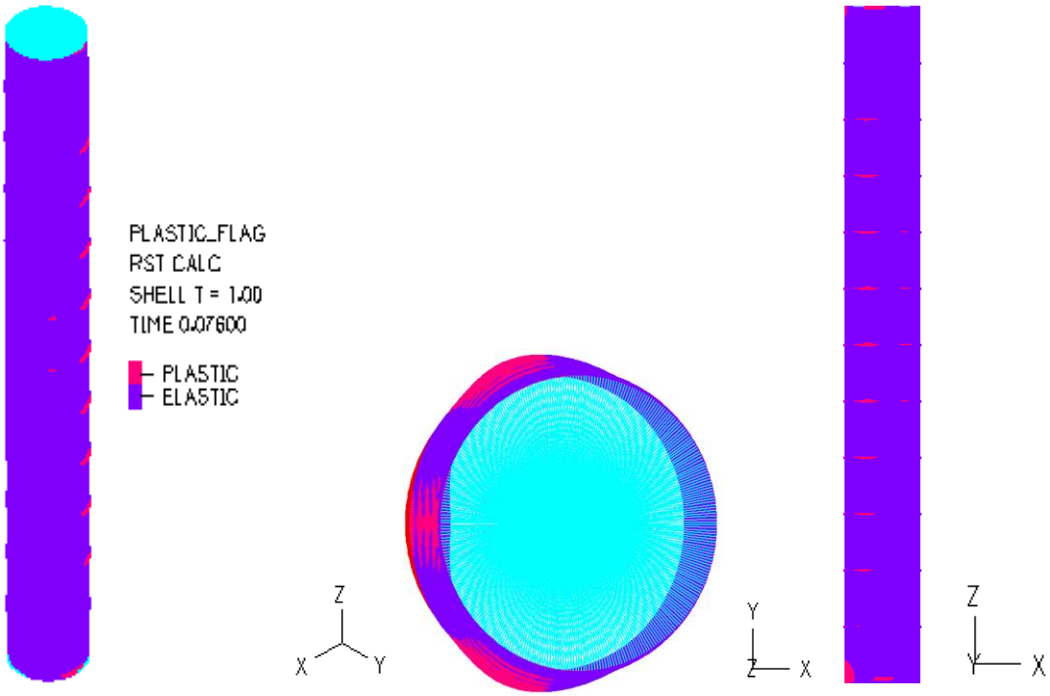

Figure 4-33: Plastic and elastic regions of the stiffened structure at failure from GMNA

4.5 COMPARISON BETWEEN THE UNSTIFFENED AND STIFFENED STRUCTURE

4.5.1 LINEARIZED BUCKLING ANALYSIS

Comparing the first buckling mode shapes of the two models in Figure 4-34, it is interesting to notice the location of buckling. In the unstiffened model, buckling occurs at the top of the structure, while at the stiffened one buckling is observed at the bottom. In both cases, the location of buckling does not correspond to the most compressed side, at the structure base, as expected by beam theory, for wind direction +X. Therefore, it is believed that the applied pressures to the walls of the shell structure are of great importance, even in the case of the stiffened structure, where the stiffeners restrict dramatically the shell deformations.

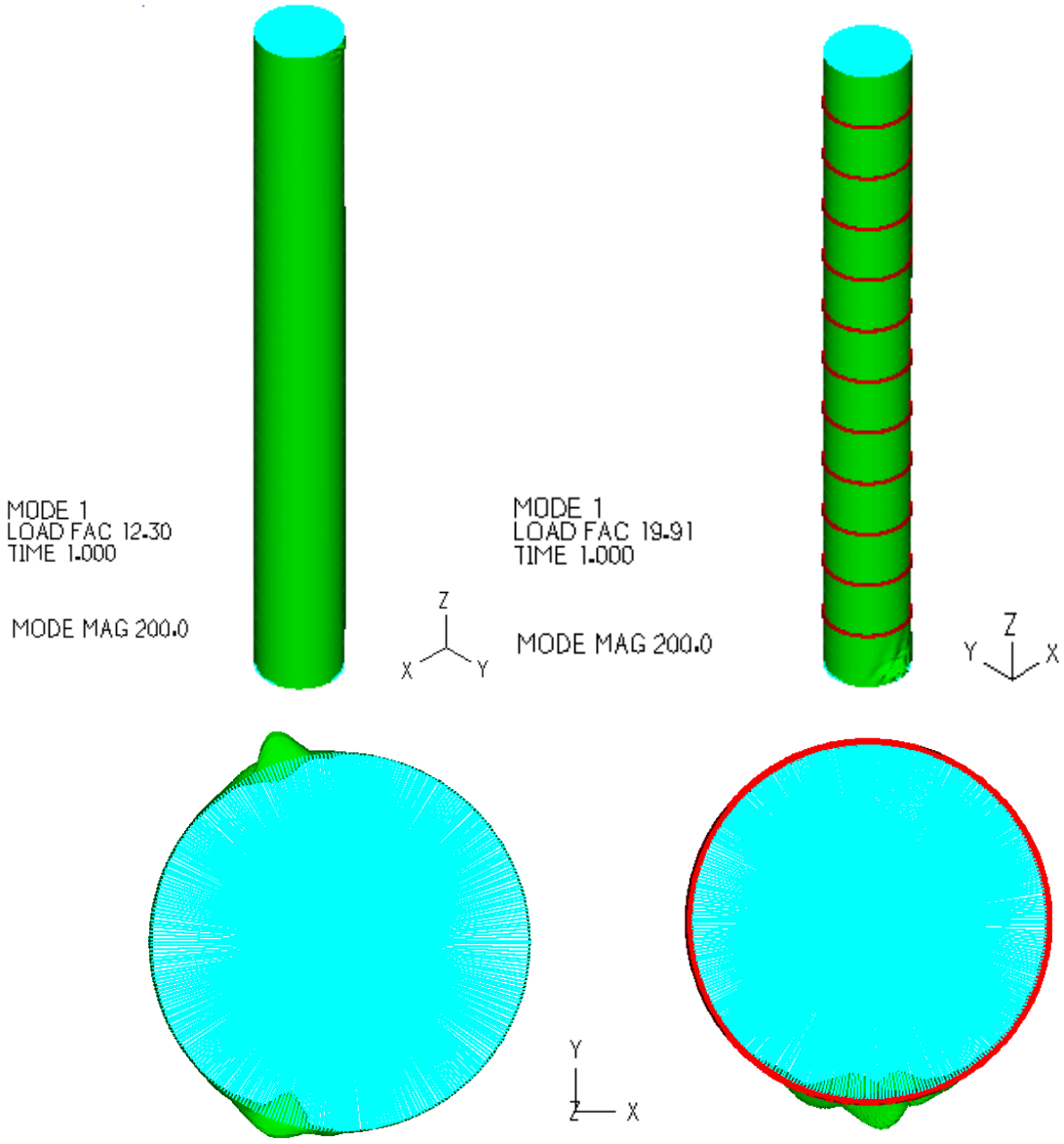

Figure 4-34: Comparison of first buckling mode between the unstiffened and stiffened structure

In order to better understand the predictions of the LBA, one should look into the deformation views and the stress distribution found with Linear Elastic Analysis. In Figure 4-35, the results obtained by Linear Elastic Analysis are presented. It is observed that the unstiffened shell deforms not only as a cantilever, but also local deformations of the thin walls appear. The latter type of deformation leads to

important changes of the cross-sectional shape (something similar to the philosophy behind the ovalization phenomenon). The presence of stiffening rings restricts the deformation of the shell structure and the change of the cross-sectional shape is significantly reduced.

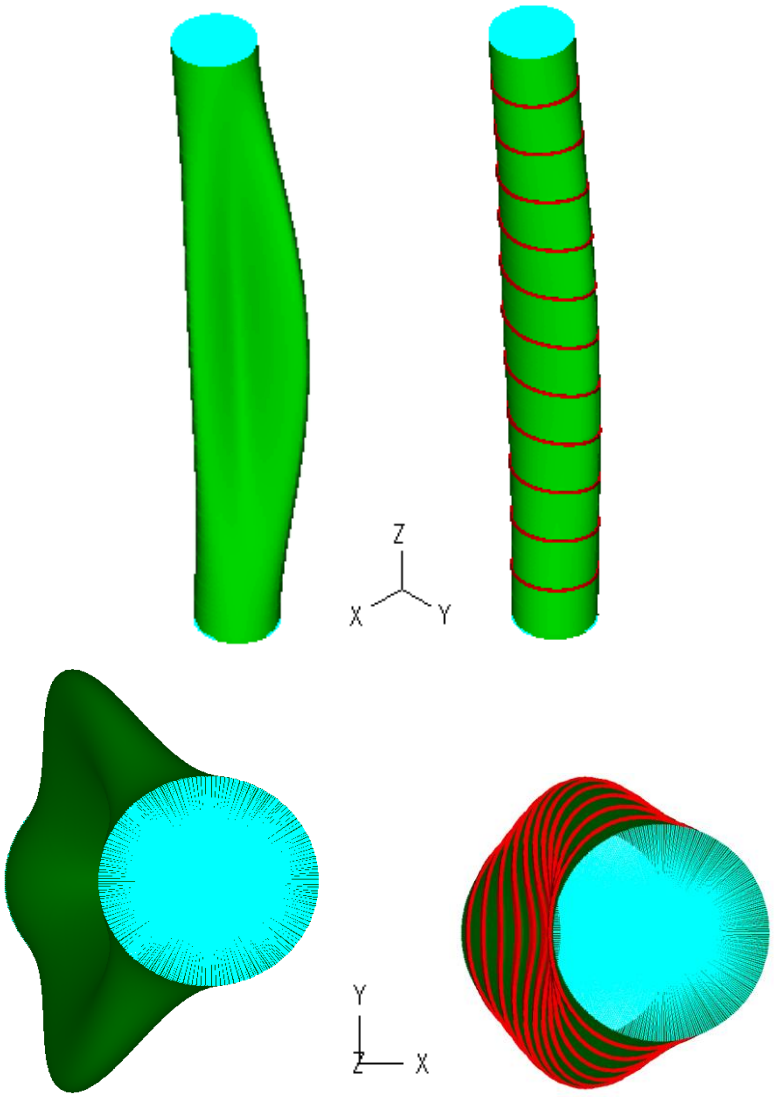

Figure 4-35: Comparison of deformed shapes according to Linear Elastic Analysis between the unstiffened and stiffened structure

This has an effect on the circumferential and longitudinal normal stress distribution. As shown in Figure 4-36, the circumferential normal stresses have large compressive and tensile peaks, in the case of the unstiffened structure, while in the case of the stiffened structure, the stress distributions are smoother. It is also worth-mentioning that large longitudinal compressive stresses appear at the location where LBA predicted buckling for the first buckling mode, as shown in Figure 4-37.

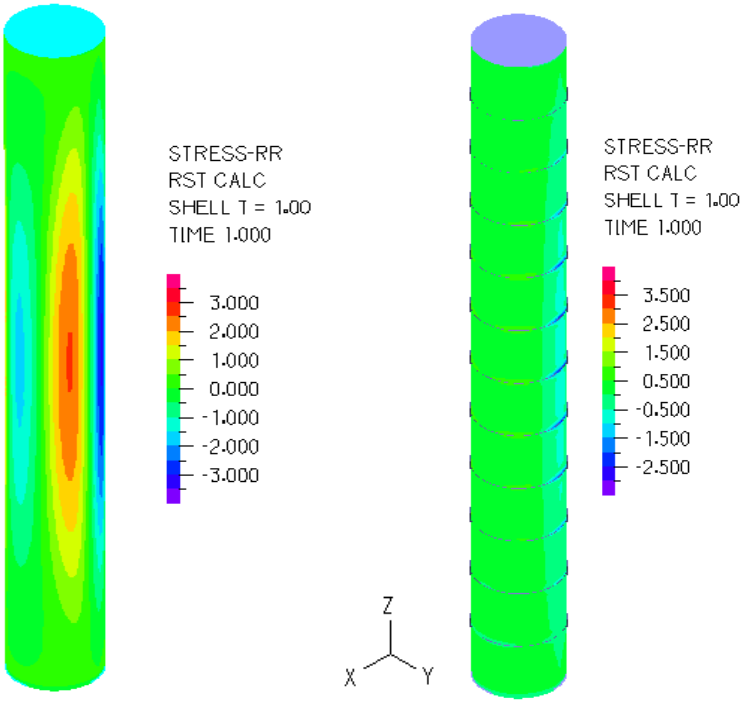

Figure 4-36: Comparison of circumferential stress distribution between the unstiffened and stiffened structure

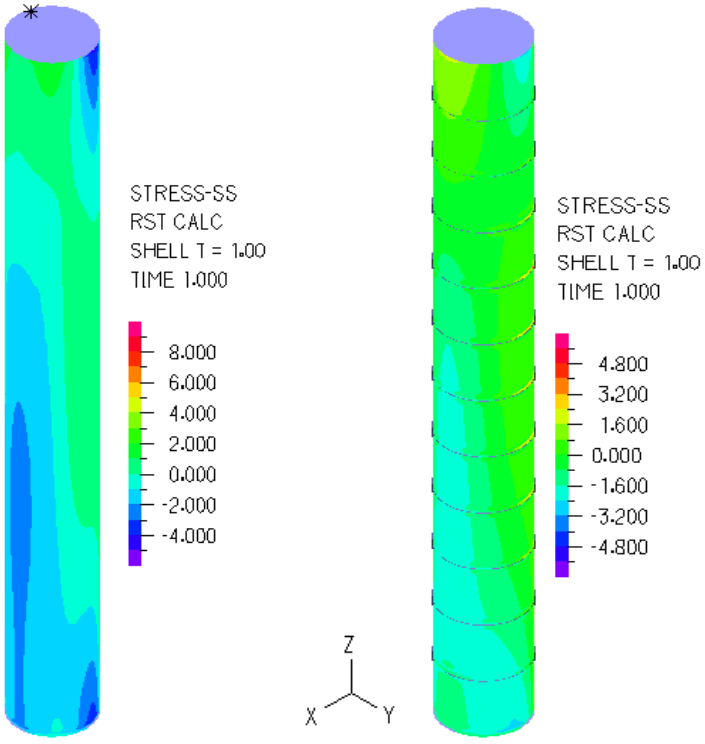

Figure 4-37: Comparison of longitudinal stress distribution between the unstiffened and stiffened structure

4.5.2 NONLINEAR RESULTS

In many cases, stiffening rings are used in industrial chimneys in order to increase the capacity of the structure. It is commonly accepted that the use of stiffening rings provides restraint against changes of the cross-sectional geometry (ovalization), while no significant increase of the bending stiffness is observed [3]. The above statement is proved looking at Figure 4-38, where a comparison between the

structural response of the unstiffened and stiffened shell structure is shown. It is noted that the elastic lateral stiffness of the structure is not significantly affected by the presence of the stiffening rings. This practically means that the cantilever component of deformation is not affected by the rings. On the other hand, the bearing capacity of the structure is enhanced by the rings, as illustrated in the results obtained with LBA, GNA, MNA and GMNA of stiffened model. The largest increase is observed for the cases that the material is assumed to be elastic. GNA of the stiffened structure predicts a collapse load factor that is approximately 2.8 times larger than the one corresponding to GNA of the unstiffened structure. The collapse load factor based on GMNA is approximately 1.35 times larger in the case of stiffeners. Obviously, the limitation imposed by material yielding decreases the effectiveness of the stiffening rings. It is, therefore, concluded that the higher the material yield strength (that is the more elastic the material) the larger the effect of the stiffening rings on the capacity seems to be.

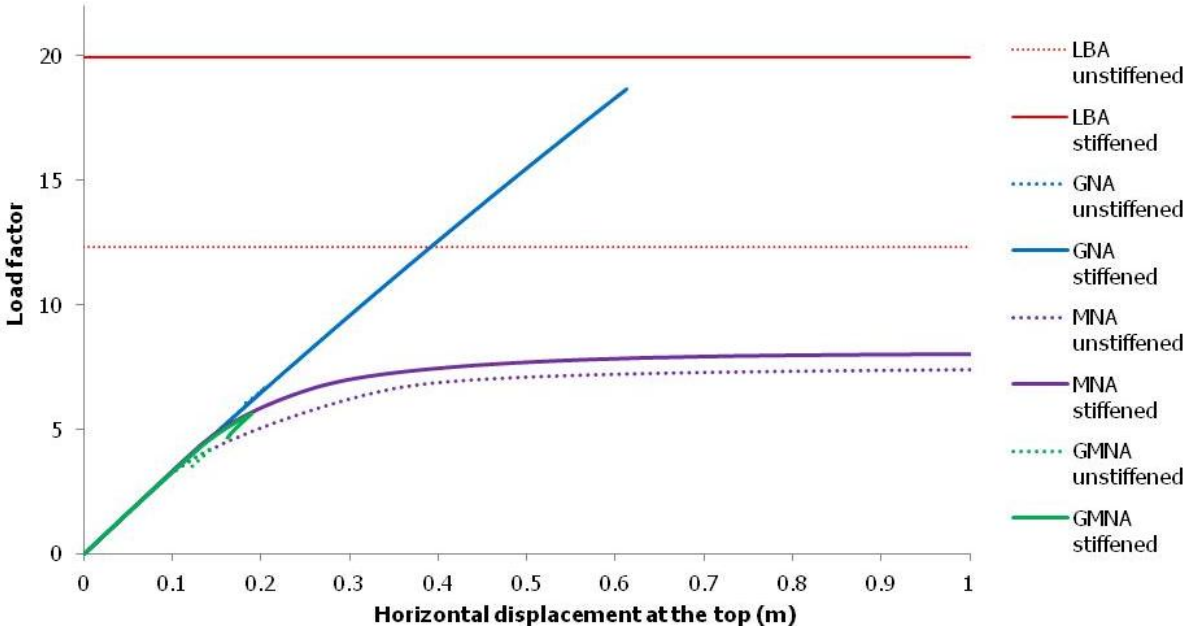

Figure 4-38: Comparison of equilibrium paths between the unstiffened and stiffened structure

A comparison between the deformed shapes of the unstiffened and stiffened structure and the plastified regions at failure are presented in Figure 4-39 and Figure 4-40 respectively. It can be seen that the use of the stiffening rings leads to a mild deformation of the shell and restricts the change of the cross-sectional shape to some extent. The stiffening rings are activated and for this reason they deform and get plastified, too.

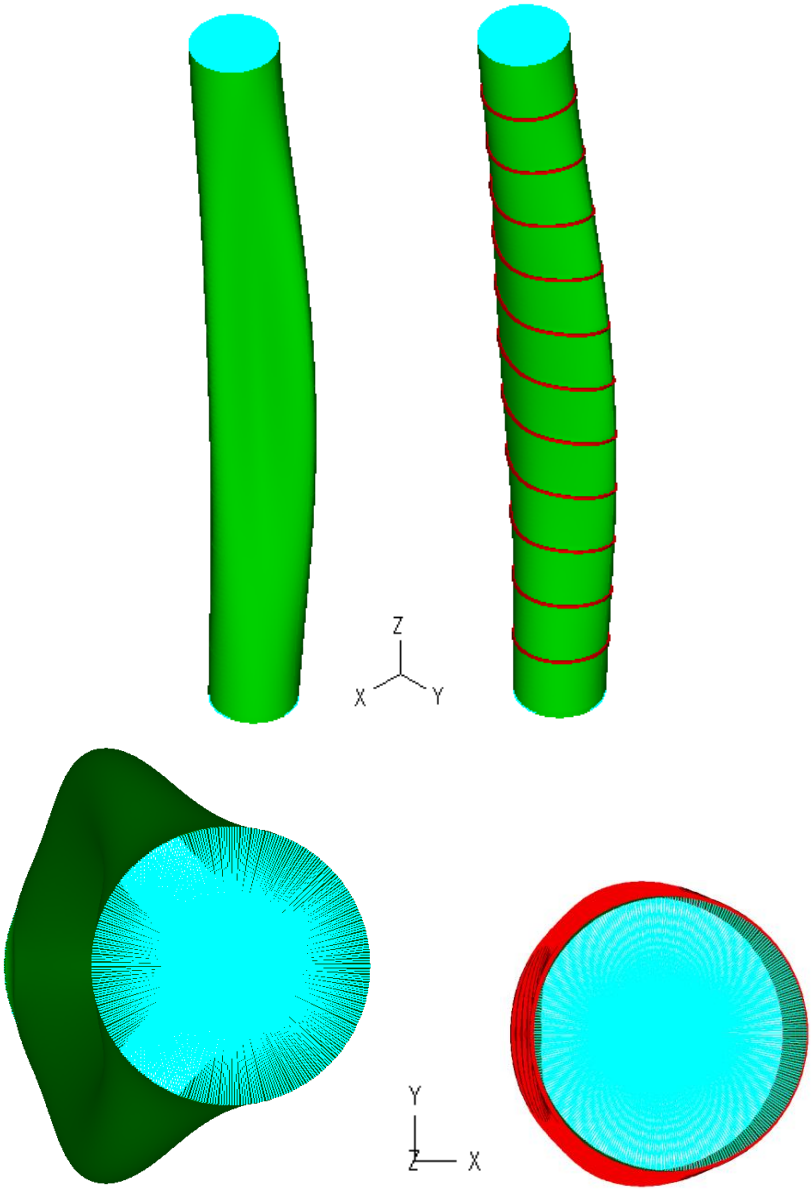

Figure 4-39: Comparison between the deformed shapes of the unstiffened and stiffened structure at failure from GMNA

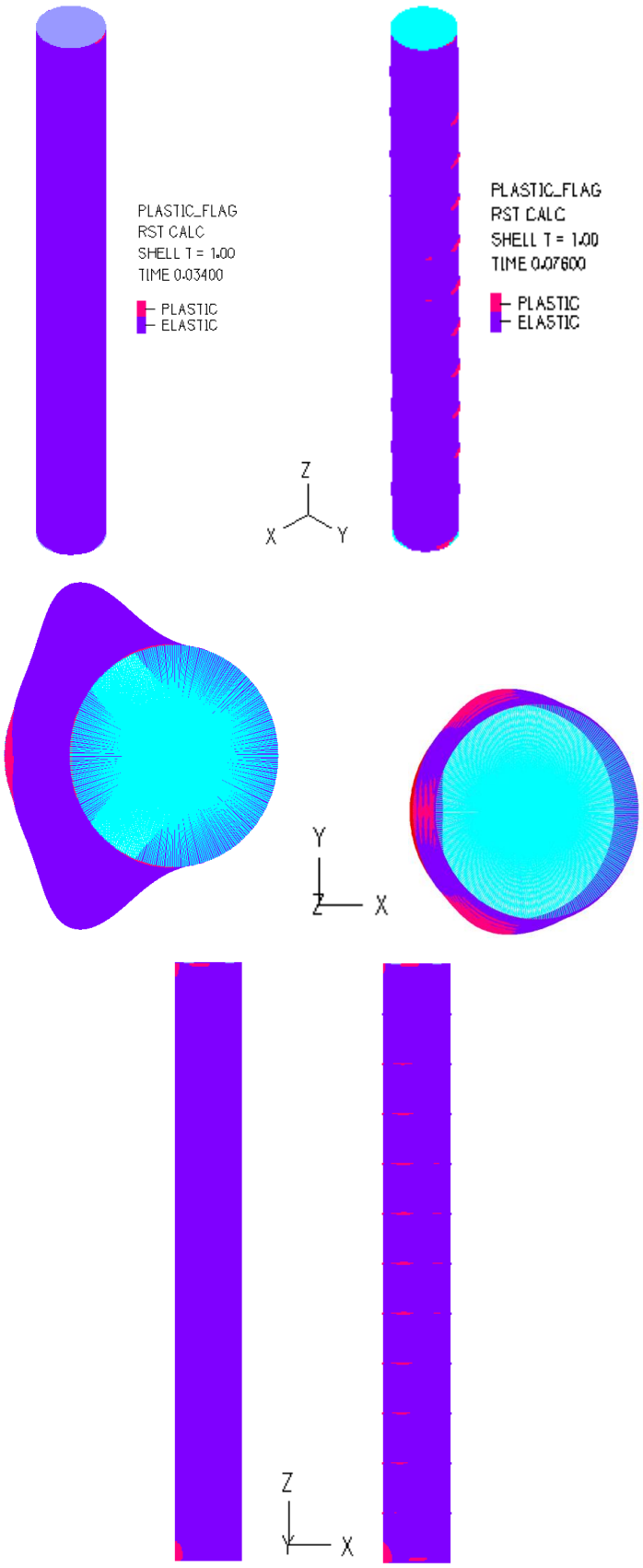

Figure 4-40: Comparison between the plastification views of the unstiffened and stiffened structure at failure from GMNA

4.6 COMPARISON BETWEEN ANALYTICAL AND NUMERICAL RESULTS

In this section, a comparison between the already calculated analytical results (section 3.3.2) and the numerical results takes place. It is pointed out that the analytical calculations are related to the unstiffened structure. According to a more accurate analytical approach than the presented one in chapter 3, the internal forces N, M are obtained by a Linear Elastic Analysis based on the emulated 3-Dimensional model, on which wind pressure (Table 4-2) is applied. According to beam theory, these internal forces are considered at a base point connected through rigid links with the bottom circumference. Thus, the final values of the analytical load factors follow:

If in Eq. (3-12) the total axial force is replaced by the numerical reaction N=1811kN instead of the simplified calculation of 1863kN, then the normal stress results σ_N=6.3MPa. Furthermore, in Eq. (3-13), the bending moment is replaced by the numerically calculated value of M=10981.1kNm and, therefore, the resulting bending stress is σ_B=22.07MPa. The final total stress value is, from Eq. (3-14), σ_{tot}=28.4MPa and this is adopted throughout the following analytical calculations.

Eventually, considering the afore-calculated value of σ_{tot}, the corresponding buckling load factor, based on Elastic Buckling Theory, is defined by Eq. (3-16), and results in λ=16. The corresponding analytical collapse load factor λ by CICIND is equal to λ=3.76 (from Eq. (3-22)).

4.6.1 COMPARISON BETWEEN BUCKLING LOAD FACTORS

The analytical buckling load factor is equal to 16, while the numerically obtained buckling load factor is equal to 12.3. This practically means that the analytical prediction is unsafe and highlights that, using beam theory considerations in combination with the use of classical elastic buckling theory, cannot be of practical use, as many important features are not taken into account in such case.

4.6.2 COMPARISON BETWEEN COLLAPSE LOAD FACTORS

In this section, comparison between the numerically obtained results with GMNA and the analytical results found with the use of the CICIND provisions is made. It should be noted that GMNA takes into account geometrical and material nonlinearity in the most efficient way a numerical tool can offer today. Initial imperfections are not taken into account, according to a type of buckling mode shape, but the significant deformations induce a type of imperfection, as also stated in previous sections. On the other hand, the analytical approach refers to the unstiffened structure and takes into account initial imperfections, geometrical and material nonlinearity, but, in a simplified way, that contains many assumptions. In Figure 4-41, it is obvious that a load factor equal to 4.25 has been found, for the unstiffened structure with GMNA, which is close to the one found by using the provisions of CICIND (3.76). In Figure 4-42, a detail of the equilibrium paths is presented in the region in which the GMNA's equilibrium path reaches its maximum load factor. It is observed that plastification appears for a load factor smaller than the one that corresponds to failure according to CICIND. This means that the CICIND load factor is not associated with the first yield, in this specific case, according to the numerically obtained results. Nevertheless, it remains on the safe side being smaller than the collapse load factor found with GMNA.

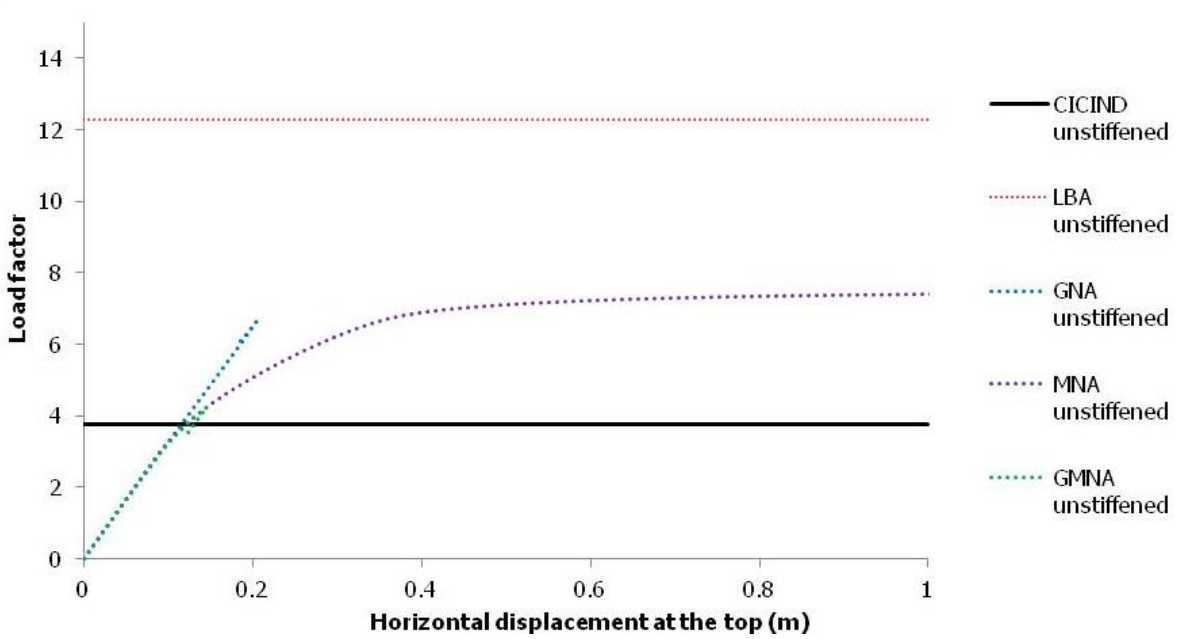

Figure 4-41: Comparison of equilibrium paths between the analytical and numerical approach

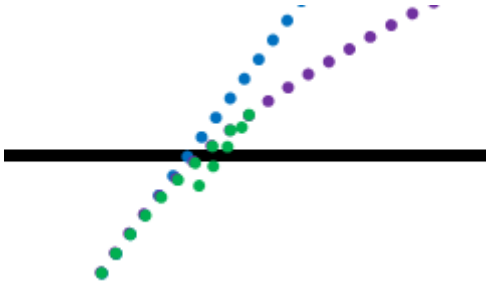

Figure 4-42: Detail of equilibrium paths of the analytical and numerical approach

4.7 SUMMARY AND CONCLUSIONS

In the present chapter, the results obtained for the unstiffened and stiffened structures were presented by making use of both numerical and analytical procedures, but mainly focusing on the numerical ones. The results were presented by means of equilibrium paths, deformed shapes and spread of plastifications. The main conclusions can be summarized as:

1) A mesh size of 0.07m proved to be sufficient for the numerical modeling of both unstiffened and stiffened structures, such as the ones presented herein. This result was verified by performing mesh sensitivity analyses, including LBA and nonlinear analyses.

2) Buckling and failure takes place in regions, in both the unstiffened and stiffened structures, that cannot be predicted by making use of beam theory that is based on simplified assumptions. This differentiation is mainly attributed to the fact that the direct application of wind pressures on the thin shell walls and their corresponding deformation are not taken into account by simplified beam theory.

3) The unstiffened structure collapses due to a combination of geometrical and material nonlinearity. Its deformed shape is significantly modified due to the direct application of pressures to its walls. As a result, the cross-sectional shape was no longer circular, in the cases investigated.

4) The stiffened structure collapses mainly due to material nonlinearity, as the geometrical one is significantly mitigated by the stiffening appearance of the circumferential rings.

5) The provisions of CICIND were found to be satisfactory, as far as the collapse load factor of the unstiffened structure (based on GMNA) is concerned, for the specific case investigated. Nevertheless, the conclusion that they will be satisfactory for other cases cannot be drawn, because their assumptions are not valid, as proved by the region of failure.

It is also concluded that, since the stiffener impact was considered as significant for the structure response, different parameters of stiffeners, such as the stiffener intervals and their stiffness, could be investigated, not only for investigation reasons, but also for optimization between capacity and economy. Such investigation follows in the next chapter.

5 IMPACT OF STIFFENER CHARACTERISTICS

5.1 INTRODUCTION

In this chapter, the impact of the stiffener spacing and of the stiffener stiffness is investigated. It was concluded in the previous chapter, that due to the thin shell of the structure and also due to wind pressure, local phenomena dominate against the overall buckling as a cantilever, in both the unstiffened and the stiffened structure, for 5m intervals of stiffeners. Such a conclusion was extracted by the performed nonlinear analyses and appropriate snapshots at the time of collapse. It was also noted that the stiffeners contribute significantly to the structure's capacity and also to the reduction of local deformation, and specifically, to the reduction of the changes of the cross-sectional shape. Hence, in the context of this chapter, the parameters of stiffener spacing and stiffness are investigated through linear and nonlinear numerical analyses.

5.2 IMPACT OF STIFFENER SPACING

Initially, different stiffener spacing cases are investigated. The chimney shell characteristics, for all the spacings and both for linear and nonlinear results, remain the same as the ones described in section 4.2. The stiffener's geometry and material do not change, too. The different spacing cases range from 20m to 2.5m. The cases of the unstiffened structure and of 5m spacing have already been presented, but they are shown here too, for completeness and comparison reasons. The investigated spacing cases are the following:

- 20m stiffener spacing (two stiffeners)
- 10m stiffener spacing (five stiffeners)
- 5m stiffener spacing (eleven stiffeners)
- 2.5m stiffener spacing (twenty three stiffeners)

5.2.1 IMPACT OF STIFFENER SPACING ON LINEAR ANALYSIS RESULTS

For all the spacing cases, LBA was carried out first in order to find the upper bound of the capacity of the structures.

5.2.1.1 UNSTIFFENED MODEL

As it was described thoroughly in the previous chapter, it is worth-noticing that the first buckling mode of the unstiffened model indicates buckling at the top, as shown in Figure 5-1, and even more, towards Y-Direction. Looking at the plan view, the deformation is almost symmetrical, due to the symmetrical wind pressure distribution. The buckling load factor to which the first buckling mode corresponds is equal to 12.3.

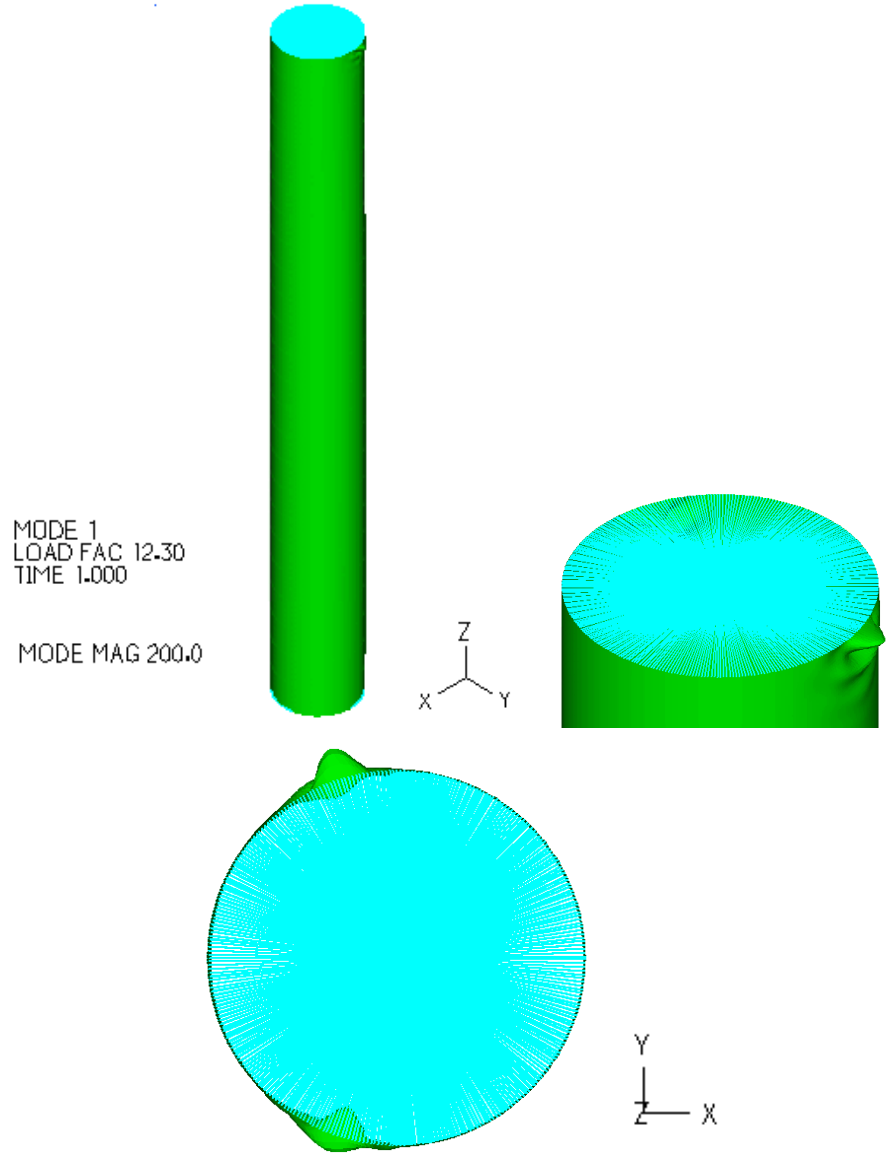

Figure 5-1: First buckling mode views of the unstiffened model

5.2.1.2 20 METERS SPACING

Initially, a spacing of 20m is investigated. In such a case, local buckling appears along a stiffening ring, as shown in Figure 5-2. This highlights the fact that the limited number of stiffening rings leads to their being significantly stressed. The buckling load factor is equal to 15.26, a value larger than the one found for the unstiffened structure.

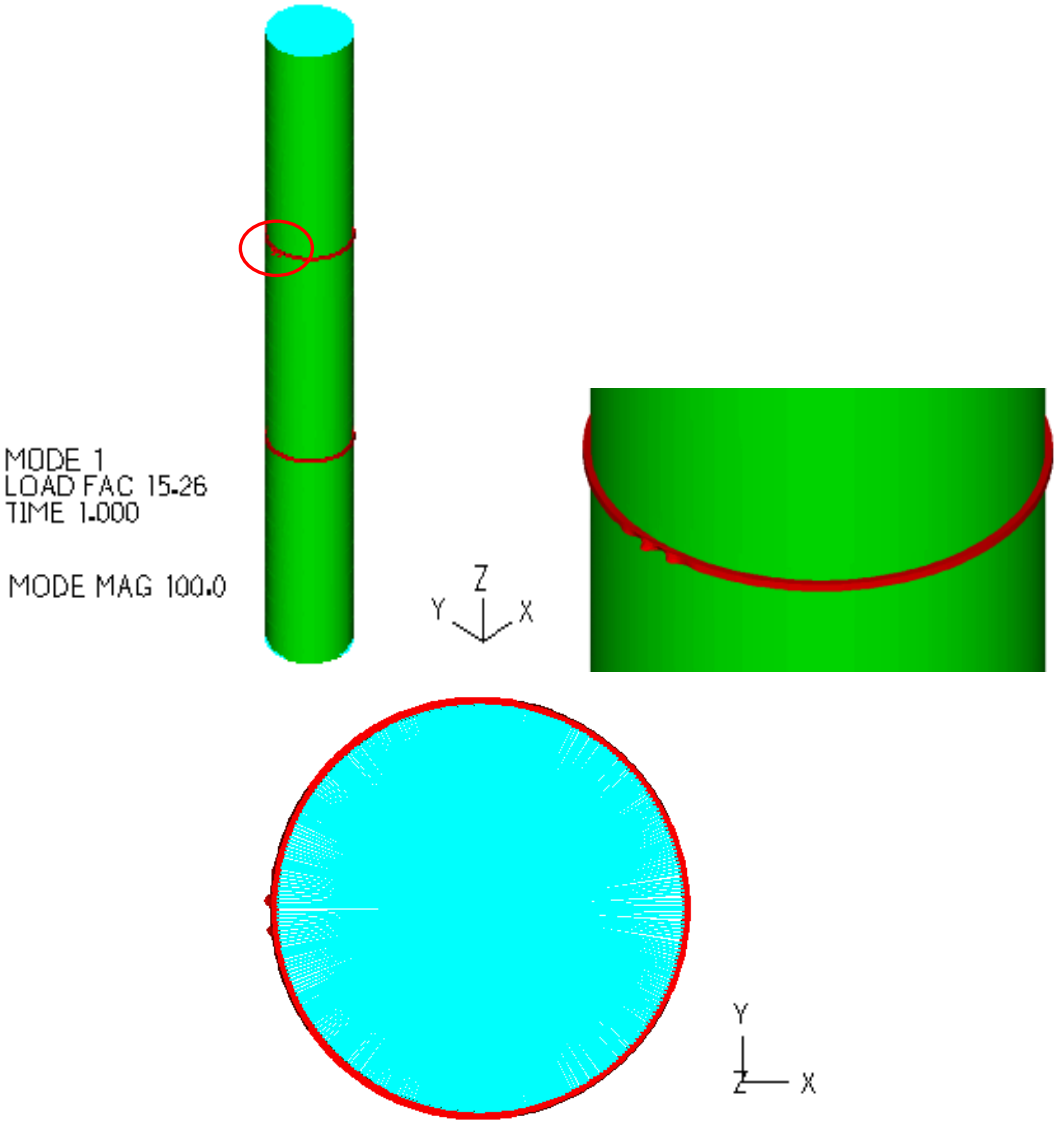

Figure 5-2: First buckling mode views of the stiffened model with 20m stiffener spacing

5.2.1.3 10 METERS SPACING

In this case, buckling is also observed in one of the stiffeners. Figure 5-3 shows the first buckling mode shapes. It is calculated that the strength increase is of the order of 14%, compared with the previous spacing case of 20m. The buckling load factor of the first buckling mode is equal to 17.42.

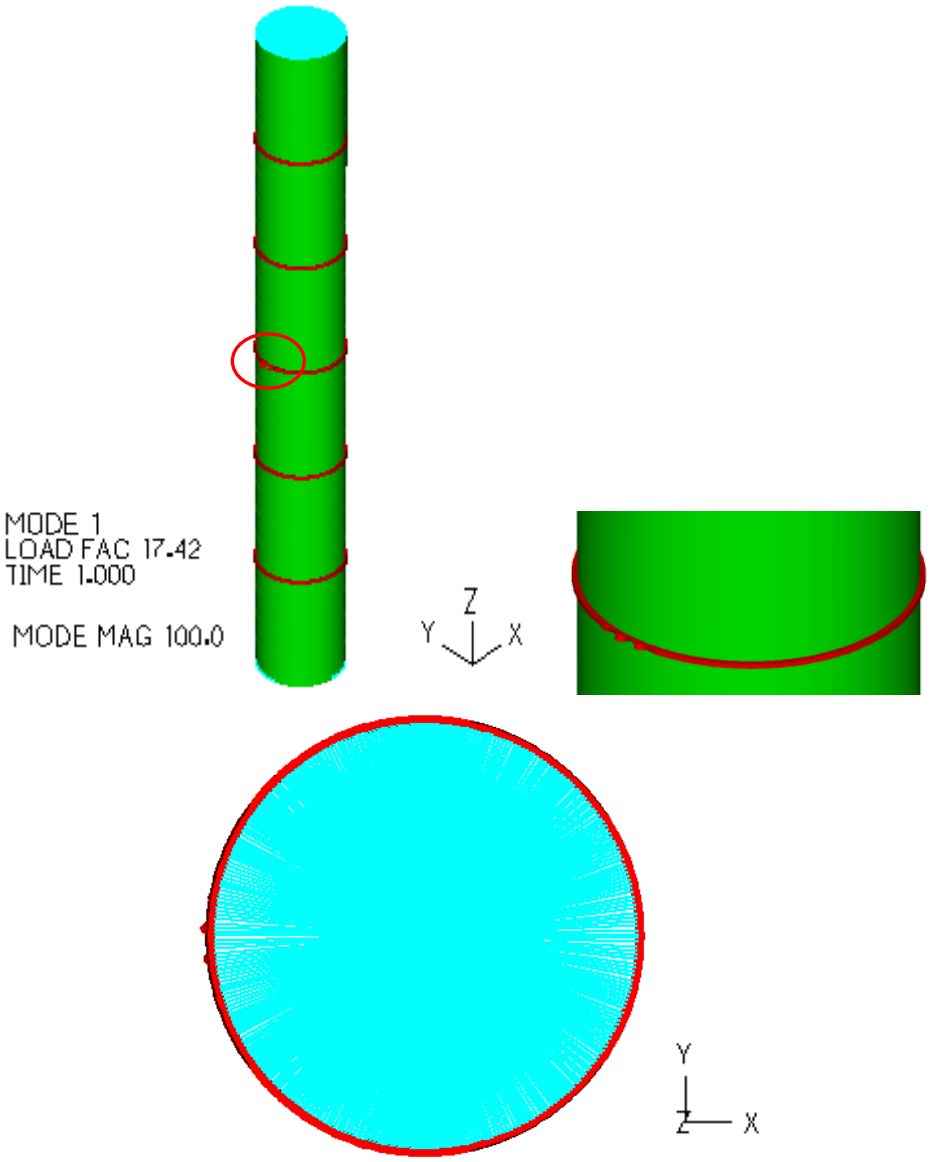

Figure 5-3: First buckling mode views of the stiffened model with 10m stiffener spacing

5.2.1.4 5 METERS SPACING

The spacing of 5m was thoroughly presented in the previous chapter. It is worth-mentioning that buckling appears in the shell for this case, as depicted in Figure 5-4, contrary to the stiffener spacing of 20m and 10m. This practically means that the number of the stiffeners is large enough to avoid appearance of buckling in one of the stiffeners. Another important thing to note is that buckling appears along Y-Direction that comes in contrast with what classical beam theory would predict. This differentiation is clearly attributed to the significant effect of wind pressure that modifies the cross-sectional shape, making a classical beam model inappropriate. The buckling load factor is this case is equal to 19.91.

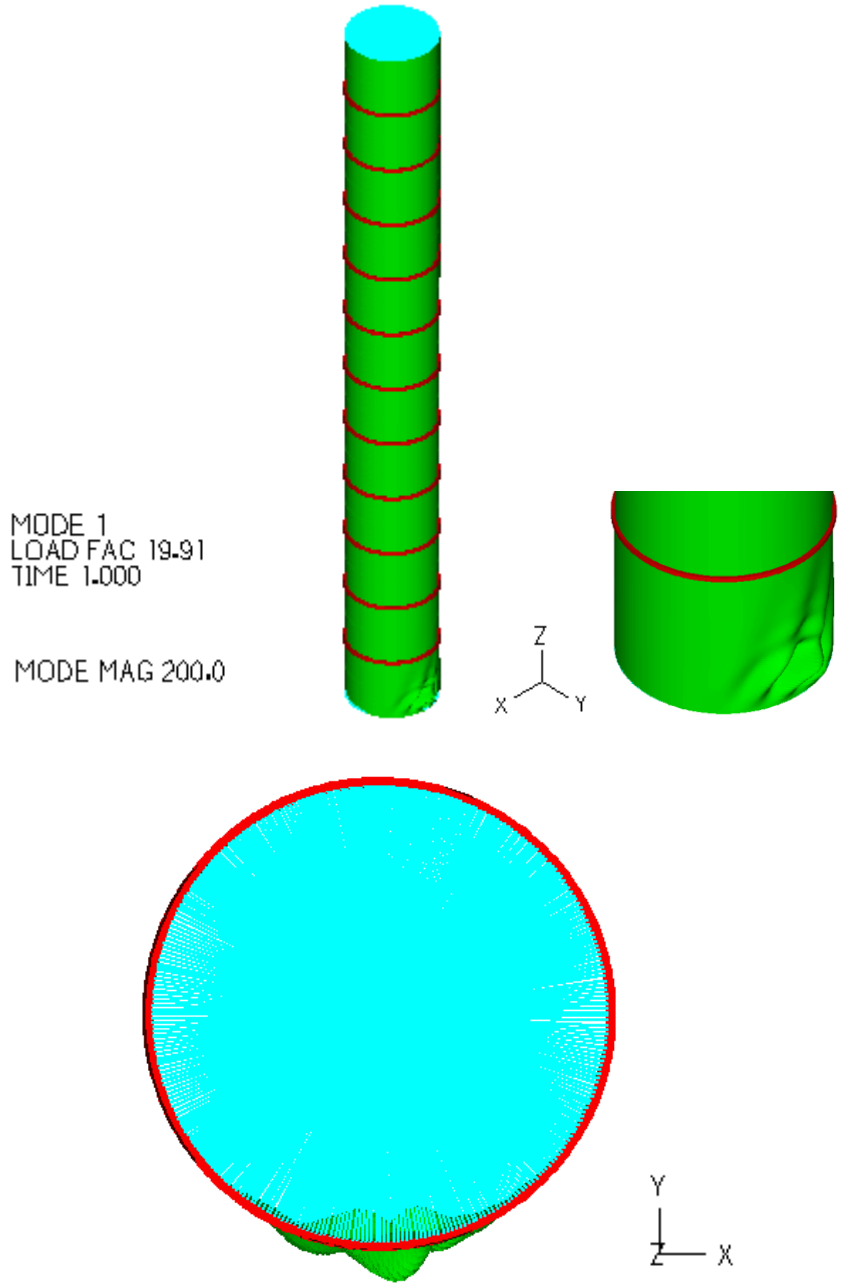

Figure 5-4: First buckling mode views of the stiffened model with 5m stiffener spacing

5.2.1.5 2.5 METERS SPACING

At last stage, a stiffener spacing of 2.5m is investigated. The fact that buckling appears, again, along Y-Direction (Figure 5-5) is related to cross-sectional shape changes, as mentioned for the case of 5m spacing. The strength increase between the previous (5m spacing) and the present case (2.5m spacing) is almost 9%. The buckling load factor of the first buckling mode is equal to 21.65.

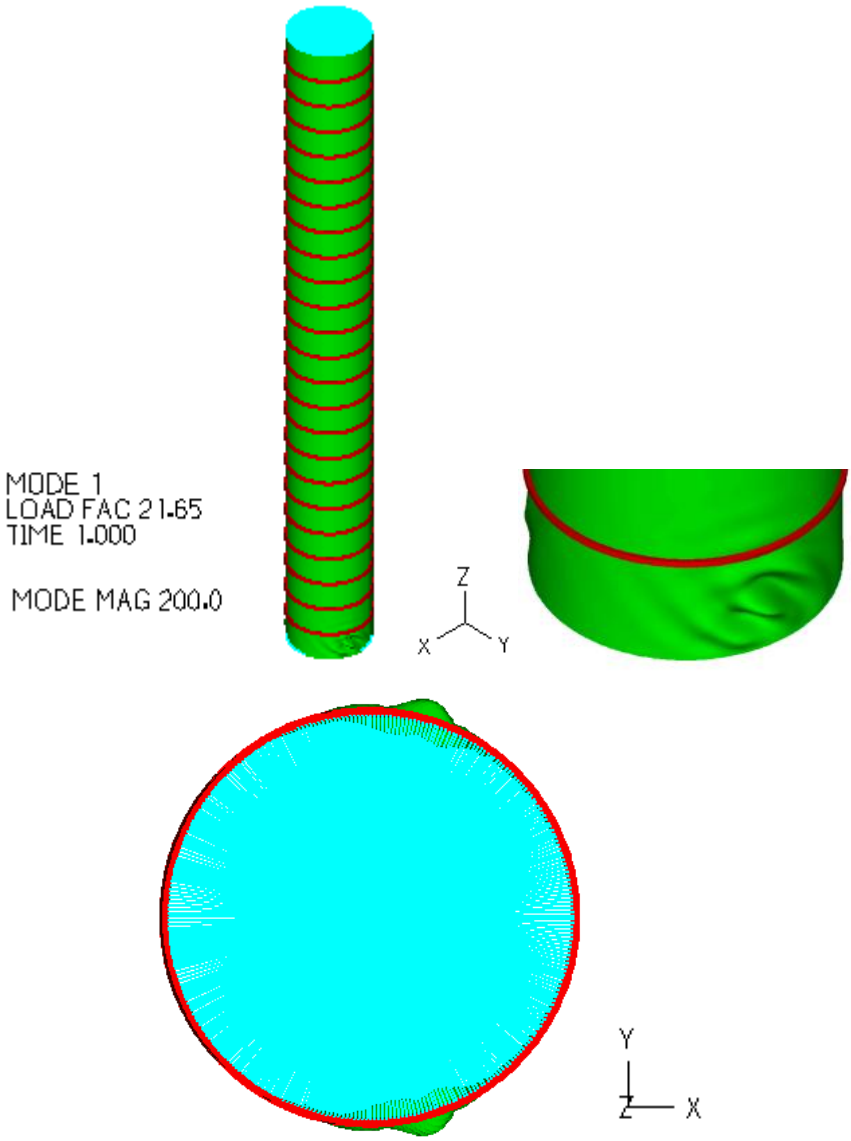

Figure 5-5: First buckling mode views of the stiffened model with 2.5m stiffener spacing

It can be seen that the larger the number of the ring stiffeners that are used, the smaller cross-sectional deformation that appears. For this reason, it is expected that a large number of stiffeners leads to behavior closer to the one predicted by classical beam theory. Additionally, the use of a large number of stiffeners decreases the possibility of failure along them.

5.2.1.6 COMPARISON OF BUCKLING LOADS FOR VARIOUS SPACINGS

Based on Figure 5-6, it can be observed that the strengthening that is achieved is smaller as we approach a very dense arrangement of stiffeners. For instance, if only two stiffeners are used in the unstiffened structure, a strength increase equal to 24% is observed. On the other hand, making use of more than ten times more stiffeners (23 stiffeners when having a 2.5m spacing) leads to an increase equal to 76% in the buckling load factor. This increase is not proportional to the much larger number of stiffeners that have been used in the very dense arrangement of stiffeners. This means that the design engineer should carefully balance the advantages and disadvantages that may arise from a very dense arrangement of stiffeners in order to find an optimum solution (in terms of strength, stiffness and cost).

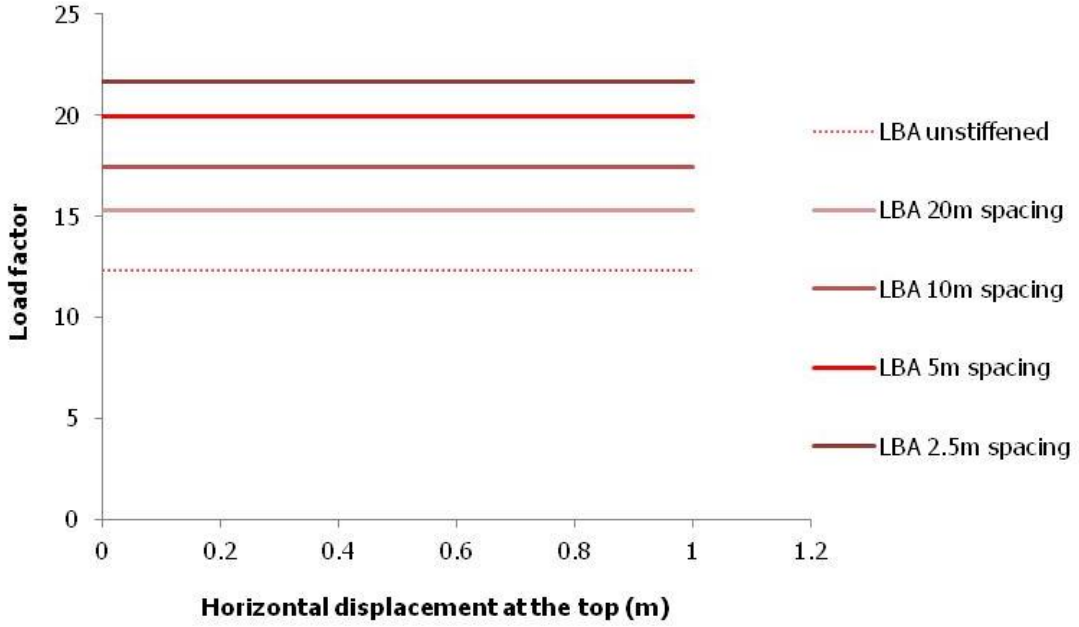

Figure 5-6: Comparison of first buckling load factors obtained with LBA between different stiffener spacing cases

5.2.2 IMPACT OF STIFFENER SPACING ON NONLINEAR ANALYSES RESULTS

Nonlinear analyses of the different stiffener spacing cases follow the LBA, so as more reliable information about the chimney capacity and deformation at collapse to be extracted. The used model is the same as the one described in section 4.4.2.1, for nonlinear analyses. In this section, the equilibrium paths of linear and nonlinear analyses, for each stiffener spacing case, are shown.

Looking at the next five figures (Figure 5-7, Figure 5-8, Figure 5-9, Figure 5-10 and Figure 5-11), a first notification is that GMNA, in all stages, results in the lowest collapse load factor, compared with the other nonlinear analyses. It is therefore concluded that regardless of the number of the stiffeners on the structure, when both nonlinearities take place, the structure capacity is reduced. Since GMNA is regarded the most representative nonlinear analysis, the collapse load factor predicted by it, is considered as the closest to the realistic one. Nevertheless, it is worth-comparing the other nonlinear analyses, too, for completeness.

When no stiffeners are used, the ultimate strengths that the GNA and MNA predict are of similar magnitude. As the distance between successive stiffeners is reduced, it can be seen that the ultimate strength found with GNA becomes larger than the one obtained with MNA. This leads to the obvious conclusion that the main effect of the stiffeners is related to geometrical nonlinearity. For this reason, their effect is larger when the material is elastic. The afore-mentioned fact reminds a similar conclusion, presented in section 4.5, where comparison between the unstiffened and stiffened model had been carried out. It had been observed that ring stiffeners increase the structure's capacity more when the material is elastic or a high yield limit is used.

Another interesting conclusion is that the collapse load factors obtained with GMNA and MNA are getting closer, as smaller spacing is used. This practically means that when the arrangement of the stiffeners is very dense, the material nonlinearity is the one governing failure. Of course, as geometrical nonlinearity is still present, the ductility of the structure after the collapse load factor is much smaller in the case of GMNA when compared with MNA.

5.2.2.1 UNSTIFFENED MODEL

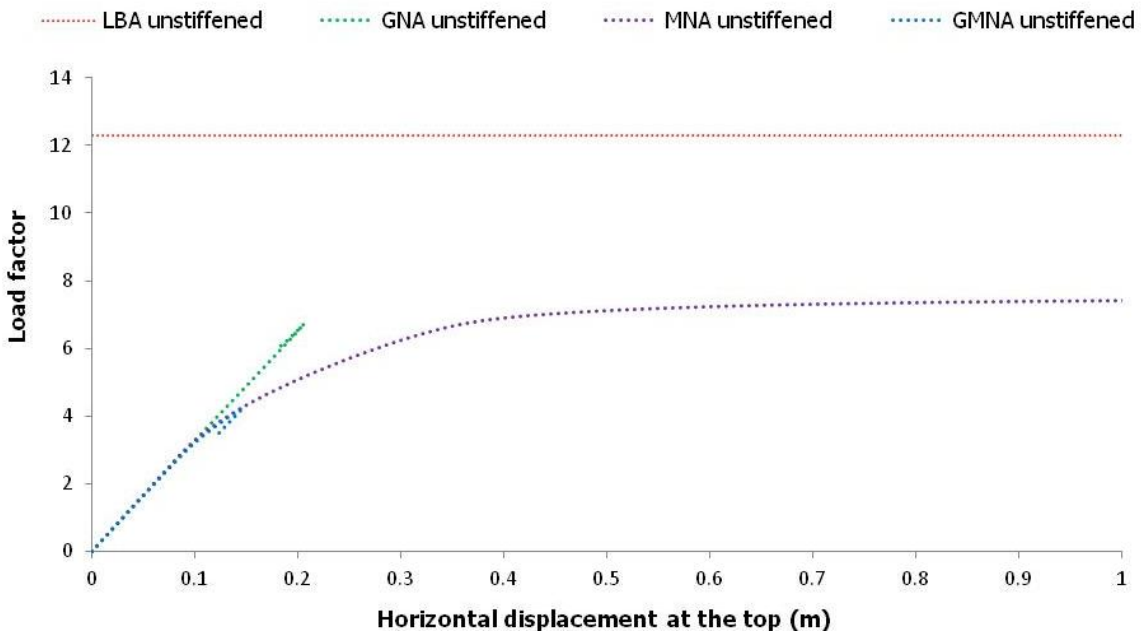

Figure 5-7: Comparison of equilibrium paths obtained with different analyses of the unstiffened model

5.2.2.2 20 METERS SPACING

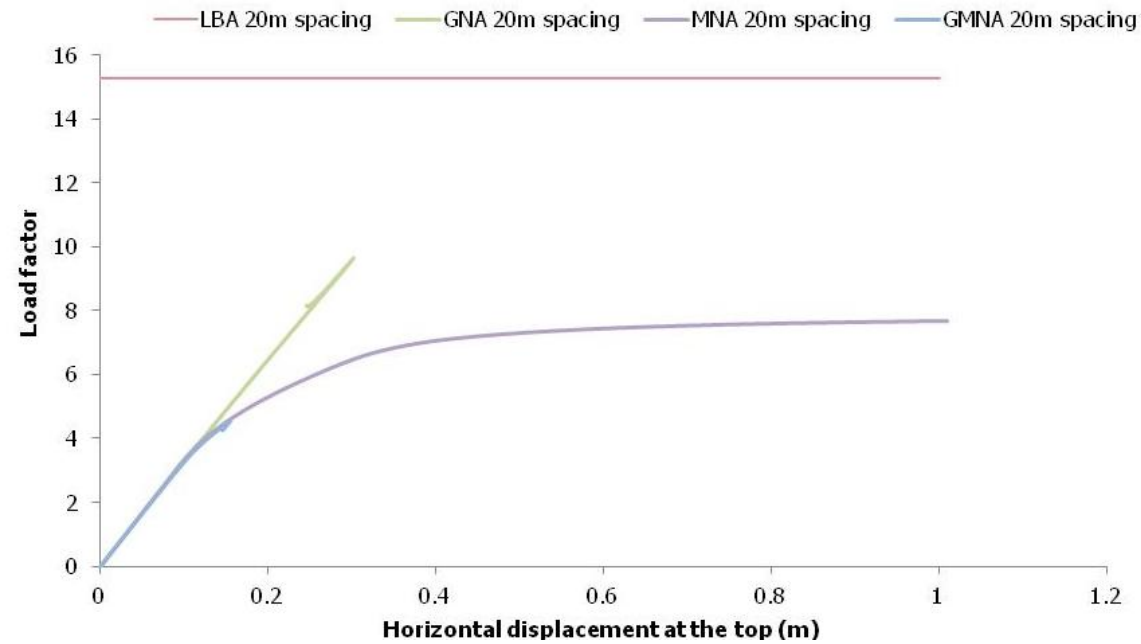

Figure 5-8: Comparison of equilibrium paths obtained with different analyses of the stiffened model with 20m stiffener spacing

5.2.2.3 10 METERS SPACING

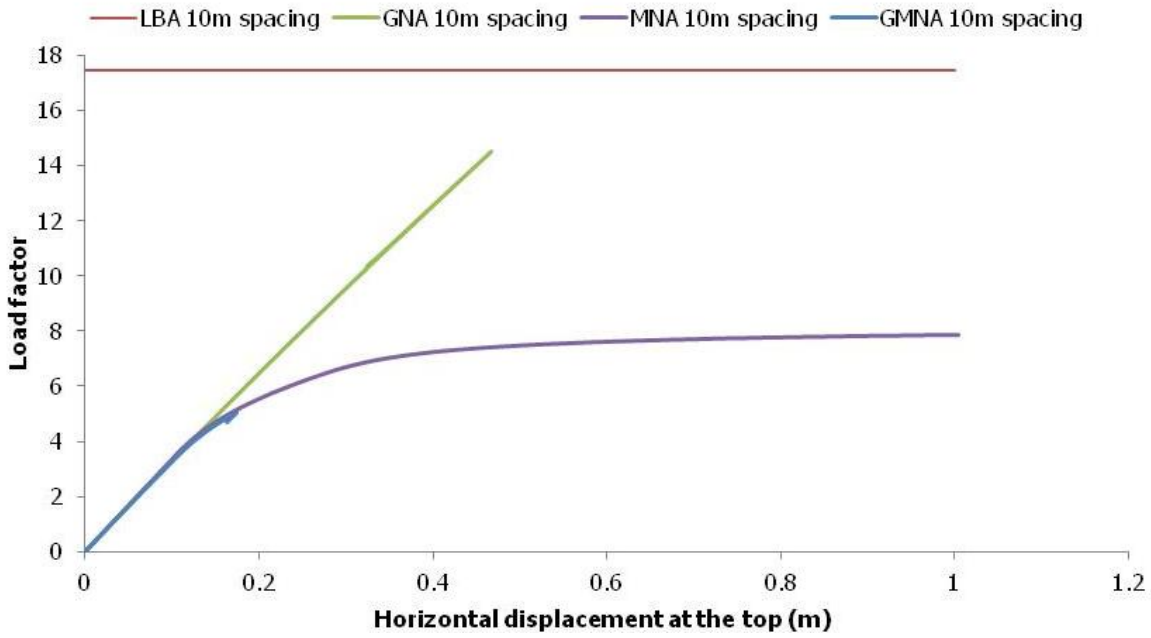

Figure 5-9: Comparison of equilibrium paths obtained with different analyses of the stiffened model with 10m stiffener spacing

5.2.2.4 5 METERS SPACING

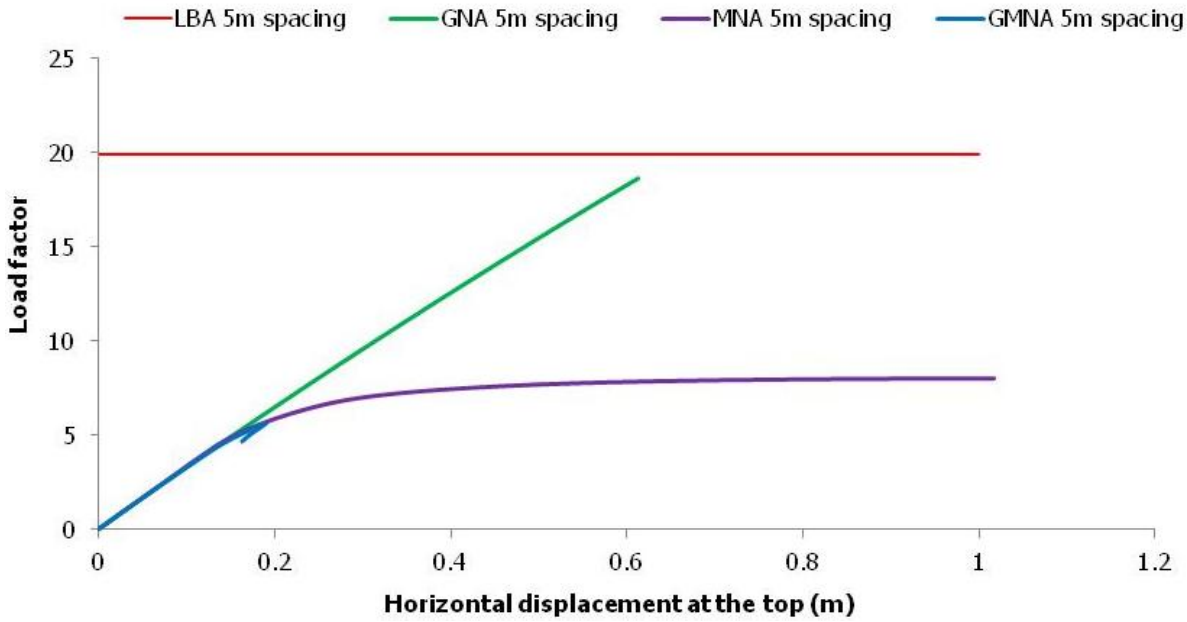

Figure 5-10: Comparison of equilibrium paths obtained with different analyses of the stiffened model with 5m stiffener spacing

5.2.2.5 2.5 METERS SPACING

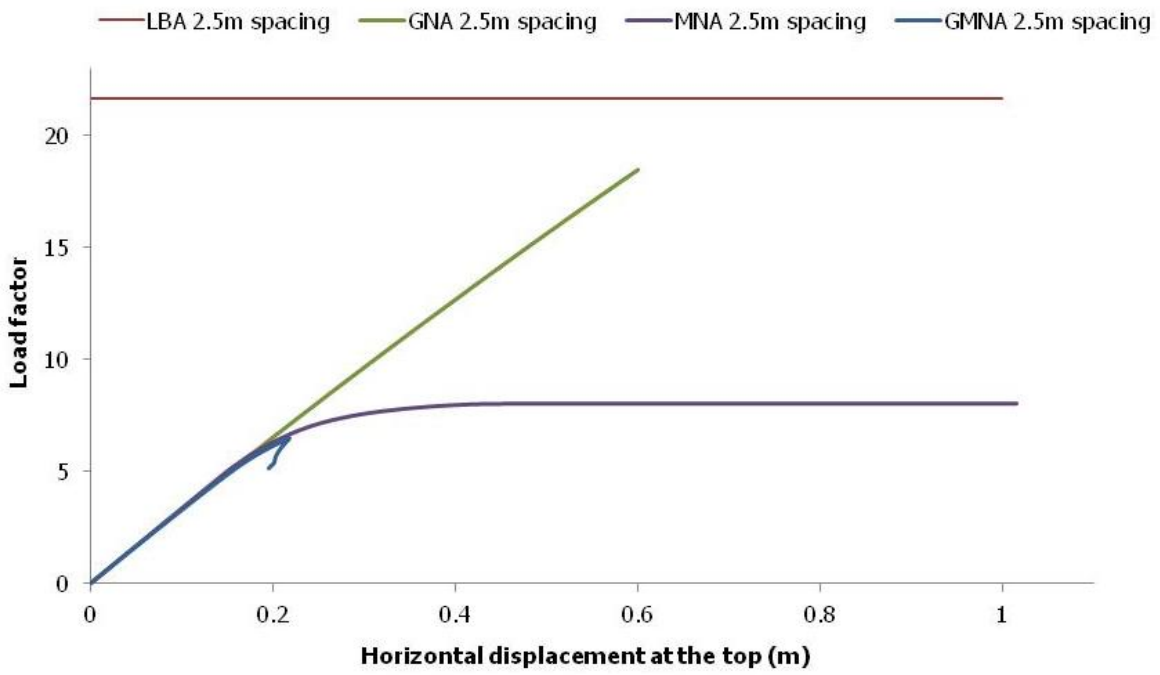

Figure 5-11: Comparison of equilibrium paths obtained with different analyses of the stiffened model with 2.5m stiffener spacing

5.2.2.6 COMPARISON OF RESPONSES FOR VARIOUS SPACINGS

- GNA results

In Figure 5-12, the equilibrium paths obtained with GNA are illustrated. The structure capacity is significantly higher in the case of the very dense stiffener arrangement than the one of the unstiffened structure. This is attributed to the fact that the denser stiffening restricts the cross-sectional changes due to the local buckling. It is also observed that regardless of the number of the stiffeners, the same stiffness is appeared in every case. Hence, it is concluded that the cantilever component of deformation is not affected by the presence of stiffeners.

It is surprising, though, that the collapse load factor of the stiffener spacing of 2.5m is slightly lower than the one of 5m spacing. This observation possibly highlights the fact that the two spacing cases deform in a different way at failure, since only geometrical nonlinearity is taken into account.

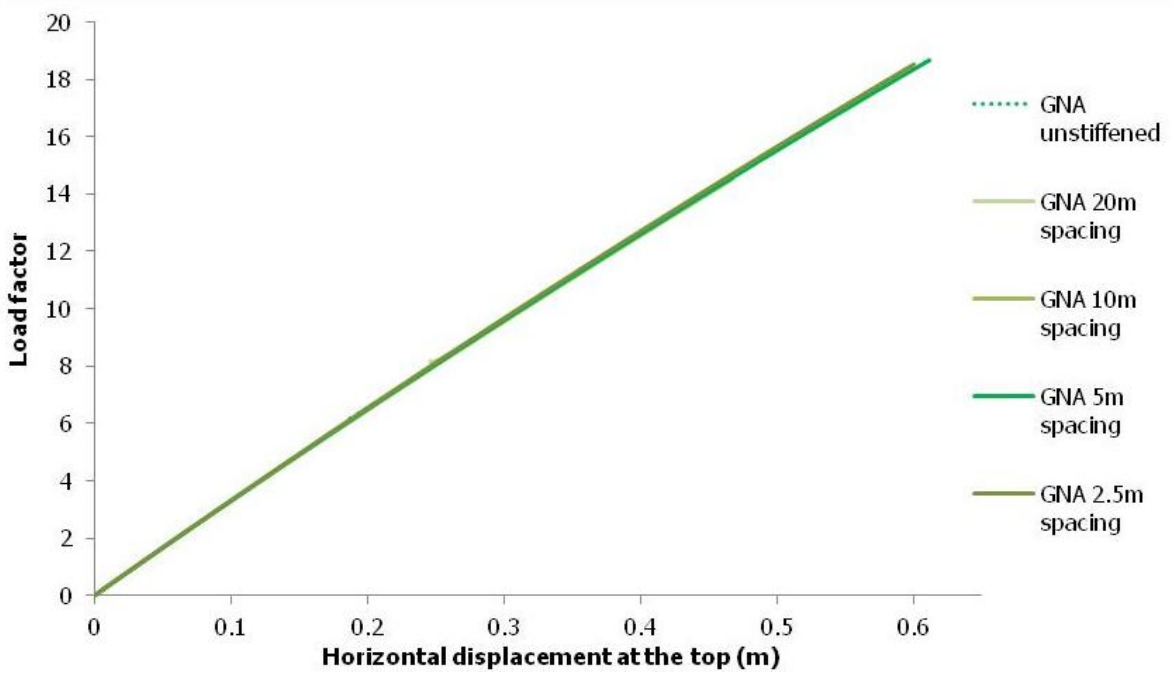

Figure 5-12: Comparison of equilibrium paths between different stiffener spacing cases obtained with GNA

- MNA results

As it was mentioned earlier in this chapter, the collapse load factors for the different spacings found with MNA remain practically at the same values (Figure 5-13). Hence, the afore-stated conclusion that the stiffeners contribute significantly to the structure capacity when geometrical nonlinearity takes place, is also drawn in this case.

However, the first yielding is significantly affected by the stiffener arrangement. Hence, in Figure 5-13 it is observed that as the spacing is getting smaller, the first yielding occurs for a higher value of collapse load factor. For instance, the first plastification for the unstiffened structure takes place at a collapse load factor equal to 3.5, while for the 2.5m stiffened structure the collapse load factor at the first yielding moment is equal to 6. It is therefore concluded that the denser the stiffener arrangement is, the more the first yielding is delayed.

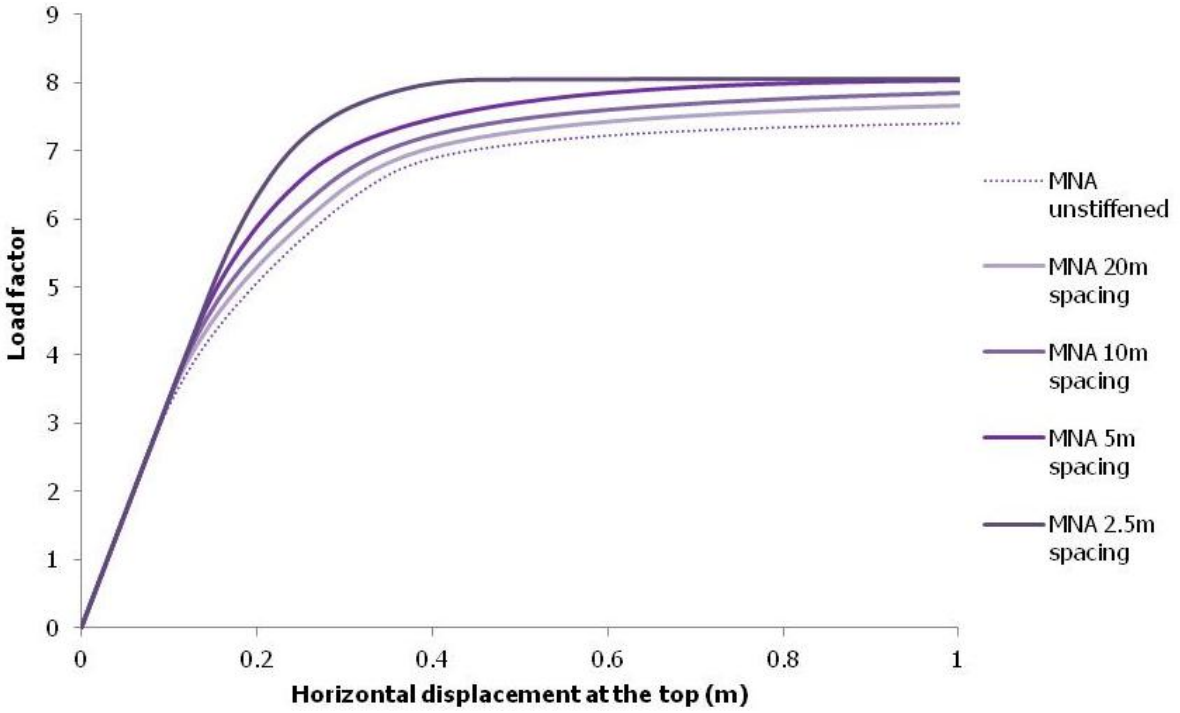

Figure 5-13: Comparison of equilibrium paths between different stiffener spacing cases obtained with MNA

- GMNA results

In Figure 5-14, it is obvious that the strengthening is bigger as a denser stiffening is used. Hence, when two stiffeners are used (20m spacing) the strength increase is 5%, compared with the unstiffened structure. On the other hand, when twenty three stiffeners are used (2.5m spacing) the strength increase is equal to 54%. This comes in contrast with the afore-presented LBA predictions. GMNA results come also in contrast with GNA's prediction about strength reduction at 2.5m spacing, compared with the 5m spacing. The last observation may be attributed to the introduction of material nonlinearity in the case of GMNA, compared with GNA.

In Figure 5-14, it is also observed that the different spacings appear the same stiffness. The stiffness is related to the cantilever component of deformation. As stated earlier, it is concluded that the cantilever deformation is not affected by the stiffener presence. The curves of the different spacing cases, though, start to diverge at different values of collapse load factors. This deviation is attributed to the first yielding, as it is more obvious in Figure 5-7, Figure 5-8, Figure 5-9, Figure 5-10 and Figure 5-11. In these five figures, it is observed that when the structure loses its initial stiffness according to GMNA, the structure according to GNA appears the same value of stiffness.

According to GMNA results shown in Figure 5-14, the increase of the stiffener number on the chimney is of great importance, as far as the capacity is concerned. Moreover, the deformation is affected dramatically by the denser stiffening. Hence, in Figure 5-15 it is observed that in the case of 2.5 spacing, smaller cross-sectional changes take place, compared with the ones of the unstiffened structure. However, the very dense stiffener arrangement does not restrict completely the local phenomena. This leads to the investigation of other stiffener parameters as well, such as the stiffener stiffness, as following.

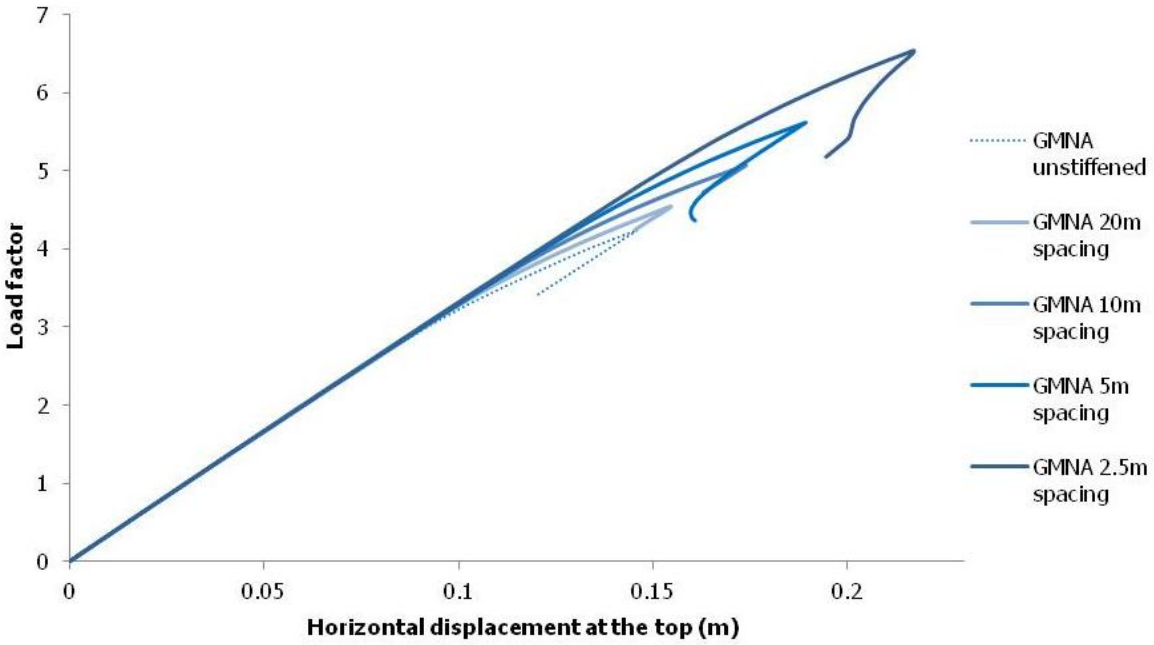

Figure 5-14: Comparison of equilibrium paths between different stiffener spacing cases obtained with GMNA

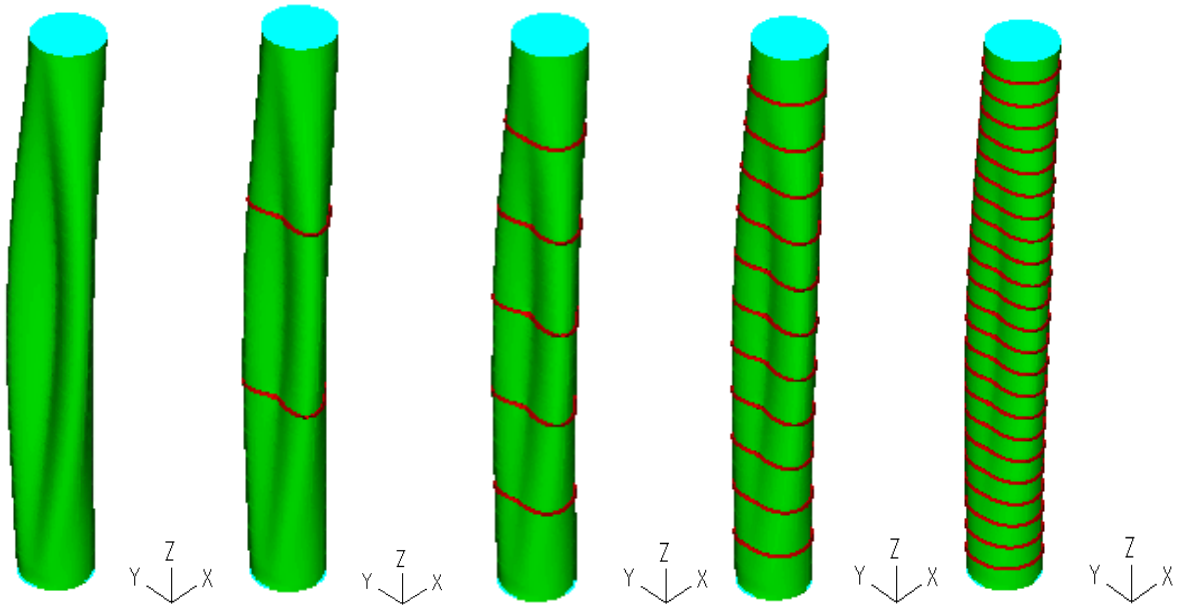

Figure 5-15: Comparison of 3-Dimensional views of deformed shapes at failure from GMNA between the unstiffened (first), the stiffened with 20m spacing (second), the stiffened with 10m spacing (third), the stiffened with 5m spacing (fourth) and the stiffened model with 2.5m spacing (last)

Summarizing, the load factors of the different analyses and for the different stiffener spacing cases are showed in Table 5-1.

Table 5-1: Comparison of chimney's load factors between the different analyses and different stiffener spacing cases

	LBA	GNA	MNA	GMNA
Unstiffened	12.3	6.73	7.42	4.24
20m spacing	15.26	9.63	7.67	4.54
10m spacing	17.42	14.53	7.85	5.06
5m spacing	19.91	18.68	8.03	5.62
2.5m spacing	21.65	18.50	8.05	6.53

5.3 IMPACT OF STIFFENER STIFFNESS

Although the use of very stiff and elastic rings is not a very realistic option, it can be proved useful for identifying the effectiveness of the specific ring cross-section (L120x120x10) that is employed in the present investigation. It is expected that very stiff and elastic rings prohibit cross-sectional deformations to a very significant extent [3]. In the finite element model, the chimney shell material is the same as the one described in section 4.2. The stiffener material changed to elastic in all cases (even in nonlinear analyses) and rigid ($E=2.025x10^{11}$), so as very stiff stiffeners to be created. As far as the other characteristics are concerned, they remain the same as the ones described in section 4.2. Throughout this chapter, the case of 5m spacing with rigid and flexible rings is investigated.

5.3.1 IMPACT OF STIFFENER STIFFNESS ON LINEAR ANALYSIS RESULTS

The buckling load factors obtained with LBA are presented in Figure 5-16. The stiffened structures have buckling load factors that are larger than the one corresponding to the unstiffened structure. Hence, the effect of the stiffening rings (flexible or rigid) is obvious. The unexpected fact is that the buckling load factor using rigid rings is lower than the one using flexible rings. The first buckling load of the rigidly stiffened structure is equal to 17.26 and the first buckling mode shape is shown in Figure 5-17. It can be seen that the region at which local buckling appears coincides with the beam theory's prediction for +X-Direction of the wind.

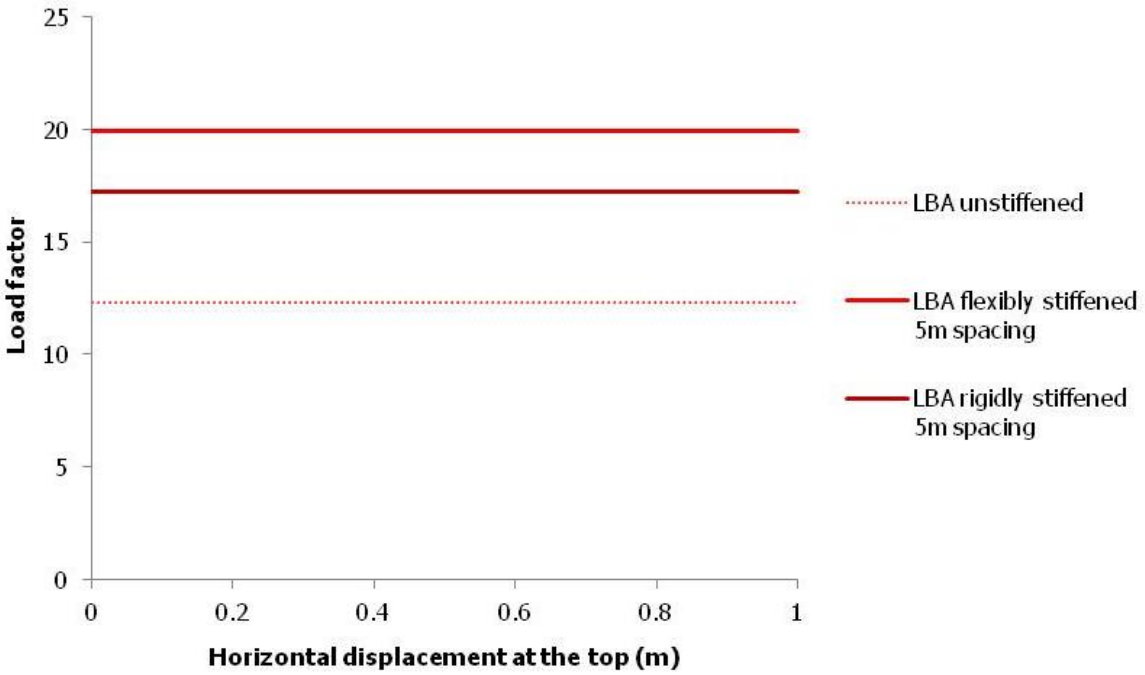

Figure 5-16: Comparison between the buckling load factors of the unstiffened, the flexibly stiffened and the rigidly stiffened model with 5m spacing obtained with LBA

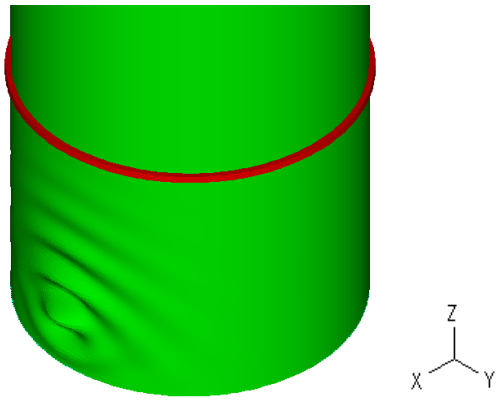

Figure 5-17: First buckling mode of the rigidly stiffened structure with 5m spacing

5.3.2 IMPACT OF STIFFENER STIFFNESS ON NONLINEAR ANALYSIS RESULTS

5.3.2.1 GNA RESULTS

In Figure 5-18, the equilibrium paths obtained with GNA for the unstiffened, the flexibly stiffened and the rigidly stiffened model are depicted. It is interesting to observe that the presence of stiffeners (flexible or rigid) leads to a significant capacity increase, as it has already been stated in the previous section. This highlights that the ring stiffeners contribute significantly to the reduction of cross-sectional changes, since in GNA only geometrical nonlinearity is taken into account. Additionally, it is worth-mentioning that the buckling load factor obtained with LBA (=17.26) is practically of the same magnitude as the collapse load factor found with GNA (=16). Hence, it is concluded that prebuckling deformations are of insignificant importance when rigid rings are used, because they dramatically restrict the local deformations due to wind.

In the case of rigid rings, the cross-sectional changes are restricted completely and the chimney buckles as a cantilever (Figure 5-19). This comes in contrast with the deformation of the flexibly

stiffened structure (Figure 5-20). The surprising fact is that the rigidly stiffened structure has a lower collapse load factor than the flexibly stiffened one.

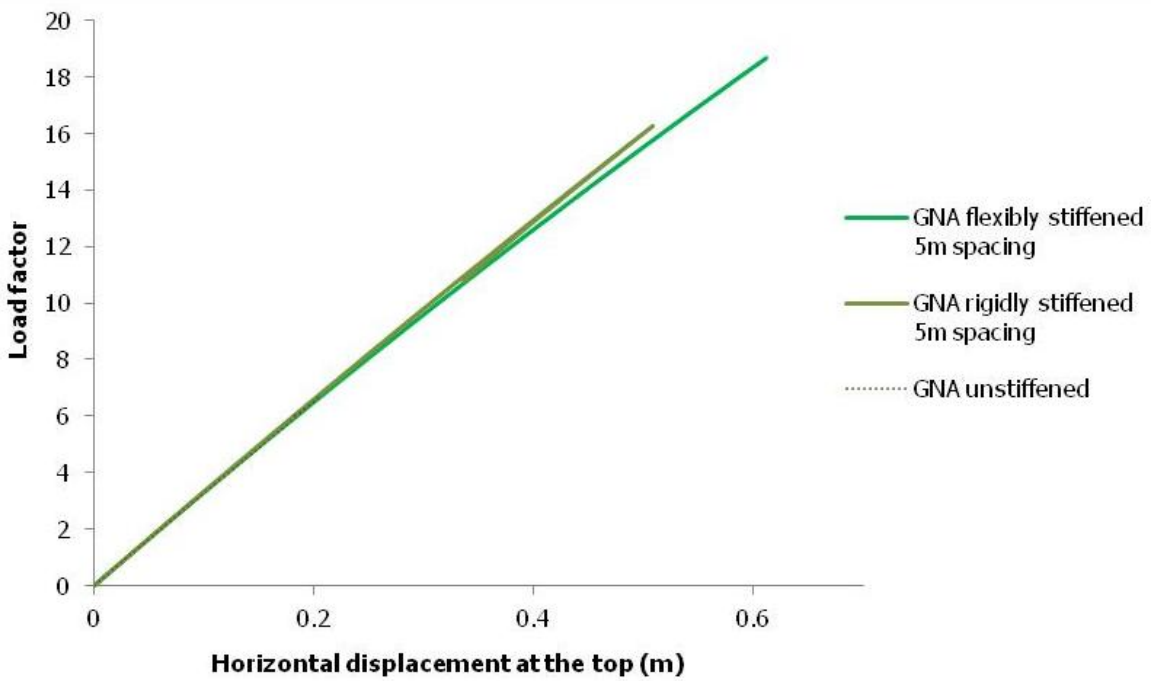

Figure 5-18: Comparison of equilibrium paths of the unstiffened, the flexibly stiffened and the rigidly stiffened model with 5m spacing obtained with GNA

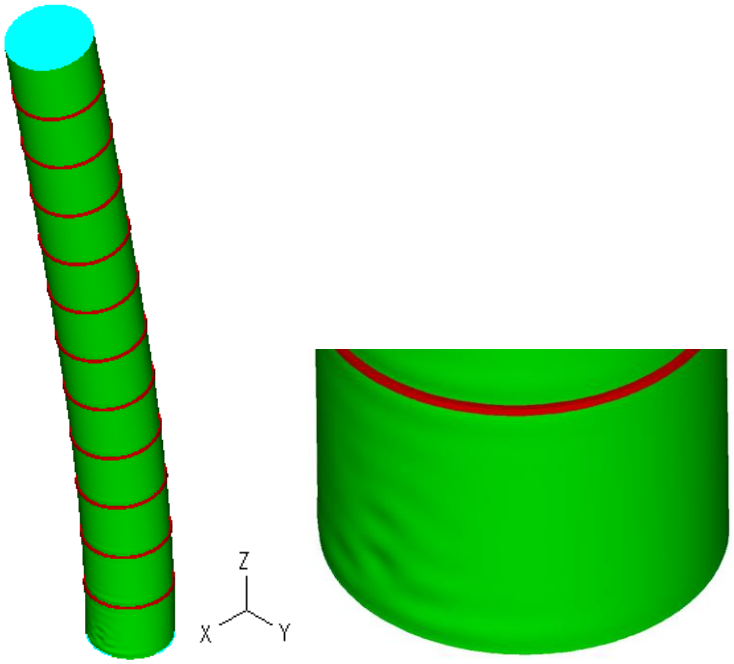

Figure 5-19: Deformation and local buckling at the base support according to GNA of the rigidly stiffened structure

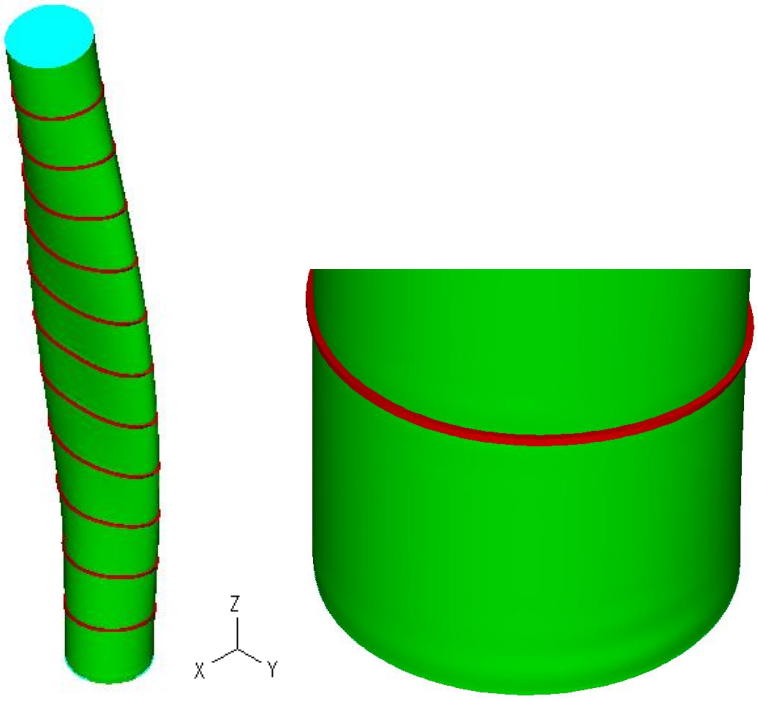

Figure 5-20: Deformation and close view of the base support according to GNA of the flexibly stiffened structure

5.3.2.2 MNA RESULTS

In Figure 5-21, the equilibrium paths found with MNA for the unstiffened, the flexibly stiffened and the rigidly stiffened model are depicted. The same conclusion as the one drawn by the previous analyses that the stiffened structures have higher capacity than the unstiffened structure is also found by MNA. In this case, though, the two stiffened structures have practically the same capacity. This leads to the conclusion that the capacity of the structure is not affected by the stiffener stiffness when only material nonlinearity is taken into account. However, the value at which the first yielding occurs is lower in the case of flexible rings than the one of rigid rings. Hence, the stiffener stiffness affects the time of first yielding in the structure.

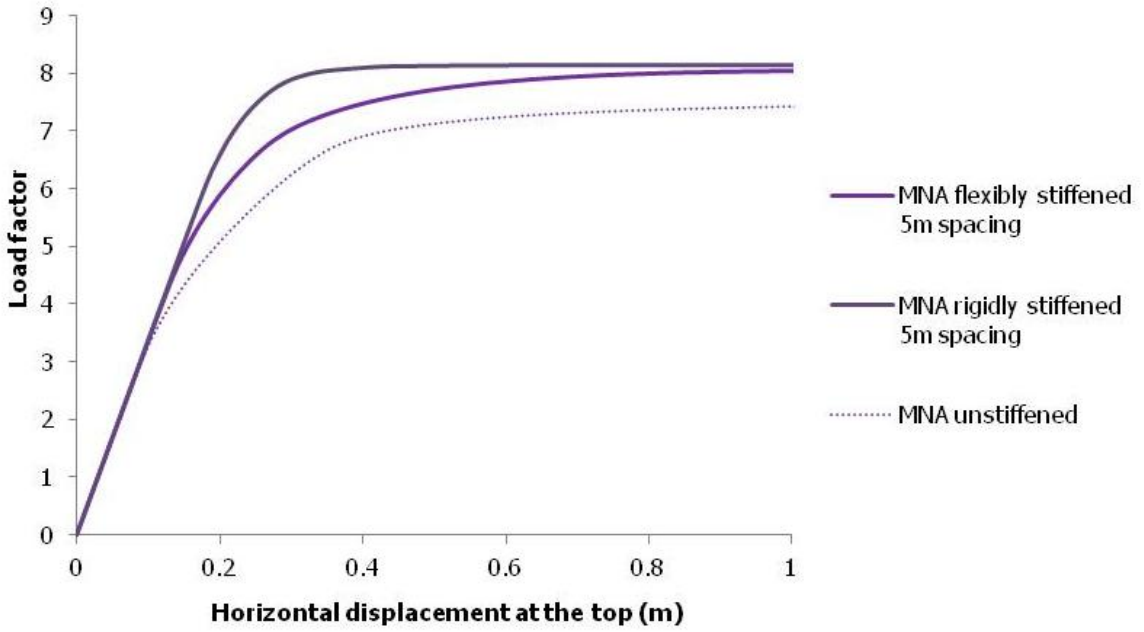

Figure 5-21: Comparison of equilibrium paths of the unstiffened, the flexibly stiffened and the rigidly stiffened model with 5m spacing obtained with MNA

5.3.2.3 GMNA RESULTS

The results obtained with GMNA are presented in Figure 5-22. It can be observed that the use of rigid and elastic rings does not increase the structure capacity, compared to the use of flexible and elastoplastic rings. This observation is similar to the one based on MNA. It is also observed in Figure 5-23 that the collapse load factor at which according to GMNA failure occurs corresponds to geometrical and material linearity according to GNA's and MNA's equilibrium path, respectively. Though, the combination of the two nonlinearities in GMNA leads to a reduced collapse load factor that is affected by both the material and geometrical nonlinearity. However, since MNA's collapse load factor is significantly lower than the GNA's one, it is concluded that material nonlinearity governs the failure time. Another interesting observation is that using rigid rings the structure behaves elastically until the collapse load, while using flexible rings the stiffness is reduced before the failure.

As shown in Figure 5-24 and Figure 5-25, no cross-sectional changes are observed in the rigidly stiffened model, but an overall (bending) buckling and yielding at the structure base are noticed. Hence, the structure behaves like a cantilever with the presence of rigid rings.

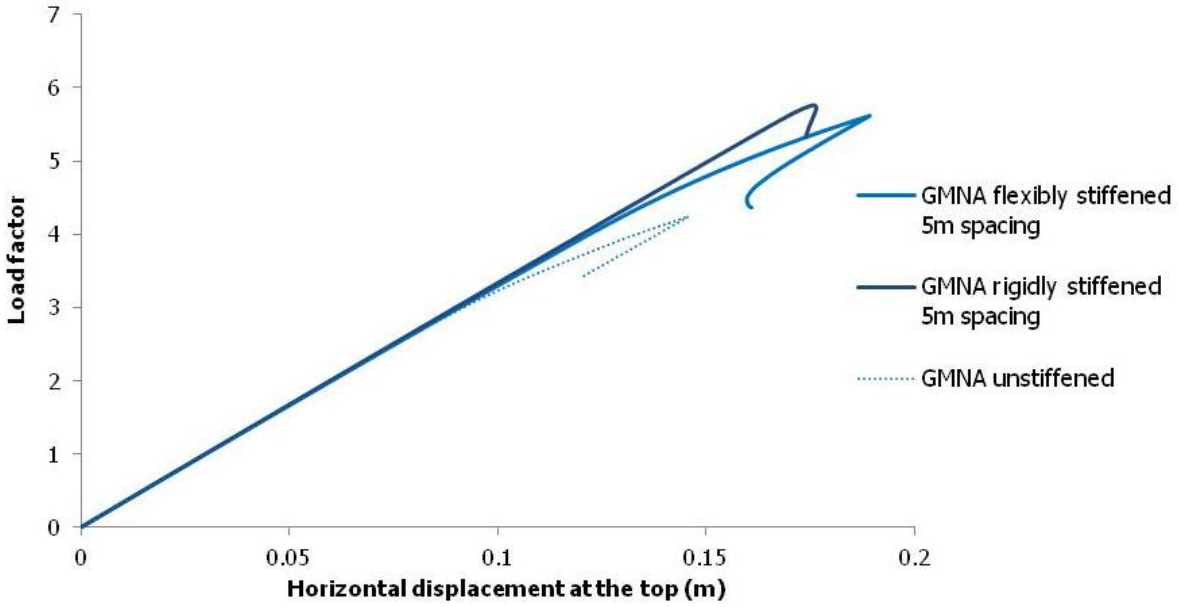

Figure 5-22: Comparison of equilibrium paths of the unstiffened, the stiffened and the rigidly stiffened model with 5m spacing obtained with GMNA

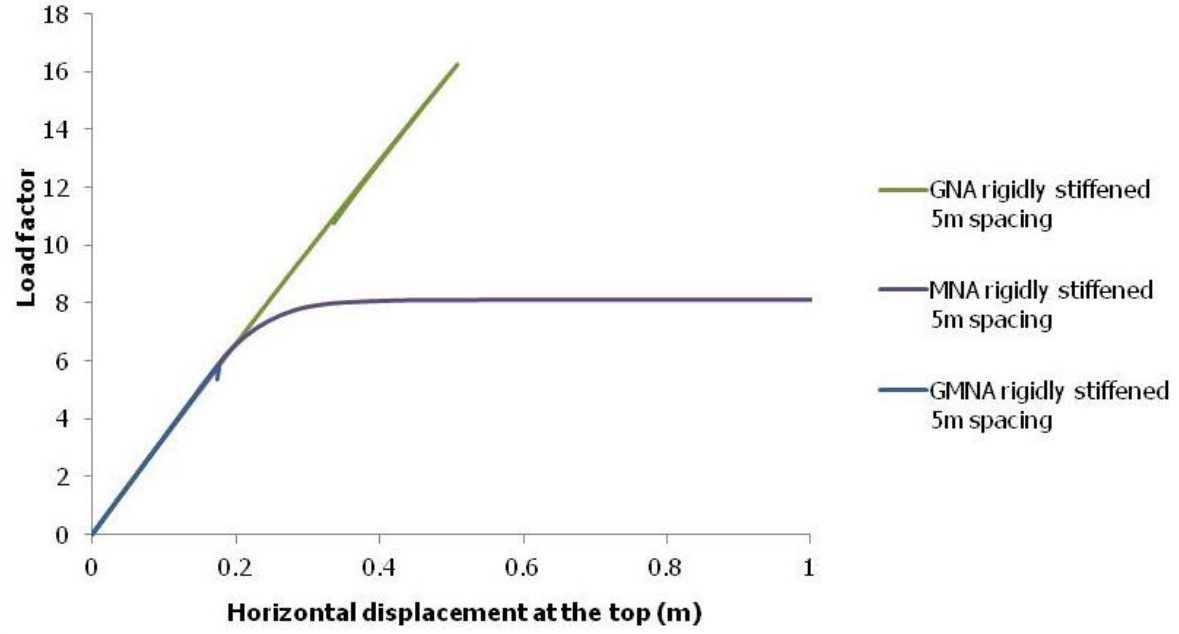

Figure 5-23: Comparison of equilibrium paths of different analyses of the rigidly stiffened model with 5m stiffener spacing

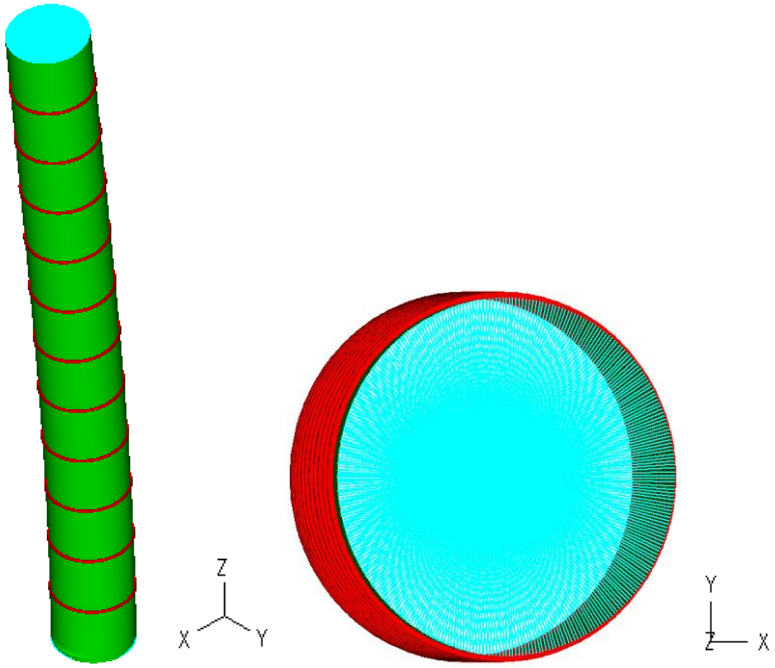

Figure 5-24: 3-Dimensional view and plan view of deformed shapes of the rigidly stiffened structure with 5m spacing at failure obtained with GMNA

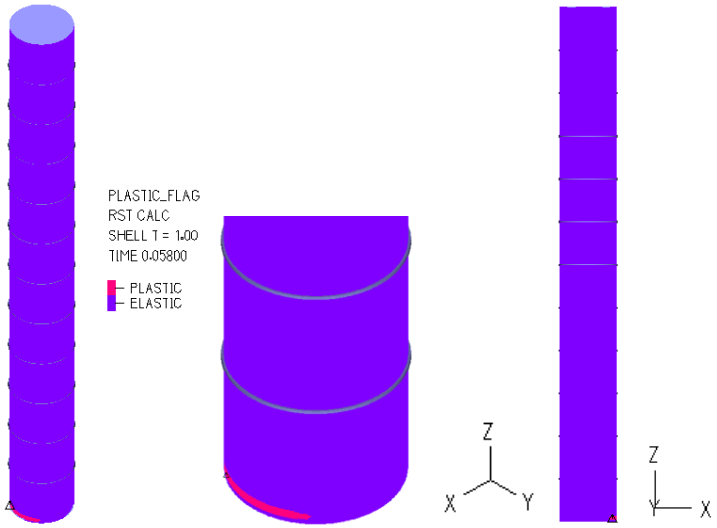

Figure 5-25: Plastic and elastic regions of the rigidly stiffened structure with 5m spacing at failure obtained with GMNA

5.4 SUMMARY AND CONCLUSIONS

In the present chapter, a parametric investigation was presented. Initially the stiffener spacing and later the stiffener stiffness were investigated. For this reason, numerical results were presented for every spacing and stiffness case by means of equilibrium paths, deformed shapes and plastification views. The stiffener spacing ranges from the value of 20m to 2.5m. Investigating the stiffener stiffness, two stiffened structures were compared: the flexibly stiffened and the rigidly stiffened one. In the rigidly stiffened model, rigid and elastic rings were used. Some substantial conclusions drawn in this chapter include:

1) When the arrangement of the stiffeners is very dense, the material nonlinearity is the one governing failure, since the local deformations are significantly restricted by the denser stiffening.
2) The stiffness of the structure is independent of the presence of the stiffeners. Hence, the cantilever component of deformation is not affected by the stiffener spacing.
3) The first yielding is significantly affected by the stiffener arrangement. Hence, as the spacing is getting smaller, the first yielding occurs for a higher value of collapse load factor.
4) The increase of the stiffener number on the chimney is of great importance, as far as the capacity and the local deformations are concerned. Hence, denser stiffening leads to higher strength and significant restriction of cross-sectional changes.
5) When the structure is rigidly stiffened, the prebuckling deformations are significantly reduced, because the stiffeners completely restrict the local deformations due to wind.
6) The capacity of the structure is not affected by the stiffener stiffness. Hence, both the flexibly and the rigidly stiffened structure collapse at similar loads.
7) The failure of the rigidly stiffened structure is governed by material nonlinearity, since the rigid rings restrict completely the local deformations and, thus, the cross-sectional changes. This leads to an elastic behavior of the structure as a cantilever until collapse due to yielding.

6 CONCLUSIONS FOR DESIGN PRACTICE

6.1 INTRODUCTION

Main concerns of the engineers of practice have to do with the efficiency of the analytical method they use and with the effectiveness of the structural components they mobilize. These two matters are treated in the present section by making use of advanced numerical analyses.

The first matter deals with the efficiency of the analytical approach. It was described that the analytical approach is related to beam theory and to strengths obtained according to design methods. The left-hand side of the equation deals with the evaluation of the normal stress due to the internal forces appearing at the critical location. This location is at the bottom support in the case investigated. The right-hand side is related to the strength of the shell structure. This strength in the case of LBA can be the buckling stress (for elastic and perfect conditions). When a type of nonlinearity is taken into account then this strength can take various values depending on the nonlinearity. In this chapter, the evaluation of the efficiency of the analytical approach will be examined by making use of a rigidly stiffened structure for which it is expected that the analytical approaches give satisfactory results.

The second issue has to do with the effectiveness of the stiffener spacing and an effort is made to answer the question whether there is an optimum stiffener spacing or not, in terms of the final strength of the structure. This problem is also confronted by using advanced numerical analyses and the rigidly stiffened structure which is expected to behave as the most strengthened structure possible.

6.2 EFFICIENCY OF THE ANALYTICAL APPROACH FOR BUCKLING

In this section, the efficiency of the analytical approach in the evaluation of the buckling load is investigated. According to beam theory, elastic buckling failure takes place when the maximum normal longitudinal stress considered at the chimney bottom is equal to the classical buckling stress due to axial compression. Such a relationship is defined in Eq. (6-1) and is also described in section 3.3.2.1.

$$\left(\frac{N}{A}+\frac{M}{W_{el}}\right)\cdot\lambda = 455MPa \tag{6-1}$$

where:

λ is the analytical buckling load factor. It results 16 (as also calculated in section 4.6)

N is the axial force, equal to 1811kN

A is the cross sectional area, equal to 0.285m^2

M is the bending moment, equal to 10981.1kNm

W_{el} is the section elastic modulus, equal to 0.497m^3

In Figure 6-1, it is observed that the analytical buckling load factor is quite close to the numerically obtained value of the buckling load factor of the rigidly stiffened structure. Additionally, the analytical buckling load factor is smaller than the numerical one, as the latter is probably affected by the boundary conditions at the structure base [3]. In Figure 6-2, it is obvious that with the use of rigid rings the buckling appears at the structure bottom and at the compressed area due to the +X-Direction of wind predicted by beam theory.

Hence, the use of beam theory in combination with the buckling stress due to axial compression assumed in the analytical calculations, leads to a satisfactory estimation of the buckling load factor in the case of the rigidly stiffened structure. This is probably attributed to the fact that the rigid rings eliminate completely the cross-sectional changes. A possible conclusion is drawn then, that the use of the classical elastic buckling stress as critical stress in the analytical design calculations is adequate when very stiff ring stiffeners are to be used on the chimney structure. On the other hand, if an unstiffened structure is to be designed, the classical buckling theory will probably be insufficient for the design, as it is also shown in Figure 6-1.

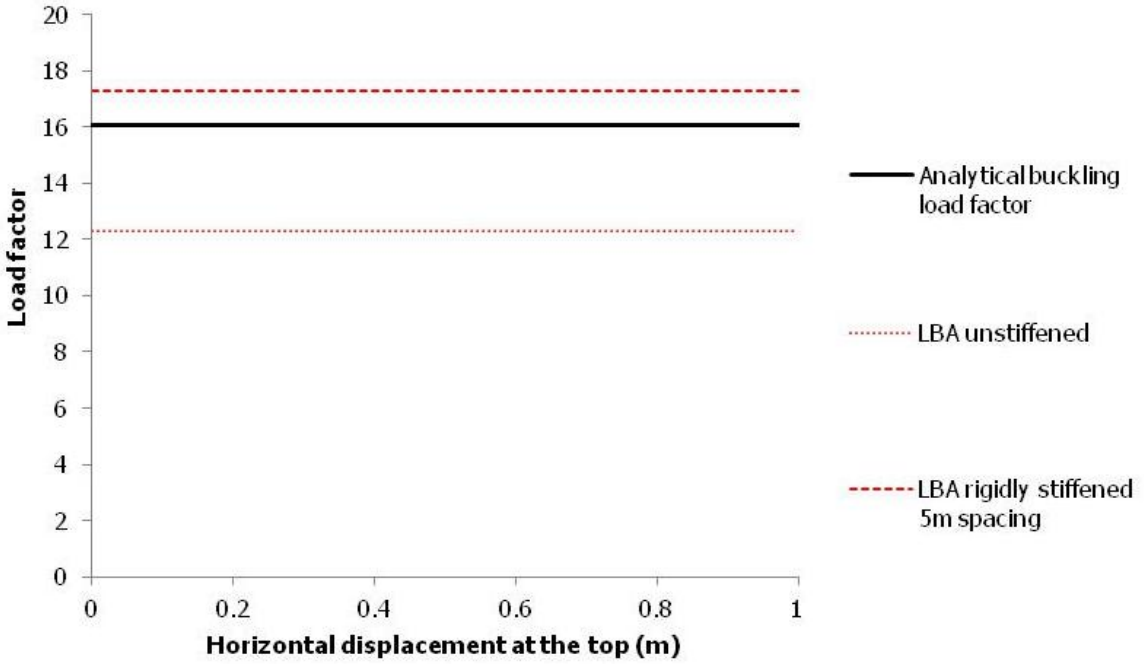

Figure 6-1: Comparison between the analytical buckling load factor and the buckling load factors of the unstiffened model and the rigidly stiffened model with 5m spacing

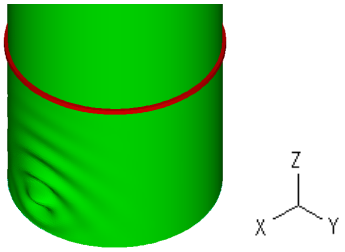

Figure 6-2: First buckling mode shape of the rigidly stiffened model with 5m spacing

6.3 EFFICIENCY OF THE ANALYTICAL APPROACH FOR NONLINEAR CONDITIONS

In this section, the efficiency of the analytical approach for the prediction of the collapse load factor is investigated by making use of nonlinear analyses.

6.3.1 GNA RESULTS

In Figure 6-3 it is obvious that in the case of the rigidly stiffened structure, the GNA collapse load factor is very close to the buckling load factor predicted by LBA. The same conclusion with the LBA results can be drawn then that the use of rigid rings eliminates the cross-sectional changes to the extent that prebuckling deformation (that cannot be captured by LBA) do not affect the final capacity. This is reinforced by the deformation views at failure obtained with GNA illustrated in Figure 6-4. It is observed that the structure behaves as a cantilever and local buckling is observed only at the structure base for +X-wind. This comes in contrast with the behaviour of the unstiffened structure, where LBA and GNA load factors are not close enough and hence the prebuckling deformations cannot be ignored.

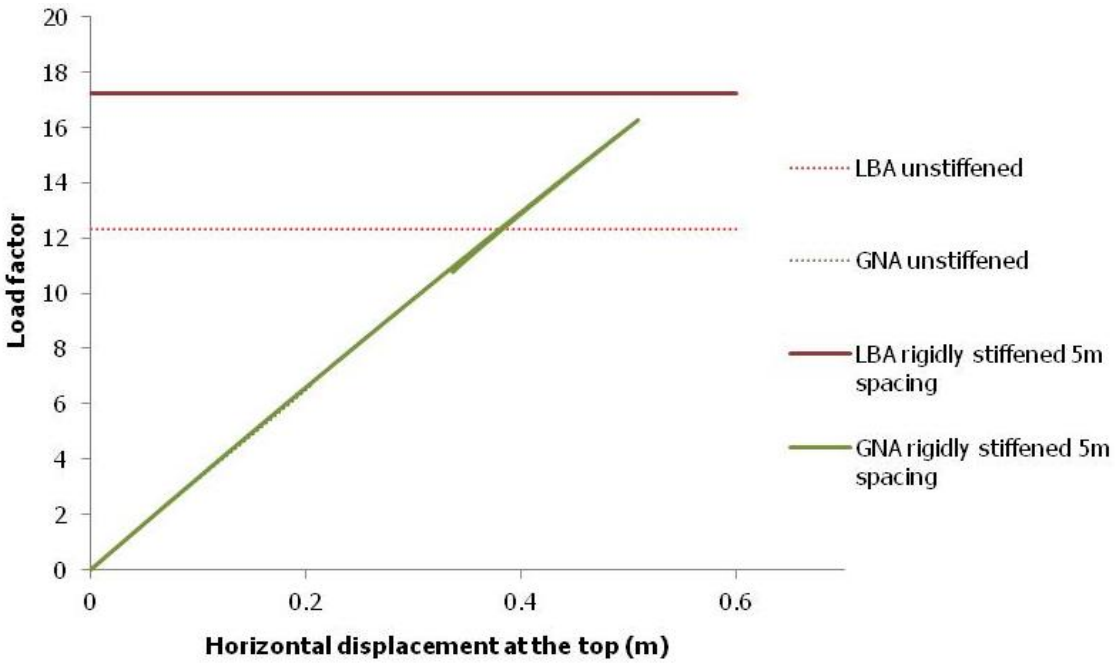

Figure 6-3: Comparison of the collapse load factors between the unstiffened and the rigidly stiffened structure obtained with GNA

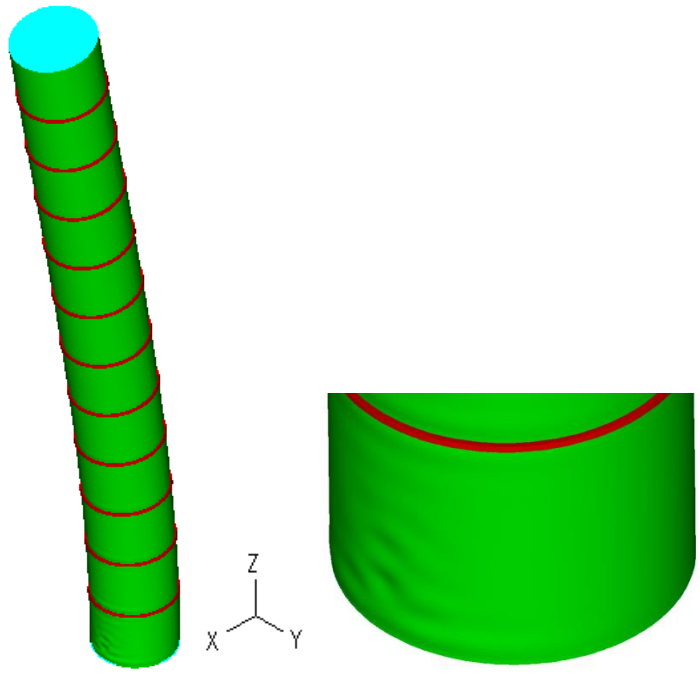

Figure 6-4: Deformation and local buckling at the base support of the rigidly stiffened structure at failure from GNA

6.3.2 MNA RESULTS

The analytical first yield load factor assuming only material nonlinearity takes place when the most stressed fiber reaches the yield stress. This is described by Eq. (6-2).

$$\left(\frac{N}{A}+\frac{M}{W_{el}}\right)\cdot\lambda = 160\text{MPa} \qquad (6\text{-}2)$$

where:

λ is the analytical first yield load factor. It is equal to 5.62

N is the axial force, equal to 1811kN

A is the cross sectional area, equal to 0.285m^2

M is the bending moment, equal to 10981.1kNm

W_{el} is the section elastic modulus, equal to 0.497m^3

In Figure 6-5 it is observed that the afore-calculated load factor assuming only material nonlinearity is very close to the first yielding predicted by the numerical results obtained with MNA for the rigidly stiffened structure. The coincidence of the two values is denoted with a red star. This leads to the conclusion that beam theory is valid for this investigated case, as also shown in Figure 6-6. Contrary to the rigidly stiffened structure, in the unstiffened model first yielding appears at a value much smaller than the one predicted by the analytical calculations assuming beam theory.

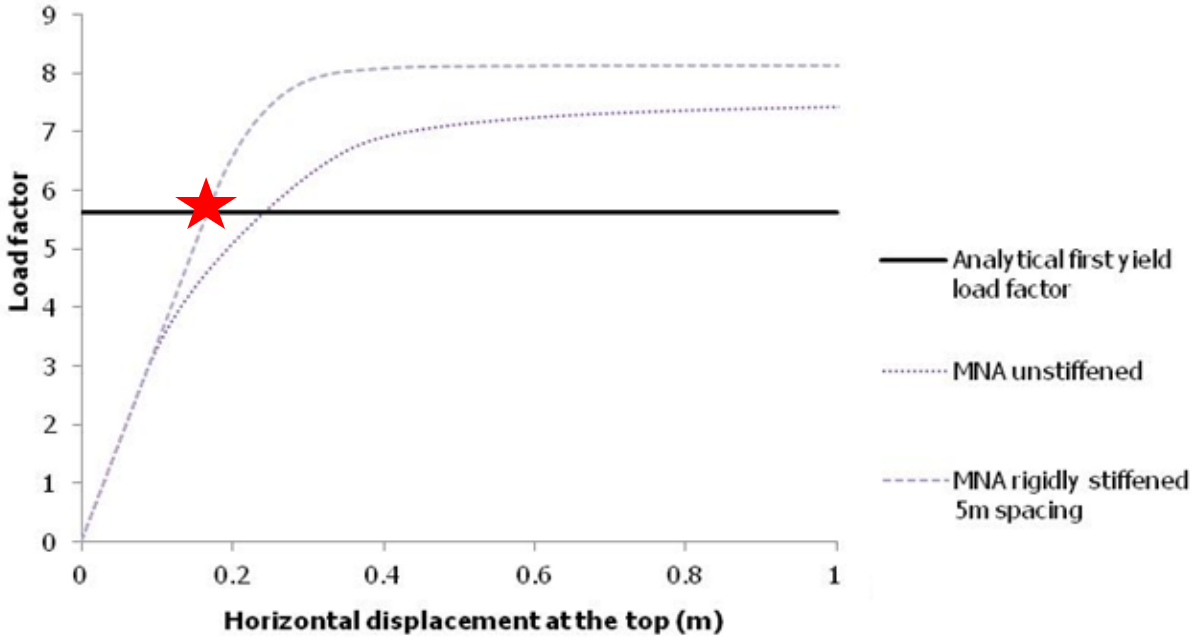

Figure 6-5: Comparison between the analytical collapse load factor assuming material nonlinearity and the time of first yielding according to MNA for the rigidly stiffened structure

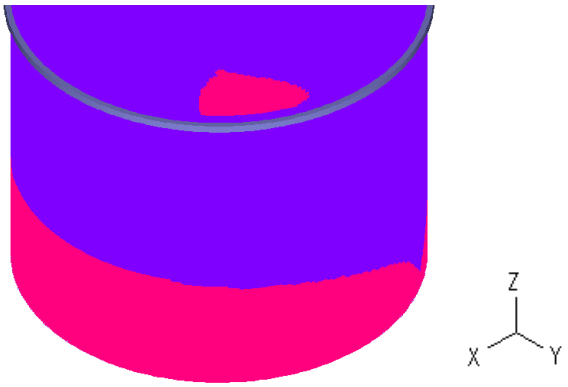

Figure 6-6: Plastification of the bottom cross-section of the stiffened structure with rigid rings at failure assuming material nonlinearity

6.3.3 GMNA RESULTS

Under conditions of geometrical nonlinearity and inelasticity, the failure stress can be considered as the one found in section 3.3.2.2 according to CICIND provisions. Hence, the analytical collapse load factor is defined in Eq. (6-3) and is thoroughly described in section 4.6.

$$\left(\frac{N}{A}+\frac{M}{W_{el}}\right)\cdot\lambda = 107\text{MPa} \qquad (6\text{-}3)$$

where:

λ is the analytical collapse load factor. It is equal to 3.76

N is the axial force, equal to 1811kN

A is the cross sectional area, equal to 0.285m^2

M is the bending moment, equal to 10981.1kNm

W_{el} is the section elastic modulus, equal to 0.497m^3

In Figure 6-7 it is observed that the numerically obtained collapse load factors of the rigidly stiffened structures are not very close to the corresponding analytical one. It is noted that CICIND guidelines take into account initial imperfections and for this reason apart from GMNA results, GMNIA results are also presented. The form of the initial imperfections is based on the first buckling mode of the unstiffened model and the magnitude is 0.85cm translation. Hence, the fact that the collapse load factor according to GMNI analysis (that is regarded as the most accurate analysis) is not close enough to the CICIND collapse load factor highlights the fact that either the beam theory is not valid in this case or the calculation of the failure stress by CICIND is not reliable or both of the previous cases.

The deformation and plastification views at failure from GMNA (Figure 6-8 and Figure 6-9, respectively) show that when rigid rings are used, failure is in accordance with beam theory (as it was in LBA and MNA). Hence, buckling waves and plastification are observed at the bottom of the chimney at the compressed side by the +X-Direction of wind.

Hence, the fact that CICIND collapse load factor does not approximate the GMNIA numerical result of the rigidly stiffened structure is probably attributed to the insufficient calculation of the failure stress by the CICIND provisions. It is concluded that the use of CICIND may lead to conservative design.

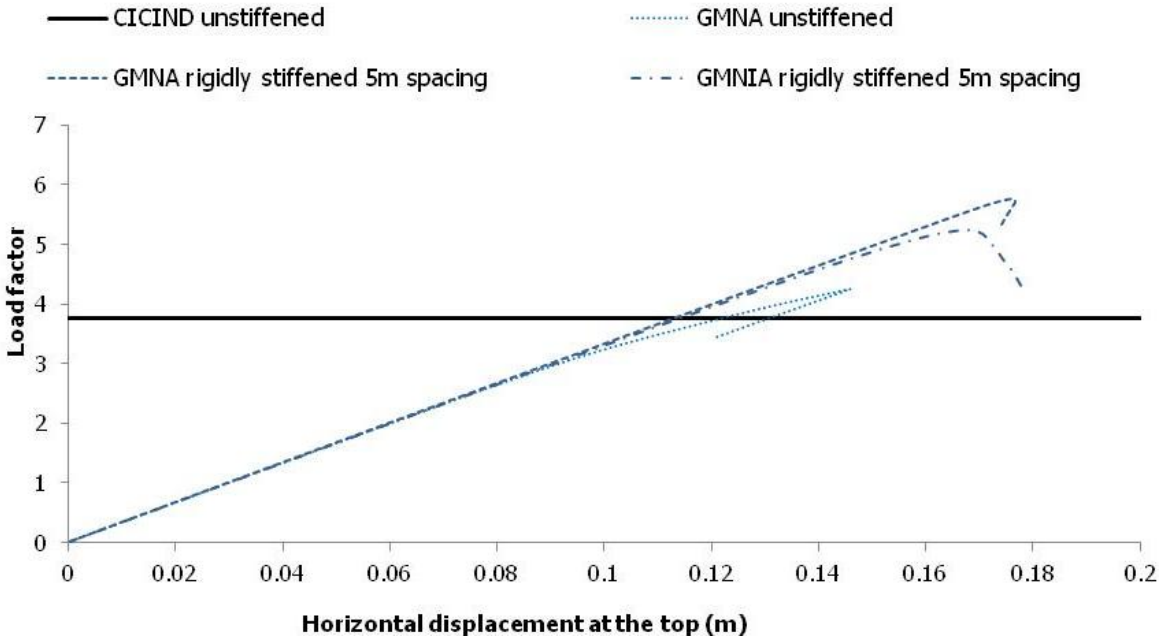

Figure 6-7: Comparison between the analytical collapse load factor by CICIND, the collapse load factors from GMNA of the unstiffened model and the rigidly stiffened model with 5m spacing and the collapse load factor from GMNIA of the rigidly stiffened model with 5m spacing

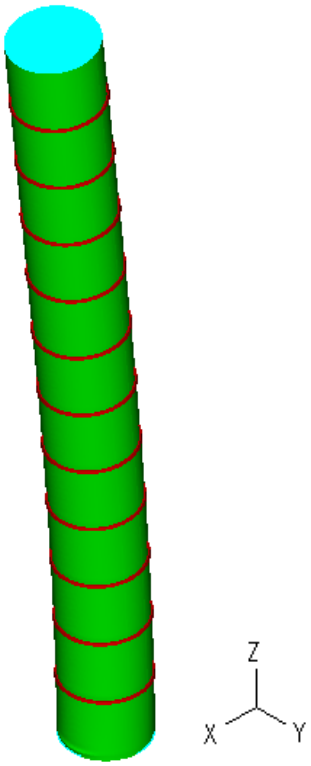

Figure 6-8: 3-Dimensional view at failure from GMNA of the rigidly stiffened model with 5m spacing

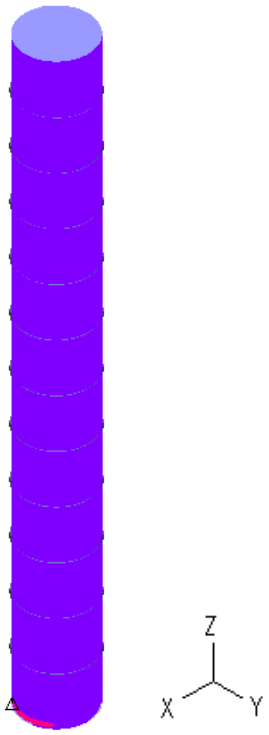

Figure 6-9: Plastification view of deformed shape at failure from GMNA of the rigidly stiffened model with 5m spacing

6.4 OPTIMIZATION CONCLUSIONS

6.4.1 MNA RESULTS

In Figure 6-10 the first yield load factors obtained with MNA for the different spacings are compared with the corresponding analytical first yield load factor. The latter has resulted by considering that failure under material nonlinearity takes place when the most stressed fiber reaches the yield stress and also assuming beam theory. This was described in Eq. (6-2).

It is observed that the analytical value 5.62 does not correspond to any of the numerically obtained values of first yielding. However, the first one is approximated as the arrangement of the flexible stiffeners becomes denser. Since the critical stress for this case (the yield stress) is undeniable, it is concluded that the beam theory is approached as the spacing becomes smaller. Hence, for a denser arrangement than 2.5m of flexible stiffeners the analytical value may coincide with the numerically obtained first yielding. The above conclusion is also shown in Figure 6-11, where the rigidly and the flexibly stiffened structures practically get plastified for first time at the same value of load factor.

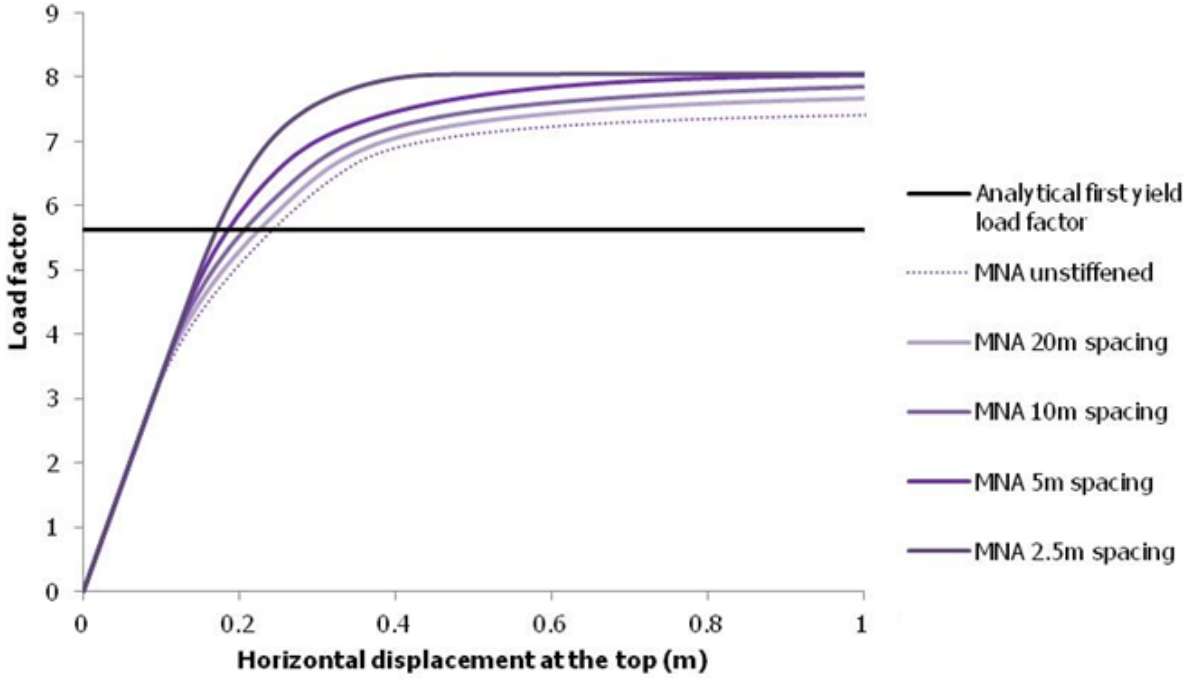

Figure 6-10: Comparison between the analytical collapse load factor assuming material nonlinearity and the load factors of first yielding obtained with MNA for the different flexible stiffener spacings

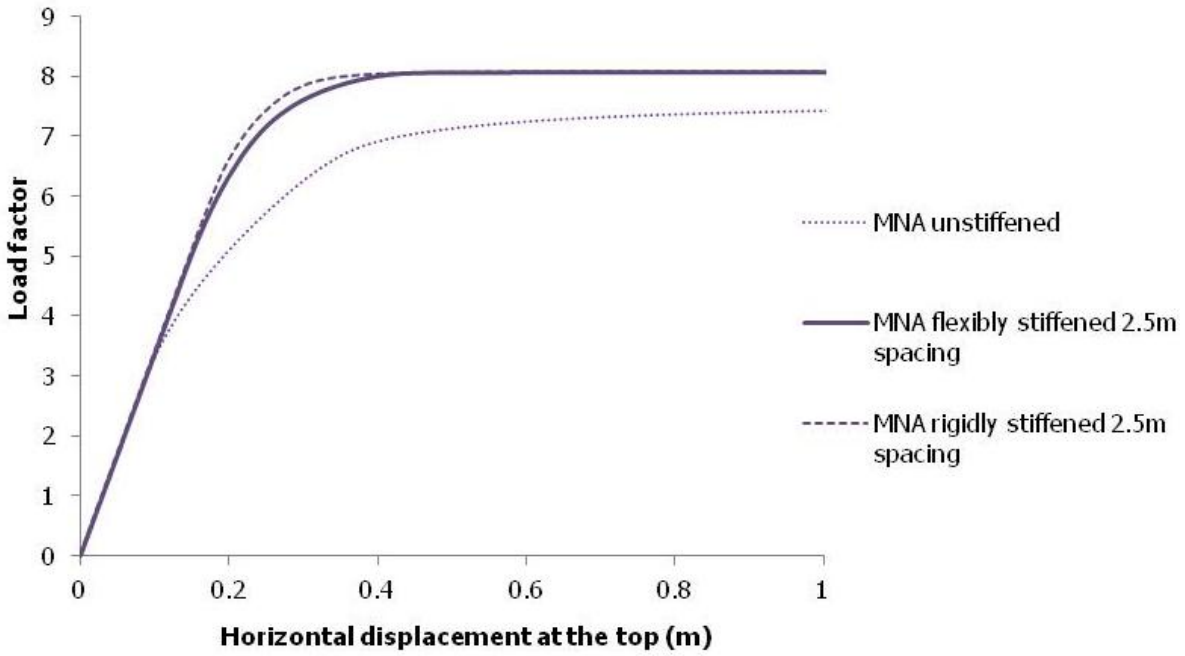

Figure 6-11: Comparison of the collapse load factors and first yielding obtained with MNA between the unstiffened model, the flexibly stiffened model with 2.5m spacing and the rigidly stiffened model with 2.5m spacing

6.4.2 GMNA RESULTS

In Figure 6-12 a comparison of the collapse load factors obtained with GMNA between the different spacing cases and the rigidly stiffened structure with 2.5m spacing is depicted. It is obvious that as the stiffener arrangement becomes denser the structure capacity of the flexibly stiffened structure approximates the one of the rigidly stiffened structure. However, the surprising observation is that the flexibly stiffened model with 2.5m spacing has a larger collapse load factor than the one of the rigidly stiffened model with the same spacing. It is hence concluded that possibly there is an optimum flexible stiffener spacing as far as the capacity is concerned. This means that for values of spacing larger than this optimum value the structure capacity reduces and tends to approximate the collapse load factor of the rigidly stiffened structure.

In Figure 6-13 the deformed shapes at failure given by GMNA for the flexibly stiffened structures are shown. It is obvious that the denser stiffening contributes to the restriction of shell deformation to a significant extent and the last case of 2.5m spacing is closer to the rigidly stiffened structure. However, a complete elimination of shell deformations is not noticed. This is also obvious in the views of plastified areas illustrated in Figure 6-14.

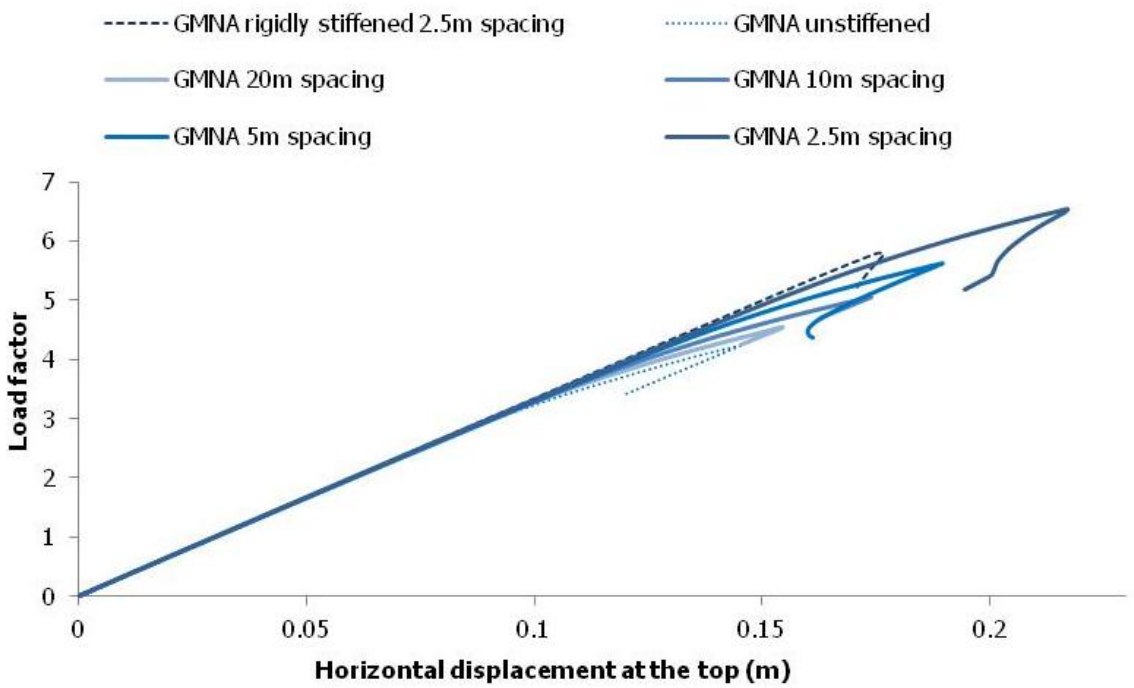

Figure 6-12: Comparison of the collapse load factors obtained with GMNA between the different flexible stiffener spacings and the rigidly stiffened structure with 2.5m spacing

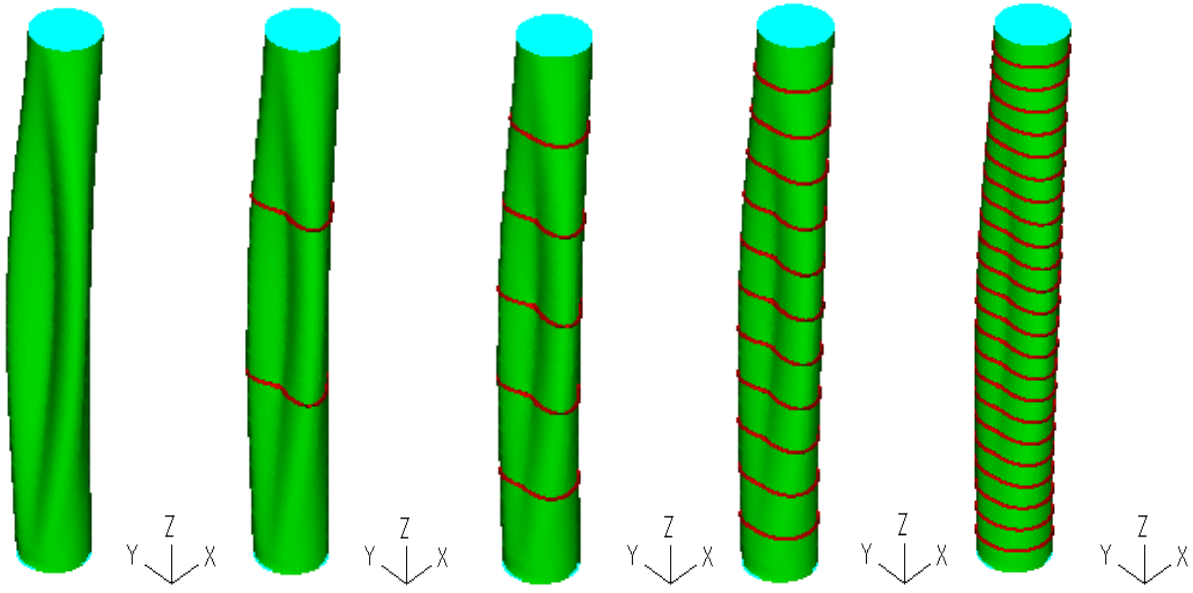

Figure 6-13: Comparison of 3-Dimensional views of deformed shapes at failure from GMNA between the unstiffened (first), the flexibly stiffened with 20m spacing (second), the flexibly stiffened with 10m spacing (third), the flexibly stiffened with 5m spacing (fourth) and the flexibly stiffened model with 2.5m spacing (last)

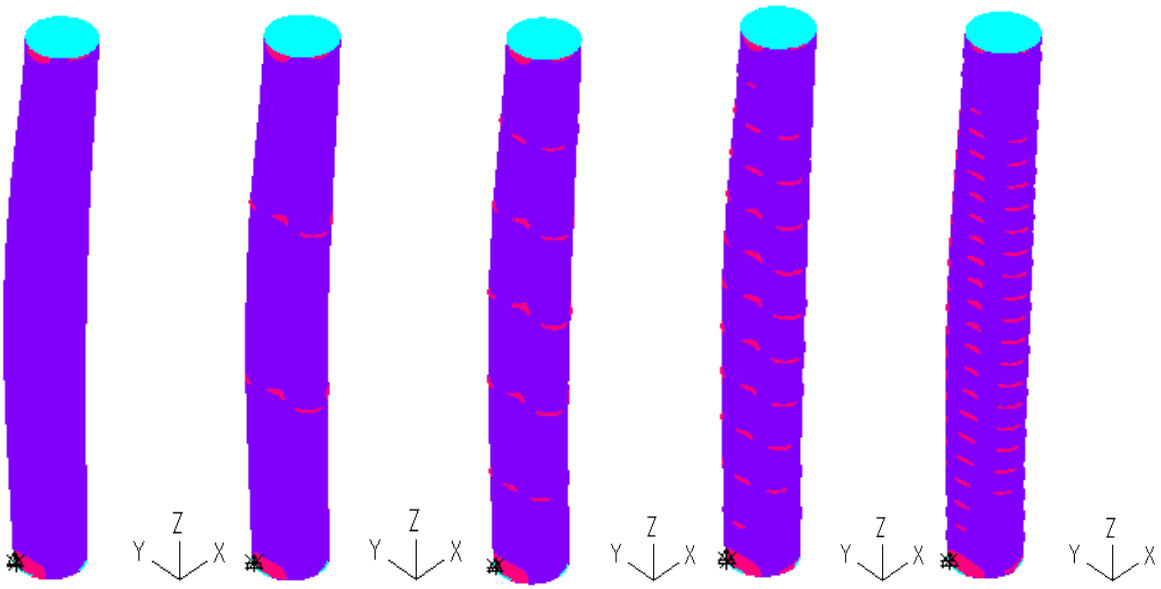

Figure 6-14: Comparison of plastification views of deformed shapes at failure from GMNA between the unstiffened (first), the flexibly stiffened with 20m spacing (second), the flexibly stiffened with 10m spacing (third), the flexibly stiffened with 5m spacing (fourth) and the flexibly stiffened model with 2.5m spacing (last)

6.4.3 LBA RESULTS

In Figure 6-15, the comparison of the buckling load factors between the different stiffener spacings of the flexibly stiffened model and the buckling load factor of the rigidly stiffened model with 2.5m spacing is illustrated. It can be observed that the rigidly stiffened structure has a smaller buckling load factor than the flexibly stiffened structure with a relatively dense arrangement of stiffeners.

The buckling modes from LBA for the different spacings are shown in Figure 6-16. In the unstiffened model, buckling is observed at the top, whilst in the last case of 2.5m buckling appears at the bottom. Despite that, even in the case of 2.5m spacing, beam theory is not valid, due to the appearance of buckling towards Y-Direction.

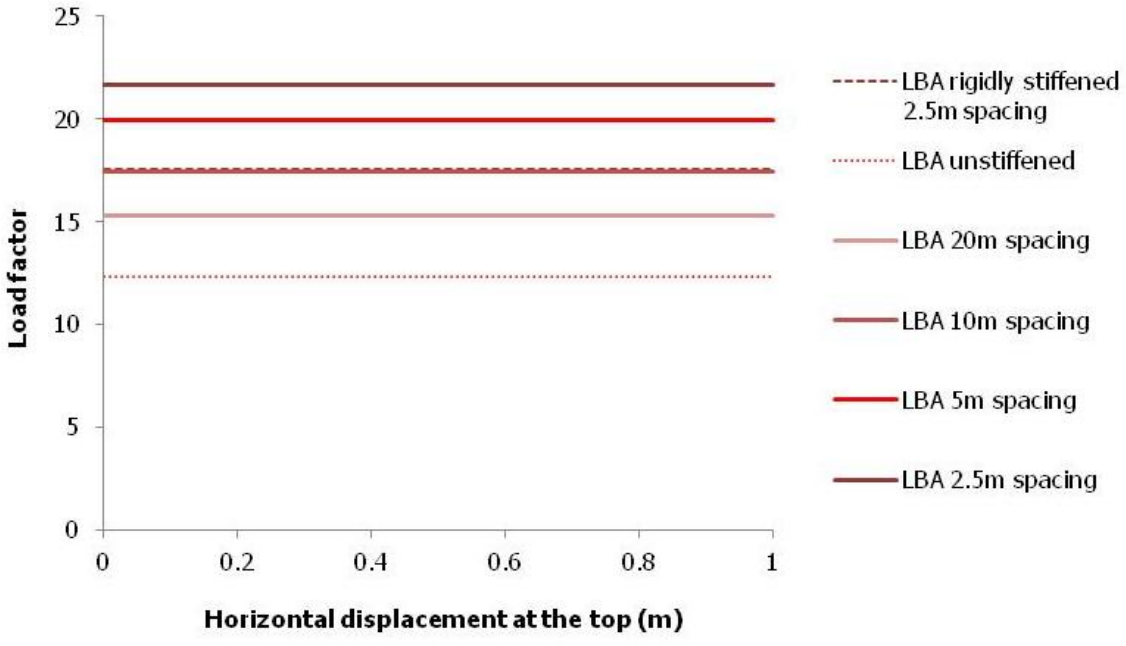

Figure 6-15: Comparison of the buckling load factors between the different flexible stiffener spacings and the rigidly stiffened structure with 2.5m spacing

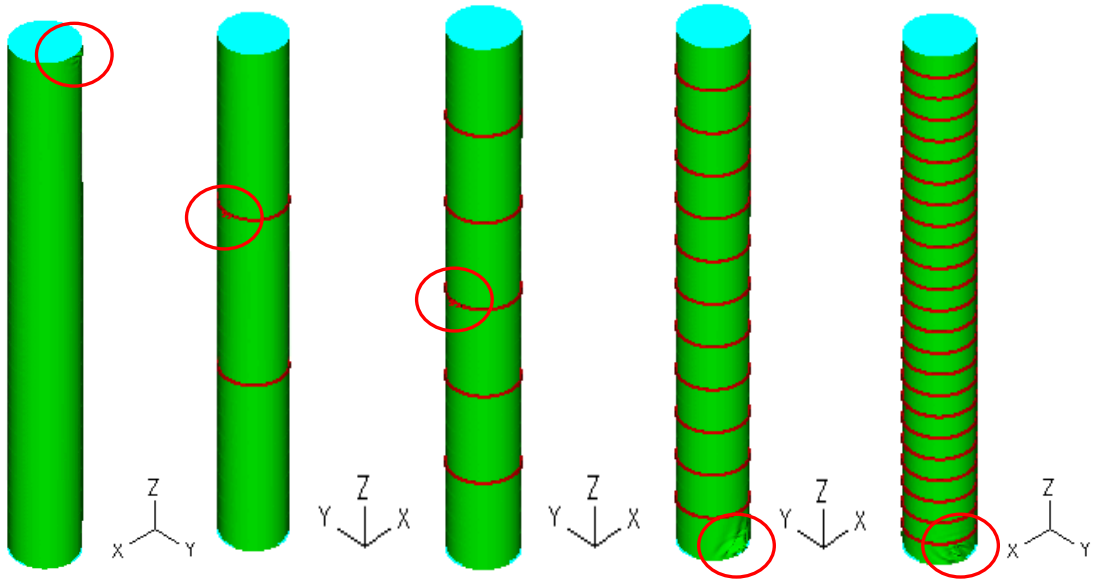

Figure 6-16: Comparison of first buckling mode shapes between the unstiffened model (first), the stiffened model with 20m spacing (second), the stiffened model with 10m spacing (third), the stiffened model with 5m spacing (fourth) and the stiffened model with 2.5m spacing (last)

6.5 SUMMARY AND CONCLUSIONS

In this chapter, some practical conclusions for the design of thin-shell chimneys were presented. These conclusions regard the reliability of the use of the classical elastic buckling stress and the failure stress predicted by CICIND in the analytical calculations. Additionally, in the context of this chapter, an optimum value of stiffener spacing was found as far as the capacity is concerned. Some of the basic conclusions drawn in this chapter follow.

1) The use of the classical elastic buckling theory in combination with the beam theory consideration for the analytical calculation of the buckling load factor is sufficient when very stiff rings are used. On the other hand, as far as the unstiffened structure is concerned, the evaluation of the buckling load factor according to this approach may be unsafe as in the case presented.

2) The failure stress and hence the structure capacity predicted by CICIND led to conservative design for the investigated case. Further research and more analyses are required for the verification of this observation.

3) It seems that there is an optimum stiffener spacing based on the specific chimney model investigated in the context of the present work. To be more specific, the denser the arrangement of the stiffeners is, the larger the capacity of the chimney model. Considering though, that the most dense arrangement of stiffeners leads to a structural response similar to the one of the rigidly stiffened structure (maximum possible stiffening of the shell structure), it is observed that there is a level of stiffening for which further strengthening reduces the capacity of the structure.

7 SUMMARY, CONCLUSIONS AND ISSUES FOR FUTURE RESEARCH

7.1 SUMMARY

The analysis and design of thin-shell structures began during the early 20th century due to the emerging requirements for designing aircrafts, spacecrafts, rockets, submarines and other types of structures. The significant differentiation of such structures from others was quickly observed, as it was found that they are particularly sensitive to geometric imperfections, local buckling and subsequent plastification.

Initially, the problem of shell buckling was investigated by making use of analytical methods in relatively simple problems, such as axial compression. Among the first researchers who worked on shell buckling were Timoshenko, Southwell and Lorenz, who established analytical methods that are widely used by modern design specifications. In the next decades, experimental tests took place and led to useful conclusions, highlighting drawbacks in the assumptions behind the analytical procedures. In the last decades, the development of computer and civil engineering sciences facilitated the use of more advanced numerical procedures.

In the present thesis, an industrial chimney of a combined cycle power plant is investigated. The thesis assumed chimney structure has a height equal to 60m, a diameter equal to 7m and a constant thickness of 0.013m. Additionally, it is stiffened by circumferential stiffeners (rings) at constant intervals of 5m. The geometric type of the stiffeners is L120/120/10. The used material is steel of grade S235 JR, according to EN 13084-7 [51]. However, due to the operating temperature, the following reduced mechanical properties for S235 are eventually used: yield stress f_y=160MPa and elasticity module E=2.025×10^{8}kN/m^2. Additionally, the Poisson's ratio is equal to 0.3. The applied loads are divided into vertical and horizontal. The first ones consist of the self-weights of the shell, the stiffeners and the equipment supposed to be present in such chimneys. The second ones are the wind loads as described in EN 1991 Part 1-4 [5].

The analytical process that is followed in this thesis is simplified making some assumptions. First of all, in the analytical calculations the consideration of beam theory is assumed. Based on the latter, the chimney behaves like a cantilever beam and, hence, the largest stress is assumed at the base of the structure, at the most compressed side due to wind. As far as the applied numerical analyses are

concerned, firstly, linear and elastic conditions are assumed, where the buckling strength is calculated, according to the classical elastic buckling theory. Secondly, nonlinear and inelastic conditions are considered, where collapse strength is found based on the guidance of the design code CICIND [4].

In the context of this thesis, numerical analyses are carried out by means of the finite element software ADINA, in order to compute the response and the capacity of the assumed chimney structure. For this reason, two types of numerical models are investigated, the unstiffened and the stiffened one. The latter is stiffened with flexible ($E=2.025\times10^8 kN/m^2$) and elastoplastic ($f_y=160MPa$) or elastic rings for nonlinear and linear analyses, respectively. Linear (LBA) and nonlinear (GNA, MNA και GMNA) numerical analyses are performed and are presented through appropriate equilibrium paths as well as snapshots at the time of failure. As strength indicator the load factor that multiplies all applied loads up to collapse is used. The comparison of the numerical results between the unstiffened and the stiffened model highlights the impact of ring stiffeners on the structure capacity and deformation. The comparison between the analytical and numerical results of the unstiffened structure leads to the investigation of the sufficiency of the assumed analytical process for the design of unstiffened chimney structures.

A parametric investigation is also conducted. In the context of that, the impact of stiffener spacing and the stiffener rigidity on structure's capacity is investigated. The stiffener spacing ranges from 20m to 2.5m. Investigating the stiffener rigidity, two stiffened structures are compared: the flexibly stiffened and the rigidly stiffened one. In the rigidly stiffened model, very stiff elastic rings are used.

Finally, some practical conclusions for the design of thin-shell chimneys are presented. Hence, the use of the classical elastic buckling theory in the analytical calculations is evaluated. Additionally, the reliability of the failure stress according to the design code CICIND [4] is investigated. Finally, an optimization investigation of the capacity in terms of stiffener spacing takes place.

7.2 CONCLUSIONS

The main concluding points of the present thesis refer to the numerical results of the two investigated structures, the unstiffened and the stiffened one, as well as to the comparison between the analytical calculations and the numerical observations. These are the following:

1) As far as the unstiffened structure is concerned, significant cross-sectional changes at the time of failure are observed. Hence, the application of the wind-pressure directly to the perimeter of the shell structure leads to a 3-Dimensional deformation of the thin shell that cannot be captured by beam theory. Additionally, the unstiffened structure collapses due to both nonlinearities (material and geometrical one), as it is noticed by the equilibrium paths of the nonlinear analyses.

2) The bearing capacity of the structure is enhanced by the rings, as illustrated in the results obtained with LBA, GNA, MNA and GMNA of the stiffened model. The largest increase is observed for the cases that the material is assumed to be elastic. This means that the limitation imposed by material yielding decreases the effectiveness of the stiffening rings. Hence, the higher the material yield strength (that is the more elastic the material) the larger the effect of the stiffening rings on the capacity will be. This also means that the (flexibly) stiffened structure collapses mainly due to material nonlinearity. Finally, the use of stiffening rings leads to a mild deformation of the shell and restricts the cross-sectional changes to some extent. However, since the latter are not fully eliminated, the beam theory is not valid.

3) The provisions of CICIND are considered satisfactory, as far as the collapse load factor of the unstiffened structure (based on GMNA) is concerned, for the specific case investigated.

Nevertheless, the conclusion that they will be satisfactory for other cases cannot be drawn, because their assumptions are not valid, as proved by the region of failure of the unstiffened model.

4) According to GMNA results of the parametric study, the strengthening of the stiffened structure is bigger as a denser stiffening of flexible rings is used. Hence, when two stiffeners are used (20m spacing) the strength increase is 5%, compared with the unstiffened structure. On the other hand, when twenty three stiffeners are used (2.5m spacing) the strength increase is equal to 54%. Moreover, the deformation is affected dramatically by the denser stiffening. Hence, in the case of 2.5 spacing (the most dense stiffening), smaller cross-sectional changes take place, compared with the ones of the unstiffened structure. However, the very dense stiffener arrangement does not restrict completely the cross-sectional changes and hence the beam theory is not valid. Finally, when the arrangement of the stiffeners is very dense, the material nonlinearity is the one governing failure, since the geometrical nonlinearity is mitigated by the very dense stiffening.

5) The use of rigid and elastic rings does not increase the structure capacity, compared to the use of flexible and elastoplastic rings. In the rigidly stiffened structure, the cross-sectional changes are completely restricted. This means that the structure behaves as a cantilever beam according to beam theory. Since local deformations are dramatically eliminated by the use of very stiff rings, the structure is governed by material nonlinearity at the failure time.

6) The use of the classical elastic buckling theory for the analytical calculation of the buckling load factor is sufficient when very stiff rings are used. On the other hand, as far as the unstiffened structure is concerned, the design according to this theory may be unsafe.

7) The critical stress and hence the structure capacity predicted by CICIND may lead to conservative design as observed by the numerical analyses performed.

8) It is possible that there is an optimum stiffener spacing as far as the overall capacity of the structure is concerned. This practically means that there is a spacing for which the capacity of the structure (especially the one related to GMNIA and combined nonlinearities) takes its maximum value and further increase in the number of stiffeners may lead to reduction of strength.

7.3 ISSUES FOR FUTURE RESEARCH

In the context of the present thesis, several numerical results related to two types of structure were presented, the unstiffened and the stiffened one. In the numerical models of these structures many assumptions took place, such as the stiffener spacing, the stiffener stiffness, the stiffener geometry, the shell and stiffener material, the shell geometry and the boundary conditions. It is known though that the analytical methods also take into account some assumptions. Hence, it is noted here that in the context of any future research, when comparison between analytical and numerical results takes place, particular attention should be paid so as these results to be directly comparable. Additionally, the target of this comparison should be in advance stated by engineers.

As far as the thesis suggestions for future research are concerned, first of all, additional experimental tests should take place. In that way, the structural response of chimneys under wind loads will be closely identified and the pressure distribution in such cases will be observed. Hence, the numerical models will be calibrated and considered as sufficiently accurate for further research.

Secondly, many numerical analyses should be performed in order to investigate the structural response of such structures by varying many parameters such as the stiffener spacing, the thickness of the shells, the height of the chimney and the diameter of the cross-section. Additionally, numerical models with breeching can be investigated, as such structures are commonly used in realistic cases. A very large number of numerical results can become a solid basis for the creation of simplified design approaches that follow closely the numerical results that can be considered as accurate as the latter will be checked against experimental ones.

Thirdly, the accuracy of CICIND is not yet fully clear according to the present investigation. It was observed that the assumptions it uses are far from the results observed numerically (such as the location of failure). Nevertheless, the final capacity seems to be satisfactory if one focuses only on the value itself. This can be more carefully examined by making use of extensive numerical analyses and checking CICIND provision's validity for other cases, too.

8 REFERENCES

[1] J.G. Teng, J.M. Rotter, Preface in "Buckling of thin metal shells", Spon Press, London, 2004

[2] M. Angelides, "Large diameter steel chimneys", CICIND Report, Vol. 29, No. 1, 2012

[3] M. Angelides, C.J. Gantes, K. Kalochairetis, CICIND funded research project, "Buckling of large-diameter steel chimneys", 2015

[4] CICIND, Model code for steel chimneys, 2010

[5] EN 1991-1-4, Eurocode 1: Actions on structures, Part 1-4: General actions-Wind actions, CEN, Brussels, 2005

[6] J.M. Rotter, "Cylindrical shells under axial compression" in "Buckling of thin metal shells", J.G. Teng, J.M. Rotter, Spon Press, London, 2004

[7] R. Lorenz, "Buckling of a cylindrical shell under axial compression", Zeitschrift des Vereines Deutscher Ingenieure, German, 1908

[8] S.P. Timoshenko, "Einige Stabilitätsprobleme der Elasticitätstheorie", Zeitschrift für Mathematik und Physik, German, 1910

[9] R.V. Southwell, Philosophical transactions of the Royal Society, 1914

[10] E. Riks C.C., Rankin, F.A Brogan, "On the solution of mode jumping phenomena in thin-walled shell structures", Computer Methods in Applied Mechanics and Engineering, 1996

[11] C.R Calladine, "Theory of shell structures", Cambridge University Press, Cambridge, United Kingdom, 1983

[12] W.T Koiter, "On the stability of elastic equilibrium", PhD Thesis, Delft University ,1945

[13] EN 1993-1-6, Eurocode 3: Design of steel structures, Part 1-6: General rules-Supplementary rules for the strength and stability of shell structures, CEN, Brussels, 1999

[14] L.A. Harris, H.S. Suer, W.T. Skene, R.J. Benjamin, "The stability of thin-walled unstiffened circular cylinders under axial compression including the effects of internal pressure", Journal of Aeronautical Science, 1957

[15] J.G. Teng, J.M. Rotter, "Buckling of thin shells-An overview" in "Buckling of thin metal

shells", J.G. Teng, J.M. Rotter, Spon Press, London, 2004

[16] L.H. Donnell, C.C. Wan, "Effect of imperfections on buckling of thin cylinders and columns under axial compression", Journal of Applied Mechanics, Transaction of the ASME, 1950

[17] N. Yamaki, "Elastic stability of circular cylindrical shells, North-Holland, Amsterdam, 1984

[18] F.W. Bornscheuer, L. Hafner, E. Ramm, "Zur Stabilität eines Kreiszylinders mit einer Rundschweissnäht unter Axialbelastung", Der Stahlbau, 1983

[19] J.M. Rotter, "Elastic plastic buckling and collapse in internally pressurised axially compressed silo cylinders with measured axisymmetric imperfections: interactions between imperfections, residual stresses and collapse", Proceedings of the International Workshop on Imperfections in Metal Silos: Measurement, Characterisation and Strength Analysis, CA-Silo, Lyon, France, 1996

[20] W. Guggenberger, "Effect of geometric imperfections taking into account the fabrication process and consistent residual stress fields of cylinders under local axial loads", Proceedings of the International Workshop on Imperfections in Metal Silos: Measurement, Characterisation and Strength Analysis, CA-Silo, Lyon, France, 1996

[21] J.M.F.G. Holst, J.M. Rotter, C.R. Calladine, "Geometric imperfections and consistent residual stress fields in elastic cylinder buckling under axial compression", Proceedings of the International Workshop on Imperfections in Metal Silos: Measurement, Characterisation and Strength Analysis, CA-Silo, Lyon, France, 1996

[22] J.M.F.G. Holst, J.M. Rotter, C.R. Calladine, "Imperfections and buckling in cylindrical shells with consistent residual stresses", Journal of Constructional Steel Research, 2000

[23] A. Robertson, "The strength of tubular struts", Proceedings of the Royal Society of London, Series A, 1928

[24] W.M. Wilson, N.W. Newmark, "The strength of thin cylindrical shells as columns", Bulletin no. 255, Univ. Illinois Engg Exptl Sta, 1933

[25] L.H. Donnell, "A new theory for the buckling of thin cylinders under axial compression and bending", Transactions of the ASME, 1934

[26] S.P. Timoshenko, "Theory of elastic stability", United Engineering Trustees Inc., New York, 1936

[27] V.I. Weingarten, E.J. Morgan, P. Seide, "Elastic stability of thin-walled cylindrical and conical shells under axial compression", AIAA Journal, 1965a

[28] N.J. Hoff, T.C. Soong, "Buckling of axially compressed cylindrical shells with non-uniform boundary conditions", Symposium on thin walled steel structures, University College Swansea, 1967

[29] B.O. Almroth, A.B. Burns, E.V. Pittner, "Design criteria for axially loaded cylindrical shells", Journal of Spacecraft & Rockets, 1970

[30] O. Steinhardt, V. Schulz, "Zum Beulverhalten von Kreiszylinderschalen", Schweizerische Bauzeitung, 1971

[31] F.W Bornscheuer, "To the problem of buckling safety of shells in the plastic range-Buckling of Shells-Proceedings of a State-of-the-Art Colloquium", (ed. E. Ramm), Springer Verlag, Berlin, 1982

[32] API Standard 620: Recommended rules for design and construction of large welded low-pressure storage tanks, 6th edn., American Petroleum Institute, Washington, DC., 1978

[33] AWWA D100–79: Standard for welded steel tanks for water storage, American Water Works Association, Denver, CO, 1979

[34] ECCS: Recommendations for steel construction-Buckling of shells, 3rd edn., European Convention for Constructional Steelwork, 1988

[35] DIN 18800-Part 4: Stahlbauten: stabilitätsfälle, schalenbeulen, Deutsches Institut für Normung, Berlin, 1990

[36] J.M. Rotter, "Buckling of ground-supported cylindrical steel bins under vertical compressive wall loads", Proceedings of the metal structures conference, Institution of Engineers Australia, Melbourne, 1985

[37] J.M. Rotter, "Pressurised axially compressed cylinders", Proceedings of the international conference on carrying capacity of steel shell structures, Brno, 1997

[38] J.M. Rotter, "Development of proposed European design rules for buckling of axially compressed cylinders", Advances in structural engineering, 1998

[39] ASME, STS-1-Steel Stacks, 2006

[40] J.M. Rotter, "The new European standards for shells and their use in analysis and design-Thin-Walled Structure", (submitted for publication), 2002a

[41] J.M. Rotter, "Shell buckling and collapse analysis for structural design: the new framework of the European standard", Festschrift Chris Calladine, Celebration volume for the 60th birthday of Prof. C.R. Calladine, University of Cambridge, 2002b

[42] G. Speicher, H. Saal, "Numerical calculation of limit loads for shells of revolution with particular regard to the applying equivalent initial imperfections", In "Buckling of shell structures, on land, in the sea and in the air" (ed. J.F. Jullien), Elsevier Applied Science, London, 1991

[43] J.M. Rotter, "Pressurised axially compressed cylinders", Proceedings of the International Conference on Carrying Capacity of Steel Shell Structures, Brno, 1997b

[44] J.M. Rotter, R. Coleman, X.L. Ding, J.G. Teng, "The measurement of imperfections in cylindrical silos for buckling strength assessment", Proceedings of the fourth international conference on bulk materials storage handling and transportation, Institution of Engineers, Australia, Wollongong, 1992

[45] X.L. Ding, R.D. Coleman, J.M. Rotter, "Technique for precise measurement of large-scale silos and tanks", Journal of Surveying Engineering, ASCE, 1996

[46] R. Greiner, P. Derler, "Effect of imperfections on wind-loaded cylindrical shells", Thin-walled structures, 1995

[47] W. Schneider, R. Thiele, "An unexpected failure mode of slender wind-loaded cylindrical shells", 1998

[48] R. Greiner, W. Guggenberger, "Tall cylindrical shells under wind pressure" in "Buckling of thin metal shells", J.G. Teng, J.M. Rotter, Spon Press, London, 2004

[49] P. Knödel, U. Schulz, "Buckling of cylindrical bins-Recent results, Proceedings of the International Conference: "Silos-Forschung und Praxis", Universität Karlsruhe, 1992

[50] M.A. Krenzke, T.E. Reynolds, "Structural research on submarine pressure hulls at the David Taylor Model Basin", Journal of Hydronautics, 1967

[51] EN 13084-7: Free-standing chimneys, Part 7: Product specifications of cylindrical steel fabrications for use in single wall steel chimneys and steel liners, 2012

[52] C.J. Gantes, "Basic concepts of nonlinear response", Notifications on the university lectures of "Nonlinear response of steel structures", N.T.U.A., Athens

[53] C.J. Gantes, K.A Fragkopoulos, "Strategy for numerical verification of steel structures at the ultimate limit state", Structure and Infrastructure Engineering, Vol. 6, Issue 1-2, 2010

[54] C.A. Dimopoulos, C.J. Gantes, "Experimental investigation of buckling of wind turbine tower cylindrical shells with opening and stiffening under bending", Thin-Walled Structures, Vol. 54, 2012

[55] M. Angelides, "Shell buckling issues in chimneys and cooling towers", CICIND Report, Vol. 30, No. 1, 2012